Engineering Model for Automatic Design of Rotor Nacelle Assemblies

For Offshore and Onshore Applications

Aksel Benlevi

Master of Science Thesis

TU Delft Delft University of Technology

Faculty of Aerospace Engineering

Engineering Model for Automatic Design of Rotor Nacelle Assemblies

For Offshore and Onshore Applications

Master of Science Thesis

For the degree of Master of Science in Sustainable Energy Technologies
at Delft University of Technology

Aksel Benlevi

August 15, 2014

Wind Energy Research Group · Faculty of Aerospace Engineering · Delft University of Technology

The work in this thesis was supported by Peperbox Gastronomy Incorporated. Their cooperation is hereby gratefully acknowledged.

Delft University of Technology
Department of
Wind Energy

The undersigned hereby certify that they have read and recommend to the Faculty of Aerospace Engineering for acceptance a thesis entitled

Engineering Model for Automatic Design of Rotor Nacelle Assemblies

by

Aksel Benlevi

in partial fulfillment of the requirements for the degree of

Master of Science Sustainable Energy Technologies

Dated: August 15, 2014

Supervisor(s):

Dr. ir. Michiel Zaaijer

Prof. dr. Gerard van Bussel

Reader(s):

Dr. Ali Elham

Table of Contents

List of Figures

List of Tables

Chapter 1

Introduction

1-1 Background

Since the late 1800's earth is experiencing an exponential growth in the human population and the resources of the planet are exploited in the same manner. Sustainable development has become inevitable in most of the aspects of human daily life. Current greenhouse gas emissions, loss of forests, land, freshwater and biodiversity is hindering the prospect of life in the planet. Speth states the situation as follows "Of all the issues, global warming is the most threatening." [19]. In order to mitigate the effects of climate change, serious measures are taken by global communities. Directives include Kyoto Protocol, European Commission 20-20-20 targets etc..

Concerns over the climate change and the scarcity of the power production from conventional sources due to the depletion of the fossil fuels are the main drivers of the climate change directives and protocols. Consequently the utilization of non-conventional sources such as solar, biomass, wind etc. has elevated because exploitation of renewable energy sources can reduce the greenhouse gases and secure energy supply[20]. Estimated renewable energy share of global final energy consumption for 2011 including traditional biomass expanded to 19% and wind energy is achieving high penetration levels. In 2012 39% of the new global renewable power added was wind power. Likewise, offshore wind energy has been dispersed among 13 countries worldwide by the end of 2012 [21]. As a result wind energy has become a norm rather than an alternative energy supply in many countries and the design of wind turbines and developing wind energy projects has become of paramount importance.

Wind turbine design is a multidisciplinary process that involves mechanical, electrical and civil engineering aspects. Many years of gained experience through learning by doing, searching and using has driven the development of the wind turbine design and its components. Most of the components of a Rotor Nacelle Assembly (RNA) consists of machine elements that has a wide spread of applications in many industries. These components are commercially available and are produced according to the acknowledged standards. Decades of experience with wind turbine applications made the RNA designs become more specialized. Each component is designed and developed in different departments of a company or even with external

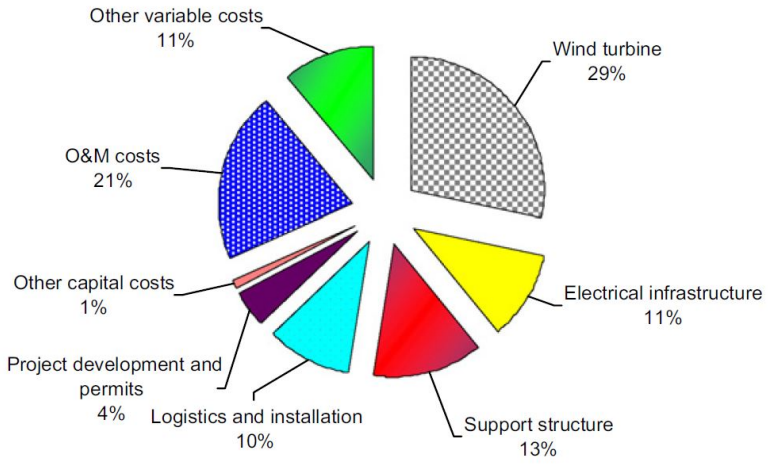

Figure 1-1: Cost breakdown for a typical OWF[1].

partners. This manufacturing and design process focuses on optimization of each component individually, without mainly focusing on the influences they have on each other.

The challenges that are addressed during the optimizations are higher reliabilities and efficiencies and lower O&M and capital costs. To overcome the challenges in different aspects a variety of drive train configurations has been proposed and utilized. These different drive train concepts differ from each other mainly with various types of generators, gearboxes and power converters. Each has their advantages and disadvantages in terms of maintainability, reliability, O&M requirements and cost.

Another approach that is taken by the wind turbine manufacturers and the project developers is to increase the size of the wind turbines in order to capture more wind energy per wind turbine. Using bigger wind turbines means decreasing the number of installations for a given Offshore Wind Farm (OWF) capacity. Reducing the number of turbines lowers the foundation, drilling, installation, maintenance and cabling costs resulting in lower Levelized Production Cost (LPC) for the farm[22]. This approach is especially important for offshore applications where the cost of support structures, electrical infrastructure, O&M, logistics and installation add up to 55% of the total estimated life-cycle cost. This is shown in Figure 1-1 [1].

Advantages of larger wind turbines as in lower operation and maintenance costs, installation and foundation costs per unit capacity and higher energy yield per wind turbine are applicable to onshore wind farms as well. However cost of the wind turbine still remains the largest share of the onshore wind farm cost. Accordingly optimizing the wind turbine performance becomes an essential factor. The size of the wind turbine technology has moved rapidly forward in the past decades. Today 5 to 6 MW wind turbines are commercially available whereas a 55 kW wind turbine was considered state of the art 30 years ago. The wind turbine capacity evolution over the years is presented in Figure 1-2. However the potential offshore market remains the main driver for large wind turbine technology development[2].

Furthermore it is important to note that attributed design parameters, such as tip speed ratio, play an important role in the design of drive train components. For instance, the flow behind the rotor rotates in the opposite direction to the rotor, as a reaction to the torque applied to

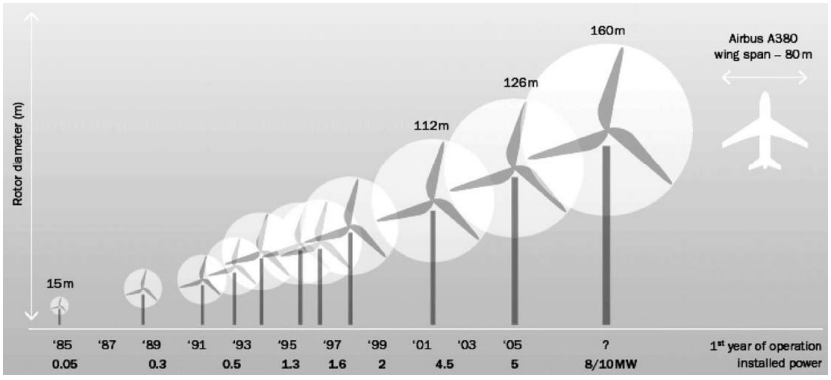

Figure 1-2: Size evolution of wind turbines over time[2].

the rotor by the flow. This rotational kinetic energy in the wake will be absent in the energy extracted by the rotor. Thus slow rotating rotors will generate higher torque and higher wake rotation losses. On the other hand higher rotational speeds will result in lower torque on the rotor and higher acoustic noise[4]. Besides the rotor that is running too fast will act as a solid wall and obstruct the wind flow, thus decreasing the power extraction [23]. Between the two mentioned rotational speeds exists an optimal value which maximizes the power coefficient. The effect of the tip speed ratio on the power coefficient of a three-bladed wind turbine in constant wind speed can be observed in Figure 1-3. The optimal tip speed ratio mainly depends on the number of blades, type of wind turbine and the air-foils used. Optimum tip speed ratio for three-bladed wind turbines is between 6 and 8, with 7 being mostly selected value[24]. The power coefficient along with the rotor diameter and losses will determine the rated power of the wind turbine. This will define the rated wind speed and the maximum rotational speed depending on the tip speed ratio and the generator type. The maximum torque and thrust are mainly influenced by the rotational speed, wind speed and the rotor diameter. The maximum torque determines the size of the gearbox and should be matched by the generator. On the other hand the number of poles in the generator has an effect on the size and stages of the gearbox that should be used. Finally the maximum thrust determines the structural design of the tower and the foundations [25]. Hence, the theoretical knowledge presented in this field suggests that there is a close dependency between components of the drive train.

1-2 Problem Analysis and Statement

When the history of wind turbine technology is considered different configurations of drive trains are observed. These concepts differ from each other by their distinctive advantages in different aspects such as maintainability, reliability, O&M requirements and cost. Accordingly superiority of each concept in particular features suggests the existence of trade-offs between components.

Additionally the theoretical approach towards the drive train components illustrates the dependency of elements with each other and the necessity of an iterative design process, that incorporates all of the constituents of the drive train. Thus the investigation in wind turbine technology concepts and physics of design leads to the problem statement.

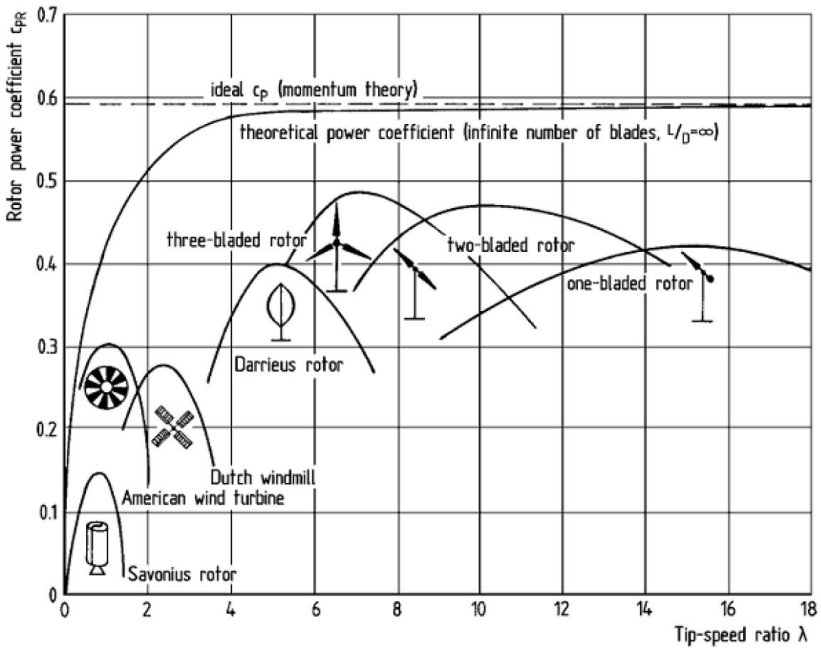

Figure 1-3: C_P - λ curves for different wind turbine types [3].

Problem Statement: There is a gap in the design process between the development and optimization of individual components in the drive train and the overall performance and cost improvements of the wind turbines in the larger scales that are achieved today.

Observation about possibilities of the drive trains and their physics shows factors in design that modifies each component in an associated manner. This exhorts the realization of a higher level optimization process that involves all components of the drive train.

1-3 The Research Objective

In order to further optimize the utilized wind turbines according to the wind class constraints for offshore and onshore wind farms this project focuses on an engineering model for (automatic) design of an RNA. Therefore the objective of the project can be stated as:

To have a validated engineering model that conducts a higher level preliminary design optimization of the rotor nacelle assembly by taking all the components into consideration.

Mainly the project extends the existing design algorithms of the wind turbine design methods, with an engineering model that does not exist. The aim of the model is to reveal the optimized design parameters of an RNA in accordance with the objective function. The model will focus on the interactions and trade-offs between the (sequential) components of the RNA. The elements that will be focused on are the rotor, main shaft, gearbox, bearings, high speed shaft and subsystems of yaw, electrical components and nacelle. Engineering design models are provided for the rotor, the gearbox and the generator only. In the course of constructing the model, the functionalities that are mostly desired by the users will be addressed. Physical models with necessary accuracy will be aimed for, as long as that they are simple enough for rapid assessments.

1-4 Approach

In order to avoid the isolated approach which neglects the optimization between disciplines, a Fully Integrated Optimization (FIO) architecture will be used. This will pass the design variables to simulation tools for cost, aerodynamics, structure etc. than the objective function and constraints will be sent back to the optimizer resulting in iterations. The approach will continue until the convergence is achieved [7].

In search of design, optimization methods will be used, thus the characteristics of the optimization problem should be noted. The objective functions and constraints will be linear and non-linear equations and a single optimization problem will be addressed with one objective function. Depending on the objective function and constraints the optimization algorithms will be gradient based (first order) or direct (zero order) with continuous and discrete design variables. Finally the different disciplines involved in the design process will lead to a Multidisciplinary Design Optimization (MDO) [7].

Formulation of the optimization problem will be done through defining the design variables, design constraints and if applicable partial safety factors for each component, and formulating the objective function. Firstly an overall analysis of RNA components will be done to see which parameters couple them. By this approach the mono-disciplinary design will be avoided. Then design integration will then be achieved by writing a shell program that ensures the communication between all codes. Most importantly due to the complexity of the problem, the design variables will be decomposed into levels. This will lead to a multilevel optimization, where each level of optimization will be carried out consecutively by fixing the design variables excluded in the corresponding level until satisfactory convergence is achieved in the objective function [7].

Initially simple working software will be formed, which will be followed by developing the software with more sophisticated engineering algorithms. Finally validation of the tool will take place. The software will be tested and analysed by applying different high level specs and comparing the results with the standards and real life RNA examples. Any problems that are encountered in this stage will lead the process back to the product development in order to implement solutions to encountered complications.

1-5 Layout of the Report

This thesis is composed of 9 chapters. Chapter 2 introduces the RNA components classified in subsystems, while functionalities and description of each component are given. Chapter 3 focuses on the optimization process and its decomposition into levels. Chapter 4 includes the engineering models that are chosen for the design tool. Chapter 5 gives information about the tools that are utilized and the structure and layout of the optimizer. In Chapter 6, the appraisal of the automatic design of RNA tool is conducted. Chapter 7 presents the utility of the tool. Finally chapter 8 and 9 gives the conclusions and future recommendations respectively.

Chapter 2

Rotor Nacelle Assembly Components

2-1 Introduction

A wind turbine is a device that converts the kinetic energy of the wind into electricity. The Rotor Nacelle Assembly (RNA) in a wind turbine consists of the rotor, nacelle and the components enclosed within the nacelle. The RNA has been divided into subsystems and each component is studied. This chapter provides descriptions of the components that are included in the RNA design tool along with their functions. Transformer and the cables have been excluded from the scope of the project, since they are considered to be located outside of the RNA boundaries. The wind turbines that will be studied in this project are variable speed horizontal axis upwind turbines with three blades and pitch control. Furthermore three types of drive train configurations will be designed in the automatic RNA design tool. First is with a Doubly Fed Induction Generator (DFIG) and a three stage gearbox, second is with a Permanent Magnet Synchronous Generator (PMSG) and a single stage gearbox and the last one is a direct drive drive train with a PMSG and no gearbox. The differences in components between the drive trains are specified under the related elements of the RNA.

2-2 Rotor Subsystem

2-2-1 Overview of the Rotor Subsystem

The rotor of a wind turbine is designed to extract power from the incoming wind and translate it to rotational movement. The rotor subsystem performs under stochastically and periodically varying loads along with steady ones. Due to the cyclic loading, fatigue becomes a major concern. On the other hand the rotor also passes the cyclic loading on to the rest of the wind turbine especially the drive train [4].

The rotor consists of three blades that are positioned at the plane of rotation. The blades are positioned 120 degrees from one another with their span axes intersecting each other at

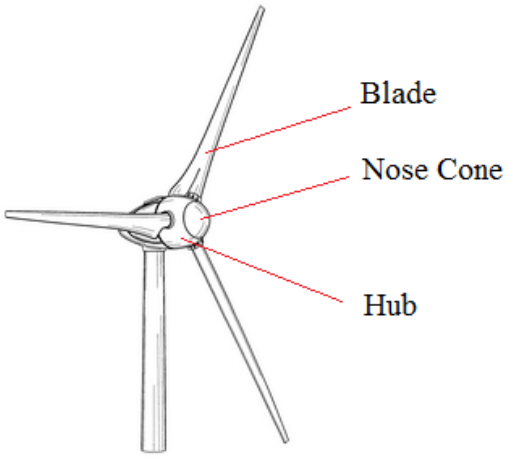

Figure 2-1: Rotor Subsystem Components

the rotor center [26]. The blades are attached to the hub and the pitch mechanism, which are covered by the nose cone. The components are shown in Figure 2-1 with the exception of the pitch mechanism which is enclosed inside the hub. The next four sections focus on the mentioned components of the rotor.

2-2-2 Blades

One of the essential elements of the rotor are the blades. These components translate the force of the incoming wind into torque for generating power [4]. Most of the commercially available wind turbine blades are made of glass fibre reinforced plastics. They are long bodies with two blade shells that are connected to a supporting web [26]. Blades are bolted to the pitch mechanism via the blade roots. The root experiences the highest moments, therefore is made ticker to withstand these moments. A variety of airfoils are utilized along the spanwise direction. Chord, twist distribution and airfoils determine the aerodynamic performance of the blades. The structural strength is established by the choice of material, manufacturing techniques and blade thickness.

2-2-3 Hub

The hub is the part of the rotor subsystem that connects the blades to the main shaft. The loads generated by the blades are transmitted through the hub. Generally hubs are made of welded or cast iron. It is one of the wind turbine's heaviest components [4]. Furthermore it provides a rigid support structure for the pitch mechanism [26]. An example of a hub is illustrated in Figure 2-2.

Figure 2-2: Typical rigid wind turbine hub [4].

2-2-4 Pitch Mechanism

The pitch mechanism is a hydraulic driven device that rotates the blades around their axis. It consists of a hydraulic actuator, rotary wheel, motor and a pitch bearing [26].

2-2-5 Nose Cone

The nose cone covers the hub and the pitch mechanism. It is connected to the hub and its purpose is to protect the pitch mechanism and the hub against environmental conditions. The material that is used to manufacture nose cones is similar to the composites that are used for the blades [26].

2-3 Drive Train Subsystem

2-3-1 Overview of the Drive Train Subsystem

The drive trains that are in the scope of the project include a power converter and all the rotating parts except the rotor and yaw subsystems. The rotating parts consist of the main shaft, couplings, gearbox, rotor bearings, brakes, high speed shaft and generator [4]. The torque is transmitted to the generator for power output. In the drive trains with three and single stage gearboxes low rotational speed and high torque is translated into high rotational speed and low torque for the use of the generator. A representative illustration of a typical drive train with a gearbox is shown in Figure 2-3.

2-3-2 Main Shaft

The main shaft is also referred to as the low speed or rotor shaft. The torque is transferred from the rotor to the rest of the drive train through this element and it also provides support to the weight of the rotor [4]. The element is a cylindrically shaped metal alloy that connects

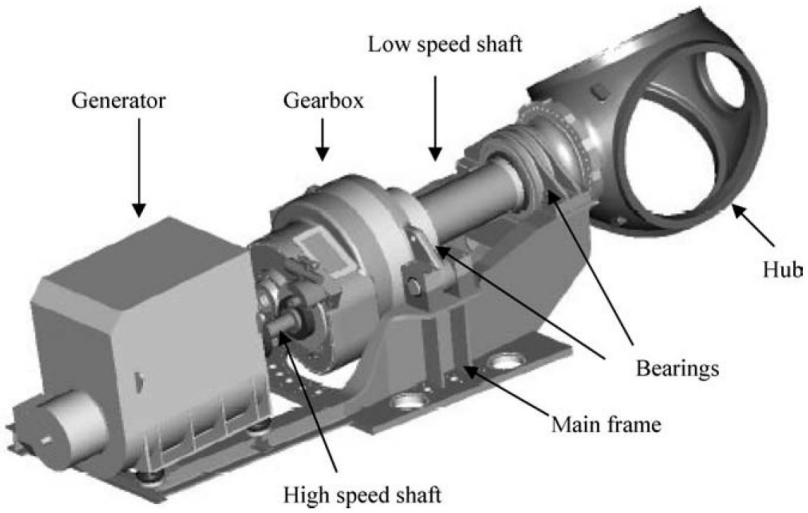

Figure 2-3: Typical drive train and associated components [4].

the hub and the gearbox. The axis of the main shaft and the rotor is the same. The main shaft is positioned by the bearings [26].

2-3-3 Rotor Bearing

The rotor bearings are used to reduce the frictional resistance between the main shaft and the nacelle bedplate. Furthermore it positions the main shaft on the same axis as the rotor. Bearings consist of an inner ring, outer ring, the balls and the cage. The inner ring is fixed on the main shaft and the outer ring is fixed upon the support of the main shaft on the nacelle bedplate. The cage holds the balls in place and balls provide the decoupled rotational movement [4].

2-3-4 Couplings

Couplings connect the shafts together. They are mainly utilized between the main shaft and the gearbox as well as between the high speed shaft and the generator. This element transmits the torque between the shafts that it is attached to and allows for small misalignments between the two rotating components [25]. On the other hand the coupling before the generator is also used for dampening the torque fluctuations [4].

2-3-5 Gearbox

In the most cases the rotational speed of the electric generator is higher than the rotational speed of the main shaft. The gearbox increases the rotational speed to the level required by the generator. This applies to the first two drive trains that are selected. Naturally these are the ones with a single stage gearbox and a three stage gearbox. Furthermore, sometimes the gearbox also has secondary functions such as supporting the main shaft bearings. There

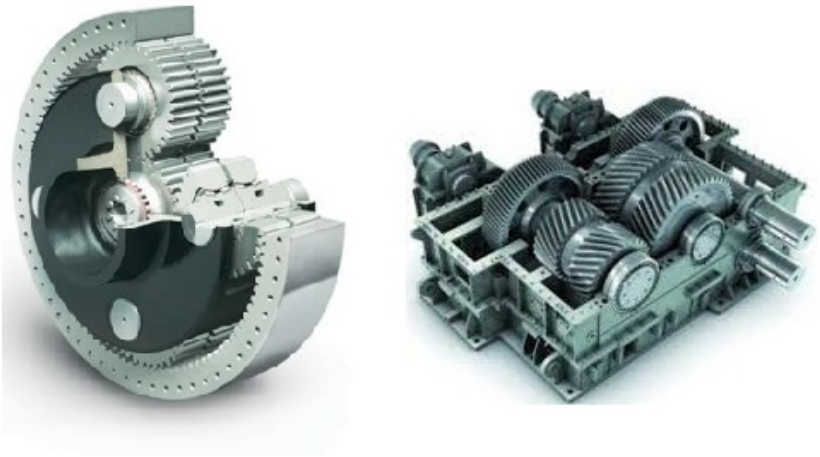

Figure 2-4: Planetary Gearbox (on the left) and Parallel Shaft Gearbox (on the right).

are two types of stages that are utilized in wind turbine applications: *i*) parallel shaft stages and *ii*) planetary stages . Examples of planetary and parallel shaft gearboxes are shown in Figure 2-4. Planetary gearboxes are composed of a sun, planet and annulus ring gears. The sun is the gear in the center and planet gears rotate around it. The annulus ring gear confines the sun and planet gears within, and is in contact with the planet gears. Parallel shaft gearboxes have a pinion (small gear) with high rotational speed and a gear with bigger radius and lower rotational speed. The first drive train with three stage gearbox includes two planetary stages and a parallel stage as the final one. On the other hand the single stage gearbox includes only a single planetary stage in the design.

The gearboxes are one of the most challenging elements of wind turbines in the operation and maintenance aspect. Besides they are one of the heaviest and most expensive components in the system [4].

2-3-6 High Speed Shaft

The high speed shaft, similar to the main shaft, is also a cylindrically shaped metal alloy. It is placed between the gearbox output and the generator shaft, thus it is not included in the direct drive drive train. It rotates around the axis of the generator. The purpose of this machine element is to transmit the rotational energy to the generator shaft. Due to the relatively lower torque transmitted, the high speed shaft is smaller in diameter than the main shaft [26].

2-3-7 Generator

The generator converts the mechanical power into electrical power. The most commonly used two types of generators in the wind turbines are: *i*) Induction generators and *ii*) Synchronous generators. First drive train with the three stage gearbox includes a DFIG as the other two have a PMSG. Generators have a horizontal rotational axis which aligns with the high speed shaft. Through the high speed shaft, high rotational speed and low torque are supplied to the rotor of the generator. Along with the magnetic field, active and reactive power is induced

in the stator of the generator. The DFIG uses electrical excitation whereas the PMSG uses permanent magnet excitation. The advantage of the PMSG is that it has no excitation losses however the excitation can not be controlled.

The stator housing of the generator is made of steel and the winding of the armature is made of copper. The wires are insulated to keep them protected from the environment and stabilize them. The exterior of the generator provides protection from condensation, dust, rain and blowing sand [4].

2-3-8 Power Converter

Some of the fundamental components used in the power converters include power transistors, silicon-controlled rectifiers and gate turn off thyristors. The most important role of the partial scale power converter is to keep the generator frequency constant while the rotor is allowed to operate with variable-speed to extract most of the energy from the incoming wind [4]. Moreover it helps to reduce power and load variations. The first drive train with the DFIG has a partial scale power converter and the other two with PMSG have a full scale power converter. However the the cost models of the NREL study includes a power converter capable of handling full power output for all of the selected drive trains.

2-3-9 Brakes

The main function of the brakes is to park the wind turbine by fixing the nacelle in position for maintenance purposes. Moreover the brakes are also used in cases of high and low wind speed shut-downs. Usually aerodynamic braking is performed before the mechanical brakes are engaged, so that the torque applied to the brakes is lower.

2-4 Yaw Subsystem

All of the commercial wind turbines have a system that aligns the rotor axis with the incoming wind direction. The designed systems in this project are upwind wind turbines therefore an active yaw system will be used instead of a free yaw system. In the active yaw system an electric motor is used to rotate the nacelle to face the wind direction. The system consists of a yaw bearing, an electric motor and a gear train. It should be able to carry the main part of the turbine and transmit the dynamic and gravity loads of the nacelle to the tower [4].

2-5 Nacelle Subsystem

2-5-1 Overview of the Nacelle Subsystem

The nacelle is the housing of the main components of the wind turbine and it is composed of the main frame and the nacelle housing.

2-5-2 Main Frame

The main frame provides a rigid support structure for components enclosed in the nacelle. Gearbox, generator and the brake are attached to the mainframe. The yaw system that is bolted on top of the tower is connected to the main frame. It is normally a rigid structure of welded or cast iron. Furthermore, it also transmits all the loads from the generator, brake and the rotor to the tower [4]. Since some of the components enclosed in the nacelle are different from each other in different drive trains (such as generators or gearboxes) the mainframes are not identical as well. These differences are reflected on the mass and cost modelling of the component.

2-5-3 Nacelle Housing

Nacelle housing provides protection to the electrical and mechanical components located inside it from the environmental conditions. It is generally made from fibreglass which is a lightweight material. On larger wind turbines the nacelle housing must have enough space to let personnel enter and perform maintenance duties [4].

Chapter 3

Optimization of the Rotor Nacelle Assembly

3-1 Introduction

The optimization of the Rotor Nacelle Assembly (RNA) will be conducted with multiple optimizers for specified components. In this section the coordination strategy and the formulation structure of the optimizers are introduced. Due to the complexity of the design a multi-level optimization will be conducted. So this section will introduce the multi-level optimization approach and the decompositions methods that are used for its application.

3-2 Multi-level Optimization

One of the reasons for establishing levels in the optimization of the system is to employ the decomposition method. At the top level the general characteristics of the system are captured and in the second lower level the individual elements in the system are modelled. The latter seizes the behaviour and the detailed description of the individual components. This behaviour is coupled with the higher level component's behaviour and (possibly) with the neighbouring components behaviour [27]. As in the relationship between the RNA and the lower level neighbouring components of generator and gearbox.

The top down analysis of the system can continue until the smallest distinguishable components and their details. Therefore multi-level analysis captures the characteristics of the system in multiple levels through a coordination strategy that is based on hierarchy of the components [27].

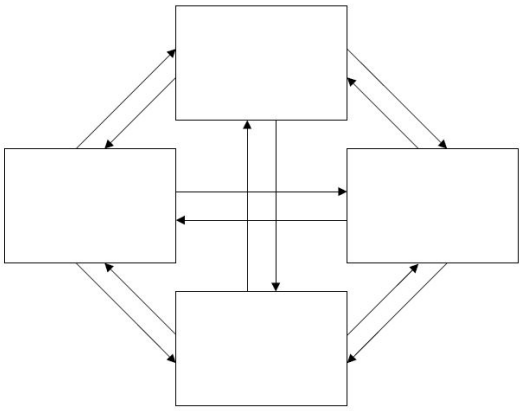

Figure 3-1: Illustration of a non-hierarchical system [5]

3-3 Decomposition of the Design Process

3-3-1 Introduction

The complex structures of today, posses distinct multiple levels of details that create a hierarchy of components going down to material level. The levels are originated from technological developments, increasing complexity of structures and advanced demands on components. The levels specified during design optimization separate the design optimization considerations of the entire system performance from the individual component performance [27].

Compact interaction between the neighbouring components is necessary to achieve better characteristics of the system. Individual optimization of the components, without taking into consideration the entire hierarchy, may lead to a non-optimal system that is a combination of optimized elements. Furthermore not all desired performances of a system are achievable by optimization of a single element [27].

Usually analysing a complex system as a whole is considered to be inefficient and unmanageable. Another approach is to decompose the system into smaller subsystems. Studying these subsystems individually could improve the feasibility and efficiency of the analysis task [5]. The main driver for the use of distributed optimization is organizing the design. Since a single designer is not able to cope with the burdening details of the system a series of design teams are appointed to distributed parts of the design process. Each team focuses on a subproblem with a given degree of decision autonomy, since some quantities from other disciplines related to the interdisciplinary interaction are necessary for the design. This kind of approach fits with distributed optimization methods naturally due to the multi-level structure of the decomposition. The second motivation for distributed optimization is the computational savings. Event though the local optimizations do not benefit from this approach the global optimization benefits from it considerably [28].

Four divisions of system partitioning methods have been identified in the literature: *i*) by aspect *ii*) by object *iii*) matrix and *iv*) sequential. Aspect decomposition divides the system according to disciplines. Such as partitioning an automotive design into structural, aerodynamic and dynamic disciplines. Object partitioning separates the system into components or

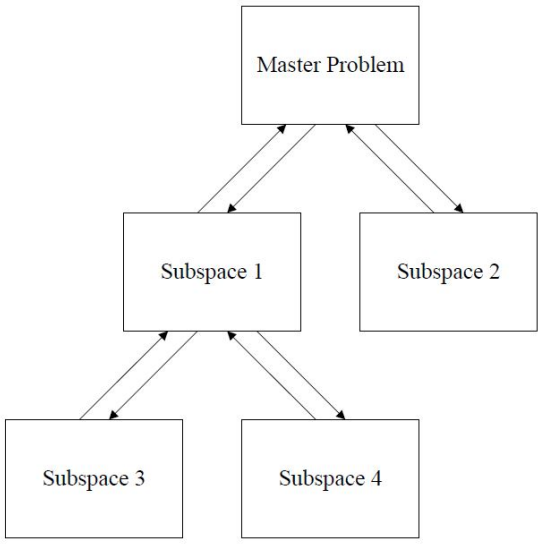

Figure 3-2: Illustration of a hierarchical system [5]

functions. In this case the automotive design would be decomposed into body, power-train and suspension subsystems [5]. Matrix partitioning is used with large systems of mathematical equations. As in an example of transportation of goods with given number of supply depots and their units of supply goods, the number of demand centres with their units of demand along with the cost of shipping between depots and centres [29]. Lastly the sequential partitioning is applied to flow processes, such as manufacturing or chemical processes, where a flow of current, mass, heat or even information is involved [30] [5]. This project utilizes aspect and object partitioning methods as the subproblems are constructed by separating them by disciplines and/or components.

According to Wagner and Papalambros a decomposition method for mathematical programming (MP), partitions the original problem variables and functions, and implements an appropriate coordination strategy. Even though the partition and coordination are distinct stages of the decomposition method they are dependent on each other. The coordination strategy commonly utilizes some attributes that usually allow partitioning, are outcome of partitioning or both. The fundamental idea behind the decomposition methods is to reformulate the original MP into a smaller set of problems that are solved independently while coordinated by a master problem (coordination strategy) [30]

System decomposition is characterized by the pathways of communication (coordination strategy) as well [5]. In this context two methods are defined: hierarchical and non-hierarchical. Hierarchical methods are named after the property that allows the subproblems to be solved individually in case the coordinating variables are fixed temporarily. This suggests a natural flow and hierarchy of information in the system [30]. While a hierarchical system will only allow communication between the parent and child, the non-hierarchical system will have no constraints on the coordination strategy. Figure 3-1 shows a non-hierarchical system with no restrictions on the flow of information whereas Figure 3-2 illustrates a hierarchical system where flow of information is restricted. In the light of these definitions, it can be commented that the system at hand is a hierarchical one. This can be observed by the consecutive flow

of energy from the rotor to the generator and also from the design process. Once the rotor design is accomplished one can deduct the torque applied on the drive train which will be used in the design of the gearbox, generator and other successive mechanical components. This shows a natural flow of information from top, the rotor, to the rest of the elements.

3-3-2 Engineering Design Requirements

The design process requirements are represented by three bodies: *i*) functions *ii*) constraints and *iii*) objective function. The functions express the objectives and duties of the system and its components. The constraints determine the boundaries of the applications. Therefore any design that is confined within the boundaries set by the constraints and executes the functions, is considered an adequate solution. However the degree of the predominance of the solution is determined by the objective function, which is a quantitative indication of the effectiveness of the design [31].

The core concepts and configurations of the RNA components are represented in Chapter 2. These demonstrate the overall function of the system and the sub-functions of each component, therefore the functions will not be discussed further in this chapter. However, due to the fact that the system at hand is composed of elements that work with mechanical, structural, electrical and magnetic principles, higher level constraints can be mentioned [31]:

- Under extreme and normal conditions the structures may not fail due to instability
- Fatigue damage accumulated over lifetime may not be a reason for structural failure
- During accidents the structures may fail with acceptable consequences
- Large deflections may not hinder the functionality of the components
- The interfaces between the components must be geometrically compatible
- During extreme and normal conditions the materials may not degrade
- The surrounding environment may not be disturbed above an acceptable level, that is defined by regulations
- Maintenance of the system should ensure the continuation of the functionalities of the system

The objective function of a Fully Integrated Optimization (FIO) architecture should administer a common goal for all the disciplines involved in the system [7]. The objective function should be able to weigh the advantages and the disadvantages of the disciplines involved. Thus for the design process of the RNA, reducing the production cost for unit electricity is considered as the objective function, which can be expressed as the Levelized Production Cost (LPC) [31]. The LPC is commonly used in the literature for displaying the feasibility of the electricity generating systems and is formulated as follows [32]:

$$LPC = \frac{\sum_{t=0}^{T_{life}} (C_t - R_t)(1+r)^{-t}}{\sum_{t=0}^{T_{life}} E_t(1+r)^{-t}} \tag{3-1}$$

where:

C_t = total costs for year t,

R_t = total revenues for year t such as subsidies,

E_t = total electricity production in year t,

T = economic life time,

r = real interest rate.

3-3-3 Partition of the Design Process

Generally the partition of an engineering design is obvious due to the various disciplines and/or components involved. However there may be decompositions that need physical interpretations that are not obvious. In these cases, especially for larger systems where the physical interactions are more detailed, a better and more advantageous way of analysing the system can be explored. Two hierarchical decomposition methods are identified: *i*) primal and *ii*) dual decomposition methods. Primal decomposition methods use structures where the linking among the subproblems happens through common variables. On the other hand the linking among the subproblems happens through common constraints in the dual decomposition methods [33]. A hierarchical primal decomposition synthesis is applied to the design optimization at hand. Because design variables such as rotor diameter or tip speed ratio change the design of the other components as well, the linking between the subproblems occurs through design variables rather than constraints.

In order to have a straightforward utilization of the model, short computational times are of vital importance. Therefore simple models with necessary accuracy are selected for the implementation of the tool. More detailed models have more design variables and need more computational times. As the scope of the project is to achieve a preliminary design optimization tool for the RNA, this approach is considered suitable [31]. The design variables and the constraints of the RNA are selected and elaborated qualitatively according to the chosen configurations (drive trains) that are given in chapter 2. In the analysis of a direct drive drive train the gearbox design variables and constraints are simply not included in the analysis.

Firstly the functional dependence table of the RNA has been constructed. This was done by forming a table with design variables as the columns and constraints as the rows. The design variables and constraints that were accounted for are illustrated in Figure 3-3. The dependency of each design variable upon the constraints is expressed by an " x ". The system design is defined by a number of design parameters and variables. A complex system is designed or optimized by determining the values for design variables that result in the best system response depending on some recognized criteria. Whereas the design parameters are fixed throughout the design process as the system inputs, the design variables can be changed by the designer [5]. Therefore the left side of Figure 3-3 is formed by the design parameters that are set up by the user inputs such as the wind site class and the rated power of the RNA. In most cases RNAs are designed to meet the requirements of a certain wind class and the rated power of the turbine is customarily decided by the portfolio managers, therefore these values are fixed in the real-world design processes and it will be the same for this project.

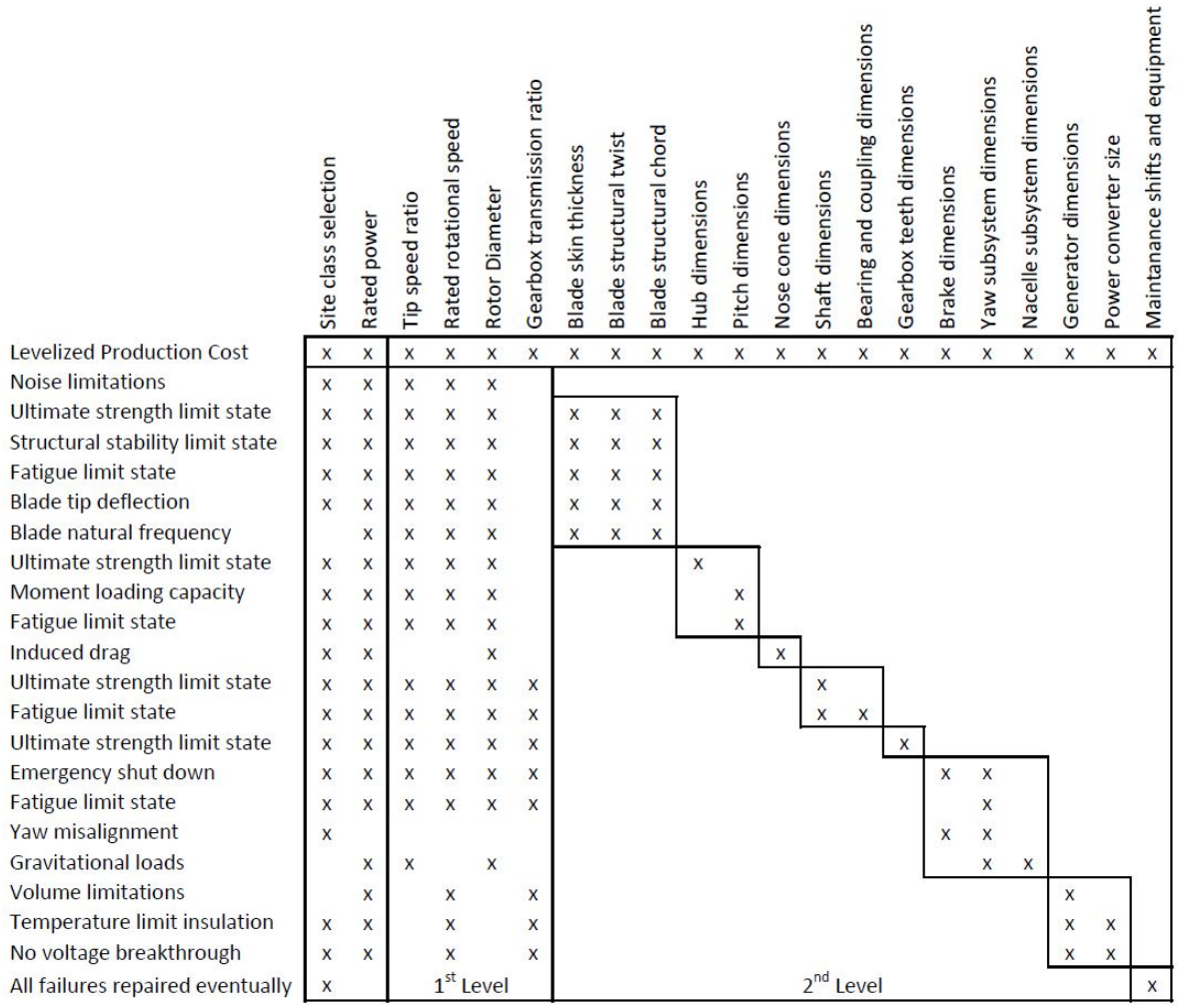

Figure 3-3: Overview of design variables and their appearance in the objective function and constraints

In order to cast the problem into a block angular structure as it is shown in Figure 3-3 the coordinating variables were identified. The selection of the coordinating variables separates the optimization process into two levels. The design variables that are present in the master problem are the coordinating variables and the ones that are in the subspaces are called local variables [30]. Separation of the tip speed ratio, rated rotational speed, rotor diameter and gearbox transmission ratio has allowed the partitioning of the system. This is due to the high level of dependency of the system on these variables. Thus the coordinating variables form the first level of master problem and the rest constitute the second level of subproblems.

The suitable structure for the synthesis has been achieved by identifying the connected components in the second level [33]. On the right hand side eight clusters can be observed along the diagonal of the matrix. These clusters are organizing the subspaces in the hierarchical system. The first cluster gather the design variables and the constraints of blades. The blade constitutes a group of its own due to its high number of constraints and local variables. On the other hand close physical and structural relations were observed for the following

combinations of components:

- Hub and pitch mechanism
- Shafts, bearings and couplings
- Brakes, yaw subsystem and nacelle subsystem
- Generator and power converter

The rest of the components along with the maintenance shifts and equipment have been selected to be singular component subspace. In this analysis two of the partitioning methods can be identified: *i*) aspect and *ii*) object. The aspect partitioning (by discipline) can be seen in the subspace of the generator and the power converter, where electrical system is distinguished from the rest. Whereas the object partitioning (by components or functions) can be observed in the rotor subspace where a single component constitutes a subproblem on its own.

3-3-4 Sequencing of the Design Process

Based on the formulation structure two types of distributed system optimization structures have been identified. The first one is the alternating approach where the optimization iterates between solving the master problem and the subproblems. The second one is the nested formulation and is generally named multi-level or bi-level programming problem. Nested methods are coordinated by a master program and for the evaluation of the master program, functions of all the subproblems should be solved previously [28].

The partition of the system in Section 3-3-3 has resulted in a multi-level optimization which indicates that the problem formulation is a nested one. This type of bi-level problem primarily is composed of a higher level master program with coordinating variables and an objective function to be minimized together with lower level subproblems with local variables that are eliminated from the higher level master problem. The optimization takes place by fixing the coordinating variables and solving for the lower level subproblems. Since the local constraints are separated, by fixing the coordinating variables the subproblems can be solved in parallel. This multilevel optimization is called nested because for each iteration of the master problem all of the subproblems have to be solved [28].

One source of difficulty in the nested formulations may be the higher number of equality constraints that is introduced to the master program than the number of coordinating variables. This could lead to failure in searching for a feasible solution to the problem. Also another issue is the convergence speed which depends on two factors. First is the cost of solving the subproblems and the second is the cost for restoring coupling by solving the master problem. The cost of restoring coupling is expected to be low in the following condition: When the number of linking variables in a nested formulation is lower than the number of the local variables. So the convergence speed of the formulation is faster [28]. Since the block angular structure revealed four linking variables with fifteen local variables, the condition mentioned above is not assumed to be an issue.

Chapter 4

Modelling the Rotor Nacelle Assembly

4-1 The Rotor

4-1-1 Introduction

This section includes the models that are chosen for the design of the rotor, the design variables, state variables (variables that are dependent on the design variables) and the constraints that are involved in the optimization of the rotor. The models are studied under two sections, namely aerodynamic and structural design relations of the rotor.

4-1-2 Aerodynamic Design Relations of the Rotor

Chord and Twist Distribution

First the chord and twist distributions of the rotor blade are determined. The analysis is conducted with the blade element momentum theory that combines the blade shape and performance. The assumptions that are presumed to reach an ideal blade shape, which is also called as the 'Betz optimum rotor', in the blade element momentum theory are:

- There is no drag; thus drag coefficient, $C_D = 0$.
- There is no wake rotation; thus $a' = 0$.
- The axial induction factor in each annular stream tube is; $a = 1/3$.
- There are no losses due to a finite number of blades (i.e. no tip loss)

Under the given assumptions the analysis results in the chord, c, and inflow angle, ϕ, distributions:

$$\phi = \tan^{-1}\left(\frac{2}{3\lambda_r}\right) \tag{4-1}$$

Table 4-1: Angle of attack and lift coefficient of aerofoils for maximum lift over drag ratio

Aerofoil Type	Angle of Attack $\alpha\,(^\circ)$	Lift Coefficient C_L
DU00W401	6.5	1.027
DU00W350	9	1.368
DU97W300	7.5	1.256
DU91W2250	4	0.952
DU93W210	3	0.888
NACA64618	4	0.898

$$c = \frac{8\pi r \sin\phi}{3BC_L\lambda_r} \tag{4-2}$$

where λ_r is the local tip speed ratio, B is the number of blades and C_L is the lift coefficient. First, the desired number of blades, B, a design tip speed ratio, λ, the rotor radius, R, and an aerofoil with known lift and drag coefficients depending on angle of attack have to be chosen [4]. The number of the blades is taken as three for all of the designs in this project. Furthermore it is important to note that the rotor radius and the tip speed ratio within the nested formulations of the model will be varied by the master problem but will be fixed for the subproblem, in this case the rotor subspace. Therefore they will be already determined for the rotor design to take place. The relation for the tip speed ratio, λ, and the local tip speed ratio, λ_r, are presented as follows:

$$\lambda = \frac{\Omega R}{U} \tag{4-3}$$

$$\lambda_r = \lambda\frac{r}{R} \tag{4-4}$$

where r is the radius of the section that is analysed and Ω is the rotational speed of the rotor. For each section of different aerofoils, the angle of attack that results in the lowest drag over lift ratio should be chosen. Therefore the approximation of no drag will be as close as possible. This project only considers fixed aerofoil types for selected stations of the blade. The aerofoil types and their corresponding lift coefficients and angle of attack values for the lowest drag over lift ratios are presented in table 4-1.

Since the inflow angle, ϕ, is composed of the twist, β, and the angle of attack, α, the twist distribution can be calculated as follows:

$$\beta = \tan^{-1}\left(\frac{2}{3\lambda_r}\right) - \alpha \tag{4-5}$$

The details of the analysis, can be seen in Wind Energy explained and Wind Energy Handbook [4] [25]. The aerofoil types which are linked to the optimum angle of attack and the spanwise locations of the segments of the blade are presented in the table 4-2, for the calculation of the chord and twist distributions. The segmentation of the blade is done for further analysis of the blade. The segments of the blades will be addressed by the stations of the blade that are illustrated in table 4-2. The station numbers, chord lengths and spanwise locations will be used in the approximation of the blade chord and twist distribution calculation that is explained next up. Only the chord lengths of stations 14, 15 and 7 till 11 and the blade mass

per unit lengths from stations 1 till 4 will not be utilized during the design. But the rest will be used in the calculation of the flapwise stiffness and the blade mass calculation that are explained in the following sections.

Table 4-2: Reference wind turbine properties [6]

Station	Aerofoil Type	Spanwise Location	Flapwise Stiffness EI_{ref} (Nm^2)	Chord (m)	Mass (kg/m)
1	Circular	0.045503	19096667700	3.542	767.8930729
2	Circular	0.088889	11232900000	3.854	607.2506
3	Elliptic	0.132275	5814818706	4.167	409.2246472
4	DU00W401	0.186508	4654550000	4.557	425.84595
5	DU00W350	0.251587	2541913500	4.652	352.32025
6	DU00W350	0.316667	2022325000	4.458	338.166875
7	DU97W300	0.381746	1549023500	4.249	320.56025
8	DU91W2250	0.4446825	1051399500	4.007	293.02085
9	DU91W2250	0.511905	640990500	3.748	260.5556
10	DU93W210	0.576984	378233000	3.502	234.8319
11	DU93W210	0.642063	215098750	3.256	192.459625
12	NACA64618	0.707143	118041250	3.01	160.553725
13	NACA64618	0.772222	83959250	2.764	134.4795
14	NACA64618	0.837302	54975750	2.518	102.8078
15	NACA64618	0.891535	37171177	2.313	86.8658251
16	NACA64618	0.934921	25448000	2.086	67.7688
17	NACA64618	0.978306	7887502	1.419	46.2576864

The ideal blade design is efficient but complex to build and therefore expensive [25]. Thus using the ideal blade shape as a guide, a blade shape that is a good approximation is constructed. This approach is applied to the chord and twist distributions of the blade. For the sake of helping the fabrication, a second order polynomial function is chosen for the chord calculation in certain regions [4]. In order to do this, the chord length at three sections of the blade will be calculated. Among the stations of the blade the thickest chord at station 6, and closest stations to 70 and 90% (station 13 and 16 respectively) of the blade will be computed [25]. Through these three points a quadratic function is fitted as a function of chord distribution between stations 6 and 16. It is important to note that the best fitting line should not increase the chord length in any position, because an increase in the chord length will increase the loads and lower the power extraction. Even though a decrease in the chord length also causes power loss it decreases the loads, therefore it is preferred.

The tip of the blade and the root sections are scaled from the reference turbine. The reference turbine is taken from the NREL study of "Definition of a 5-MW Reference Wind turbine for Offshore System Development". The properties of the reference wind turbine that will be used in this project are illustrated in table 4-2 [6]. For the blade root and tip, a linear scaling relation is used. This procedure involves stations from 1 till 5 and the last station. In the interest of matching the chord distributions at the transition regions between stations 5-6 and 16-17, calculated chord lengths and reference wind turbine values at stations 6 and 16 are used. A comparison between the reference turbine rotor chord length at station 6, and

the designed chord length at station 6 will reveal the scaling factor for the root section chord distribution. Likewise the scaling factor for the tip of the blade is revealed by the comparison of the chord lengths at station 16.

The same approach is also applied to the twist distribution of the blade. This time two stations are chosen to be computed. Through these points and the twist at the tip of the blade, which is assumed to be 0°, a quadratic function is fitted. In order to compute a function that resembles the ideal blade twist distribution, one point from the inner blade section (excluding the root) and one from the outer section needs to be chosen. The stations where the structural twist will be optimized are 5 and 12. Since the root is composed of circular and elliptic sections twist cannot be considered in this region, so the twist value of station 5 is given to these sections.

The stations at which the twist and chord lengths are calculated to fit the quadratic function to are selected to resemble the ideal blade shape as much as possible under the guidance of literature studies and manual attempts.

Rotor Power

The computation of the power coefficient for the rotor power calculation, is done with the tip speed ratio - power coefficient curve that is introduced in section 1 in figure 1-3. The curve fitting for the three bladed rotor has been done, to calculate the power coefficient, C_P, according to the given design tip speed ratio.

$$C_P = -0.00024615\lambda^5 + 0.0092121\lambda^4 - 0.13246\lambda^3 + 0.89168\lambda^2 - 2.6901\lambda + 3.0781 \quad (4\text{-}6)$$

As a result the aerodynamic power can be calculated with the following formula:

$$P = C_P \frac{1}{2} \rho_{air} \pi R^2 U^3 \quad (4\text{-}7)$$

The power delivered to the drive train by the rotor is calculated with equation 4-7. The formula is used from cut in wind speed to the rated wind speed and then the power is kept constant until the cut out speed. The cut in speed and cut out speed in this project is taken as 3 m/s and 25 m/s respectively, similar to the reference turbine [6]. Besides, the losses in the gearbox and the generator are also taken into account to arrive at the power output of the Rotor Nacelle Assembly (RNA).

4-1-3 Structural Design Relations of the Rotor

The loads associated with the torque and the thrust on the blades are among the most important rotor loads on a wind turbine. In order to examine the steady loads on a wind turbine, the rotor will be modelled as a simple rigid aerodynamically ideal rotor. The details of the analysis can be found in Wind Energy Explained by J. F. Manwell [4].

Root Thickness

The chord analysis determined the diameter of the root section, therefore with a stress analysis the root thickness is examined. Generally, aerodynamic edgewise moments are of less

significance than flapwise moments. Therefore this project will focus its load analysis on flapwise stresses. The root thickness will be investigated with the maximum flapwise stress at the root. The relationship is given by the following equation:

$$\sigma_{flp,\max} = \frac{M_{flp} x}{I_b} \tag{4-8}$$

where x is the distance from the flapwise neutral axis, M_{flp} is the flapwise bending moment at the root and I_b is the area moment of inertia of the blade cross-section at the root. For a hollow cylindrical cross section the area moment of inertia is shown below [4]:

$$I_x = I_y = I_b = \frac{\pi \left(d_o^4 - d_i^4\right)}{64} \tag{4-9}$$

where d_o is the outer diameter which is equal to the chord length at the root section and d_i is the inner diameter [4]. The following relationship applies for the outer diameter and inner diameter:

$$d_i = d_o - 2t \tag{4-10}$$

where t is the skin thickness. During the design load case defined for the root stress analysis in section 4-1-5, the thrust force is composed of the drag force over the blade. The drag force for each blade element, dF_D can be displayed as follows:

$$dF_D = \frac{1}{2}\rho C_D U^2 c dr \tag{4-11}$$

The drag coefficients are found from the aerofoil type data for each station with the determined twist distribution and the design load case conditions. Hence the flapwise moment for position r on the blade can be calculated as follows:

$$M_{flp}(r) = \int_r^R \frac{1}{2}\rho C_D U^2 c \left(r' - r\right) dr' \tag{4-12}$$

$$M_{flp}(r) = \frac{1}{2}\rho C_D U^2 c \left[\frac{R^2}{2} - rR + \frac{r^2}{2}\right] \tag{4-13}$$

As a result the flapwise moment can be calculated for any position on the blade. The position of interest, in this analysis is the root section, thus along with the chord, drag coefficient and radius values of root the maximum flapwise moment is calculated.

Blade Stiffness and Thickness

The blade stiffness and thickness will be analysed in relation with the tip deflection limit state. Since the flapwise moments relate to blade tip deflection limit state, the flapwise stiffness of the blades will be investigated. The stiffness distribution of the blade is computed from the reference turbine stiffness distribution. The stiffness values for each station of the reference turbine is represented in table 4-2. The values are interpolated from the reference turbine blade structural properties for the selected spanwise locations on the blade. The stiffness of the designed turbine will be calculated with the following scaling relation [34]:

$$EI = EI_{ref} \cdot f \cdot g^3 \tag{4-14}$$

where f is the skin thickness factor, which is the ratio of the skin thickness of the designed blade and the reference blade for all sections. g is the scaling factor of the chord distribution, which can be computed by the reference turbine chord lengths and the new chord lengths of the design. Finally, EI and EI_{ref} are the stiffness values of the new turbine and the reference turbine respectively. The EI_{ref} and the chord values for the reference turbine are shown in table 4-2.

Even though a blade can sustain greater deflection without being damaged, the blade should not strike the wind turbine tower in the most critical load case for the blade tip [35]. Thus, flapwise stiffness and moment is used to calculate the blade tip deflection, y which can be represented with the following formulation:

$$y = \int_0^R \left(\int_0^r \frac{M_{flp}(r')}{EI(r')} dr' \right) dr \tag{4-15}$$

Once again the tip deflection is calculated numerically with arrays of flapwise moment and blade flapwise stiffness. Due to the different design load cases that will be appointed to the tip deflection ultimate state in section 4-1-5, the flapwise moment is calculated slightly different than the root thickness analysis. The flapwise moment is calculated with the thrust coefficient, C_T. So the, flapwise moment, $M_{flp}(r')$, can be computed as follows:

$$M_{flp}(r') = \frac{1}{3} \int_r^R \frac{1}{2} \rho C_T U^2 2\pi \left(r'^2 - r r' \right) dr' \tag{4-16}$$

$$M_{flp}(r) = \frac{1}{6} C_T \rho U^2 2\pi \left[\frac{R^3}{3} - \frac{r R^2}{2} + \frac{r^3}{6} \right] \tag{4-17}$$

In order to be consistent with the previously made assumptions in the chord and twist analysis in section 4-1-2, where axial induction factor was assumed to be 1/3, the thrust coefficient is taken as 8/9. This also allows a more conservative approach for the tip deflection analysis than calculating the actual thrust coefficients for each station with inflow and twist angles, due to the fact that the thrust coefficient during operation is highest when the axial induction factor equals 1/3.

4-1-4 Design Variables of the Rotor

The design variables of the subsystem can be defined after modelling the rotor. These are:

- λ, tip speed ratio
- R, rotor radius
- t_{root}, blade root thickness
- f, skin thickness factor

The tip speed ratio, λ, and the rotor radius, R, are appearing in functions and constraints of the other components as well that is why they are the global design variables of the first level optimization as they were mentioned in section 3-3-3. These design variables are not presented once again in the design variables of other components. The rest of the design variables (blade root thickness and the skin thickness factor) only take part in the second level optimization of the rotor.

Table 4-3: GL partial safety factors for composite material [7]

Type of Safety Factor	Symbol	Value (-)
General material factor	γ_{M0}	1.35
Influence of ageing	C_{2a}	1.5
Temperature effect	C_{3a}	1.1
Hand layup laminate	C_{4a}	1.2
Post cured laminate	C_{5a}	1.1
Total		2.94

Table 4-4: Partial safety factors for ultimate load analysis [7]

Type of Safety Factor	IEC	GL
Loads	1.35	1.35
Blade consequence of failure	1	1
Tower consequence of failure	1	1
Materials	1.1	2.94
Total	1.485	3.969

4-1-5 Constraint Relations of the Rotor

Partial Safety Factors

This section introduces several partial safety factors that will be used to construct the constraint relations of the rotor. The partial safety factors are applied to materials, failure of different components and the uncertainties in the design process [7]. However, there are many standards that prescribe partial safety factors for achieving sound wind turbine systems. The standards that are taken into consideration in this project are the International Electrotechnical Commision (IEC) and Germanischer Lloyd (GL) [36] [7].

The material safety factors of the composites are prescribed in the GL standards and are presented in table 4-3. On the other hand the material partial safety factor of the IEC is much simpler and is shown in table 4-4.

As mentioned before, the load safety factor should include the load safety factor and the consequence of failures of other components. So all the partial safety factors for the ultimate load analysis for IEC and GL standards are shown in table 4-4.

For the maximum allowable flapwise stress in relation with the root thickness analysis in section 4-1-3, the GL safety factors are used due to their conservative nature. Thus resulting in a total safety factor of 3.969. Since the model that is constructed does not include fatigue analysis due to computational times, a conservative approach on ultimate load cases is taken into consideration. As the yield stress of the composite used in the blades is assumed to be 325 MPa, along with the chosen safety factor, the maximum allowable stress at the root becomes 82 MPa. This results in the following constraint [7]:

$$\sigma_{flp,\max} < 82MPa \tag{4-18}$$

The maximum elastic deflection of the blade in the tower direction should be investigated by taking into account the partial safety factors of loads, material and consequences of failure. However this time partial safety factor for the elastic properties of composite materials should be taken into consideration as the material safety factor. The IEC standards states that the partial safety factor for the elastic properties of composite materials should be taken as 1.1. Instead a more conservative value of 1.48 is chosen resulting in a total safety factor of 2 for the tip deflection of the blade analysis.

Definition of the Design Load Cases

The limit states of ultimate strength for the root thickness analysis and the blade tip deflection should be analysed with different types of design load cases. However, a dominating design load case is chosen for each ultimate state for the sake of simplicity and computational times.

The design load cases that are described in the IEC standards were checked for the chosen NREL reference wind turbine and it was found that the governing extreme load case was the extreme wind model (EWM) with a 50-year recurrence period while the turbine is in the parking condition [7]. Hence, this design load case is applied to the root thickness analysis. The chosen design load case suggests that the flapwise moment should be calculated with the 50 year extreme wind speed. The wind velocity that has a 50-year recurrence period is defined for each wind class that is studied in this project, in section 4-4-3 and will be used for the calculation of the maximum flapwise stress of the root section. Moreover, since the wind turbine is in parked condition, the angle of attack for the drag coefficient should be found by adding up the twist distribution and the yaw misalignment, 15°, that is defined for the design load case.

The tip deflection should be analysed when the thrust force reaches its maximum value during operation. Therefore for the tip deflection limit state, the design load case is chosen as power production with the rated wind speed of the wind turbine. Furthermore, during the power production at the rated wind speed the stiffness of the blade in the out of plane direction is less than it would be in pitched idling position. Thus during the design load case for the blade tip deflection, the blade is more likely to hit the tower.

Blade Tip Deflection

To finalize the tip deflection limit state and form a constraint for the analysis, the maximum allowable tip deflection should be calculated. This distance is dependent on the blade and tower properties. The tower diameter at height of the tip, overhang, blade's tilt angle, cone angle and pre-bending defines the maximum allowable tip deflection of the blade. The values for the reference wind turbine are shown in table 4-5.

The allowable tip deflection is calculated by scaling and recalculation of distances by given properties. The tower diameter at the hub height is scaled with the relative hub height of the new turbine to the reference turbine hub height. Hub height calculation is detailed in section 4-4-1. The overhang is scaled with the rotor radius. The cone, and tilt angle are assumed to be the same for all of the designs, but the distances created due to these angles change with different values of rotor radius. It is important to note that the tilt angle is defined as the angle between the horizontal axis and the rotor shaft and the cone angle is between the rotor

Table 4-5: The properties for maximum allowable blade tip deflection calculation

Parameter	Value
Tower diameter at height of tip (m)	5.4
Overhang (m)	5
Tilt angle ($^\circ$)	5
Cone angle ($^\circ$)	2.5
Pre-bending	-

plane and the blade axis [37]. Thus the first one is related to the rotor radius, whereas the latter is related to the blade length. As a result the allowable tip deflection is scaled with the designed wind turbine. Accordingly it can be set as an upper limit to the blade tip deflection calculated in section 4-1-3, by taking into account the selected partial safety factors in this section.

Root Skin Thickness

The last constraint was formed in order to achieve consistency between the two structural design analyses conducted in the model. The skin thickness that is calculated for the root section from the maximum flapwise stress analysis and the skin thickness factor from the blade tip deflection analysis should correspond to the same root thickness. This is achieved with the following equality constraint:

$$t_{root} = t_{root\_ref} \cdot f \tag{4-19}$$

where t_{root_ref} is the reference turbine root skin thickness and equals to 10.3 cm.

4-2 The Gearbox

4-2-1 Introduction

The drive trains that are taken into consideration in this project will involve one stage and three stage gearboxes. The three stage gearbox is assumed to have first two stages as epicyclic arrangement and the last one as parallel shaft arrangement [25]. The single-stage gearbox will be a planetary configuration as it is commonly done in wind turbine gearboxes due to its compact and lightweight properties as it was mentioned in section 2-3-5 [10] [38]. In this section two types of teeth in relation with the chosen stages will be introduced: *i*) spur teeth and *ii*) helical teeth. Parallel shaft arrangements are assumed to have helical teeth and the planetary configuration spur teeth. The pressure angles of all designed gears and the helix angle of the helical gears are chosen to be 20° for the design of the gearbox [25].

4-2-2 Geometrical Design Relations of Gearbox

Even though there are many variables that can be computed in a complete gear analysis, for the simplicity of the model only the relevant parameters to the stress calculations that will be

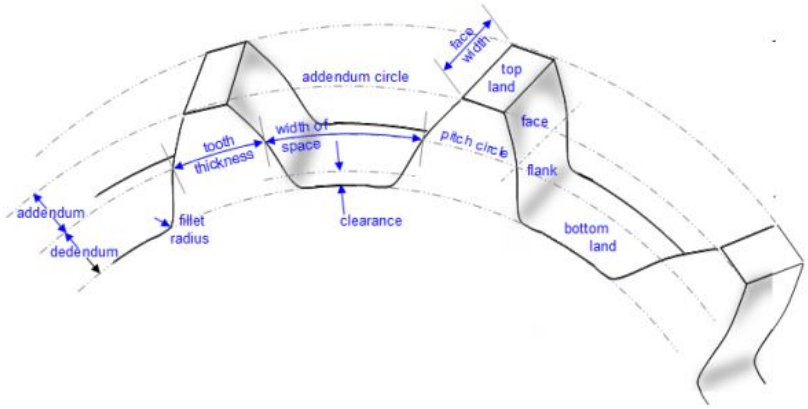

Figure 4-1: A gear schematic showing the major dimensions

analysed in the forthcoming sections are introduced. Figure 4-1 represents a spur gear with some additional geometrical dimensions.

One of the most fundamental geometrical relationship of a pinion and gear pair in a parallel stage is the gear ratio, u. The transmission ratio is the ratio of the gear and pinion diameters.

$$u = \frac{d_g}{d_{pinion}} \tag{4-20}$$

Furthermore the gear ratio applies to the relationship between the numbers of teeth, rotational speeds and torque for the pinion and the gear.

$$u = \frac{z_g}{z_p} = \frac{n_p}{n_g} = \frac{T_g}{T_p} \tag{4-21}$$

where, z ,n and T are the number of teeth, rotational speed and torque respectively for pinion and gears. The formulation takes a different form in case of planetary systems. The relationship between the sun, planets and the ring teeth numbers can be expressed as follows [39]:

$$u = 1 + \frac{z_{ring}}{z_{sun}} = 2\left(1 + \frac{z_{planet}}{z_{sun}}\right) \tag{4-22}$$

From equation 4-22 the following relationship between the teeth numbers of the gears can be computed for a planetary stage:

$$z_{planet} = \frac{z_{ring} - z_{sun}}{2} \tag{4-23}$$

The pitch is the distance between the same point on two consecutive teeth and it is defined as [9]:

$$p = \frac{\pi d}{z} \tag{4-24}$$

where d is the pitch diameter and z is the number of teeth. Another dimensional characteristic of a gear is the module, m. This value essentially is the pitch diameter divided by the number of teeth.

$$m = \frac{d}{z} \tag{4-25}$$

4-2-3 Structural Design Relations of the Gearbox

This section contains two analyses concerning the structural design of gearbox stages: *i*) bending stress and *ii*) surface fatigue. These two analyses are detailed for the selected teeth shapes and gears of the project.

Bending Stress

Firstly a bending stress analysis will be conducted. Bending stresses in a gear pair, mostly affect the base of the tooth. Therefore a gear tooth bending stress analysis will be applied. This is done by the Lewis stress formula, which allows the designer to calculate the bending stresses of spur and helical gears. It is acknowledged that this analysis does not take into consideration some of the factors that are taken into account in modern gear design procedures. Such examples are contact ratio, CR, degree of shock loading, accuracy and rigidity of mounting etc.. However, it was assumed to be satisfactory for a preliminary design process, which is the scope of this project. The Lewis equation for the bending stress is [9]:

$$\sigma_b = \frac{F_t}{bpY} \tag{4-26}$$

where b is the tooth width and is measured along the helix angle for helical gears and across the pitch line for spur gears. p is the circular pitch, F_t is the tangential force on the teeth and Y is the Lewis form factor. The Lewis form factor can be calculated for full depth and stub teeth gears with different pressure angles.The formulation of the Lewis form factor for full depth teeth with 20° pressure angle is as follows [40]:

$$Y = 0.154 - \frac{0.912}{z} \tag{4-27}$$

where z is the number of teeth in the gear. The tangential force, F_t, for helical and spur gears is generally calculated as follows [8].

$$F_t = 0.98 \cdot 10^6 \frac{P_p}{n_p r_p} \tag{4-28}$$

where P_p is the power in kW, n_p is the angular velocity in $\min^{-1}$ and r_p is the pitch radius in mm [8]. Further bending fatigue analysis that includes many newly introduced factors should be done in order to make the proper stress calculations. However in this project another approach will be adopted. A conservative safety factor will be used when the yield stress of the gear is compared with the calculated bending stresses. The yield stress of the steel is taken as 250 MPa [41]. During emergency breakdown the mechanical brake on the high-speed shaft decelerates the rotor from an over-speed to a standstill . In order to do this, the brake applies a torque about three times the rated torque. Therefore considering the above mentioned condition, the total safety factor was chosen to be 5. This factor includes the effect of the increasing torque during emergency breakdowns and the difference between the Lewis equation for bending stresses and the modern gear design procedures. It is applied in the comparison between the yield stress and the calculated bending stress.

While constructing the engineering model, it was observed that the bending stress for the smallest gear in each stage is the greatest. The reason behind it is that the lower number of

teeth in the pinion and sun lowers the Lewis form factor, which results in greater bending stress. Furthermore, the tangential force and the pitch is the same for a gear pair in contact, thus doesn't have an altering consequence. The effect of the teeth number can be further observed in equations 4-26 and 4-27. So the bending stress analysis is applied only to the suns and pinion of the stages.

Surface Fatigue

The second analysis regarding the gearbox design is the surface fatigue analysis. For helical gears at the pitch surface the sliding velocity is zero. Due to this effect the oil film gets squeezed out and surface pitting occurs. The surface fatigue stress for spur gears is calculated as follows [9]:

$$\sigma_c = C_p \sqrt{\frac{F_t}{bdI} K_v K_o K_m} \tag{4-29}$$

The surface fatigue stress for the helical gears is done by making a slight modification on the spur tooth analysis. For instance the helical gears have slightly lower sensitivity to mounting conditions, therefore 0.93 is placed in front of the mounting factor, K_m. The calculation can be made as follows [9]:

$$\sigma_c = C_p \sqrt{\frac{F_t}{bdI} \left(\frac{\cos \psi}{0.95 CR} \right) K_v K_o \left(0.93 K_m \right)} \tag{4-30}$$

where C_p is a term that relates the elastic properties of the materials into a single factor, and is defined as [9]:

$$C_p = 0.564 \sqrt{\frac{1}{\frac{1-\nu_p^2}{E_p} + \frac{1-\nu_g^2}{E_g}}} \tag{4-31}$$

where, E_p and E_g are the Young's modulus of the pinion and the gear material respectively. The modulus of elasticity or the Young's modulus of the steel is 207 GPa. ν_p and ν_g are the Poisson ratios of the materials and it is taken as 0.3 for steel [40]. Therefore C_p has the value of 191 $\sqrt{MPa}$ for all the designs. I is the geometry factor and can be calculated as follows [9]:

$$I = \frac{\sin \varphi \cos \varphi}{2} \frac{u}{u+1} \tag{4-32}$$

where φ is the pressure angle. Back in the equation 4-30, ψ is the helix angle and CR is the contact ratio. CR is the average number of teeth in contact while the gears are rotating. It is necessary that the tooth profiles are proportioned so that a second pair of teeth come into contact before the first pair leave each other [9]. The study shows that increasing contact ratios in low-contact ratio gears reduced the gear dynamic load. Therefore this project assumes a high contact ratio of 2 in this analysis [42].

K_v is the velocity factor and for high precision, shaved and ground gears can be calculated as follows [9]:

$$K_v = \sqrt{\frac{78 + \sqrt{V_p}}{78}} \tag{4-33}$$

where V_p is the pitch line velocity in ft/min and is the same for the pinion and the gear.

Table 4-6: Overload Correction Factor K_o [8] [9]

	Driven Machinery			
Source of Power	Uniform	Light Shock	Moderate Shock	Heavy Shock
Uniform	1	1.25	1.5	1.75
Light Shock	1.1	1.35	1.6	1.85
Moderate Shock	1.25	1.5	1.75	2
Heavy Shock	1.5	1.75	2	$\geq$2.25

Table 4-7: Mounting Correction Factor K_m [9]

	Face Width (in.)			
Characteristics of Support	0 to 2	6	9	16 up
Accurate mountings, small bearing clearances, minimum deflection, precision gears	1.3	1.4	1.5	1.8
Less rigid mountings, less accurate gears, contact across the full face	1.6	1.7	1.8	2.2
Accuracy and mounting such that less than full face contact exists	Over 2.2			

K_o is the overload correction factor and its value depends on the working characteristics of the driving machine and of the driven machine. For the system at hand the driving machine is the rotor of the wind turbine and if it is classified as turbines with high starting torque according to the tables provided in G. Henriot's book, it has light shocks characteristics. The driven machine is the generator and it is classified as uniform. More detailed classification of driving and driven machines can be found in G. Henriot's book [8]. According to the classifications of the machinery, the overload correction factor is taken as 1.1 These correction factors depending on application are introduced in table 4-6.

K_m is the mounting factor, that reflects the accuracy of mating gear alignment. This factor gets values according to the characteristics of support and face width [9]. Most gearbox failures do not begin as gear failures, they initiate in bearing locations due to the lack of information on the gearbox system loads. Unpredicted bearing behaviour beyond the bearing mounting location such as housing deformations is contributing to the gearbox failures faced in the wind turbines [43]. The mounting correction factor depending on the characteristics of support and the face width is given in table 4-7. Considering the situation, a support characteristics with less rigid mountings, less accurate gears and contact across the full face is taken into consideration. The mounting correction factor below 2 *in* face width is taken as 1.3 and above 16 *in* is taken as 2.2. However for the safety factors between these values, the following calculation is formulated according to the tooth width, b:

$$K_m = 0.002b^2 + 0.0075b + 1.579 \tag{4-34}$$

Ultimately, the surface fatigue stress, σ_c, should be compared to the surface fatigue strength, S_H, which is given by the following equation:

$$S_H = S_{fe} C_{Li} C_R \tag{4-35}$$

where S_{fe} is the surface fatigue strength of the steel, which is 9171 MPa for a hardness of 330 Bhn. C_{Li} is the life factor and for 10^7 cycles this value equals to 1. However throughout the lifetime of the turbine the cycle numbers can reach values above 10^9. Therefore a value of 0.65 is taken for this factor. The last one, C_R is the reliability factor and for 99.9% reliability it equals to 0.8. Thus the gear-tooth surface fatigue strength has a constant value of 4769 MPa. While the comparison is made between the surface fatigue strength and the stress a conservative value of 3 is taken as a safety factor, due to the fact that emergency brakes could increase the applied torque three times on the gearbox [9]. This value is placed in the equation 4-30 as a coefficient in front of the tangential force, F_t while the surface fatigue stress is calculated.

Once again the construction of the engineering model revealed that the greatest surface fatigue stress is observed in the smallest gear in each stage. The reason behind it is the smaller diameters of the pinion and the sun. Since all the rest of the coefficients are the same for all of the gears in a certain stage, as it can be seen from equations 4-29 and 4-30, smaller diameters result in greater surface fatigue stress. Thus the surface fatigue analysis is only applied to the sun and pinion of the gearbox stages.

4-2-4 Design Variables of the Gearbox

The design variables can be defined after modelling of the gearbox. These are:

- u_2, transmission ratio of stage 2
- u_3, transmission ratio of stage 3
- d_{pinion}, pinion diameter
- d_{sun1}, sun diameter of stage 1
- d_{sun2}, sun diameter of stage 2
- b_{pinion}, pinion tooth width
- b_{sun1}, sun tooth width of stage 1
- b_{sun2}, sun tooth width of stage 2

The design variables that are defined above are for a three stage gearbox design. In case of a single stage gearbox the design variables related to the second and third stages drop out. The design variables that are defined take part in the second level optimizations of the three and single stage gearboxes. The overall transmission ratios are shaped by the first level optimization where the tip speed ratio and rotor radius is decided. According to these values the rated rotational speed of the rotor is computed in the rotor optimizer in the second level. Since the generator rated rotational speeds are kept constant, as it will be explained in section 4-3-2, the transmission ratios of the gearboxes are dictated by the first level optimizer. Therefore the transmission ratio of the first stage does not appear as a design variable in the second level gearbox optimizations.

4-2-5 Constraint Relations of the Gearbox

The constraints are formed from knowledge based engineering relations and the structural design analyses. The first constraint that is included for the gearbox optimization is about the width of the gears. The face width is not standardized, but generally it is between the values given below [9].

$$9m < b < 14m \tag{4-36}$$

The limit of gear ratios per stage depends on the type of gear that is used. For the epicyclic gear configurations this value can go up to 15 and for the parallel gears this value can be up to 5 [39] [10].

The minimum tooth number is set to 21, due to the fact that it prevents the excessive undercut of the tooth for facilitating finishing operations and results in designs that are more resistant to surface fatigue [44].

The final two constrains are coming from the bending stress and surface fatigue analyses. The details of the analyses are presented in 4-2-3. The resulting constraints are:

$$YS_{gear} > 5\sigma_b \tag{4-37}$$

$$S_H > \sigma_c \tag{4-38}$$

where YS_{gear} is the yield stress of the gear.

4-3 The Generator

4-3-1 Structural Design Relations of the Generator

The size of the generator is correlated to the developed torque. The air gap force density is assumed to be a constant value for a wide range of machine powers. The force density is the force per square meter of active air gap surface area. The values that correspond to conventional generators used in the wind turbines are [12] [45]:

$$F_d = 25 - 60kN/m^2 \tag{4-39}$$

The force density of a generator is considered constant because it is the product of two limited phenomena. The first is the air gap flux density, which is limited due to the magnetic saturation of the material (the state reached when the magnetization of a material cannot increase further with and increasing external magnetic field). The second one is the current loading, which is limited by the power dissipation as heat. The force density can be increased by the utilization of forced liquid cooling however not without reducing the efficiency of the generator [12] [45]. The air gap force density varies depending on the type of rotating electrical machine. The air gap force density for the Doubly Fed Induction Generator (DFIG) is assumed to be 30 kN/m^2, for the permanent magnet generator with the single stage gearbox it is assumed to be 50 kN/m^2 and finally for the permanent magnet generator in the direct drive drive train it is 60 kN/m^2 [46]. By using the force density the power generated by the machine can be given as [12] [45]:

$$P = \Omega_{gen} T_{rated} = 2\Omega_{gen} \pi r_g^2 l_g F_d \tag{4-40}$$

where Ω_{gen} is the angular rotational speed of the generator, r_g is the stator bore radius and l_g is the axial stator stack length. With the introduced dimensions, the volume of the generator rotor, V_g, can be calculated [12] [45]:

$$V_g = \pi r_g^2 l_g = \frac{P}{2\Omega_{gen} F_d} \tag{4-41}$$

4-3-2 Design Variables of the Generator

In order to lower the design variables included in the generator models the generator rotational speeds of the DFIG is assumed to be 1200 rpm and for the permanent magnet generator with the single stage gearbox it is assumed to be 100 rpm in accordance with the NREL studies, where the drive trains were selected from [44] [47]. This fixes the volume of the generator for the two mentioned generators. For the direct drive it is partially the same, because the rotational speed of the generator is not fixed but is dictated by the first level optimization. Hence, in all of the cases the free design variable that can be defined is the:

- r_g, generator radius

The calculation of the generator radius and the length is conducted with an optimizer in the second level.

4-4 Relevant Rotor Nacelle Assembly Relations

4-4-1 Hub Height

The cost model for the tower, that is presented in appendix A, depends on the hub height of the wind turbine. Therefore a hub height formulation for the design is introduced. Two different hub height calculations are introduced for onshore and offshore applications in this project.

The hub height in offshore applications is composed of two parts, rotor radius and the clearance. The clearance usually takes a value between 5 and 8 m. This project assumes 8 m of clearance from the blade tips at the lowest point of their rotation to the platform (interface level). Thus the hub height, H_{hub}, can be calculated as follows [48]:

$$H_{hub} = \Delta z_{clearence} + \frac{1}{2} D \tag{4-42}$$

where $\Delta z_{clearence}$ is the clearance height and D is the rotor diameter. On the other hand the hub height for the onshore applications is taken the same as the rotor diameter:

$$H_{hub} = D \tag{4-43}$$

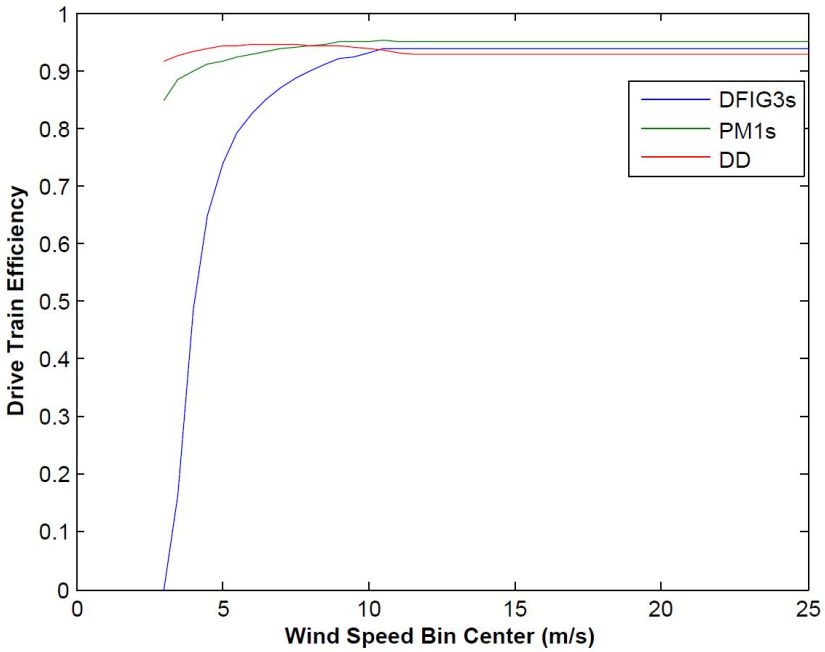

Figure 4-2: Drive train efficiencies

4-4-2 Power Curve

In order to calculate the energy yield of the wind turbine, the total power curve of the drive train needs to be found. The aerodynamic power curve is already constructed in section 4-1-2, henceforth the losses in the drive train need to be computed.

The losses of drive trains are taken from the NREL WindPACT Alternative Design study report [44]. This study provided a table of wind velocities versus drive train efficiency for different types of drive trains. The type of drive trains taken from the study are a baseline drive train with three stage gearbox and a DFIG (DFIG3s), a single permanent magnet drive train with one stage gearbox with a permanent magnet generator (PM1s) and a direct drive drive train with no gearbox and a permanent magnet generator (DD). The efficiency plots of above mentioned drive trains are illustrated in figure 4-2.

The drive train efficiencies that are given in figure 4-2 are refitted for different values of rated wind speed that is dictated by the master problem. The efficiency values from 3 m/s to 11.5 m/s wind velocities are stretched or contracted according to the relative position of the new rated wind speed to the reference turbine rated wind speed (11.5 m/s). Once the efficiency values are matched with the new wind speeds, interpolation reveals the efficiency values for the old wind speeds. This procedure is necessary to match the wind speeds and the corresponding arrays to result in the annual energy yield.

In order to reach the final power curve the rotor power curve is multiplied by the efficiency of the corresponding drive train configuration. The rated power in this curve should correspond to the input parameter given by the user.

Table 4-8: Classes according to IEC 61400-1

	Offshore	Coastal	Inland
Class	1	2	3
Average wind speed at hub height [m/s]	10	8.5	7.5
50 years wind speed (10 minute mean at hub height) [m/s]	50	42.5	37.5
Turbulence Intensity class	C	B	A
Reference value at 15 m/s	$I_{15} = 0.12$	$I_{15} = 0.14$	$I_{15} = 0.16$
Wind speed distribution	Weibull $k = 2$ (Rayleigh)		
Wind shear exponent	0.2		
Air density $[kg/m^3]$	1.225		

4-4-3 Energy yield

In order to calculate the energy yield first the wind turbine class of the design should be known. The wind turbine class is an input to the model by the users. The wind turbine classes are identified in IEC 61400-1 standards according to the wind speed and turbulence parameters. In this project three types of wind turbine classes will be studied. The wind sites that are investigated are offshore, coastal and inland [49]. The specifications of the wind classes are shown in table 4-8. The turbulence intensities are not linked with the classes directly, so one can also study classes of 1A or 3B. A, B and C are designating high, medium and lower turbulence characteristics respectively.

The values given in table 4-8 allow for the probability density function of the wind speed distribution to be calculated. The distribution of wind speeds over an extended period of time is calculated with a Weibull function with shape parameter, k, of 2. This specific function of Weibull distribution is called as the Rayleigh function and can be calculated as follows:

$$P_R = \frac{k}{a}\left(\frac{U}{a}\right)^{k-1} e^{\left(-\left(\frac{U}{a}\right)^k\right)} \tag{4-44}$$

where k is the shape or form parameter and a is the scale parameter. a is calculated with the gamma function and the annual average wind speed at hub height, V_{ave}.

$$a = \frac{V_{ave}}{\Gamma\left(1 + \frac{1}{k}\right)} \tag{4-45}$$

The result of the gamma function is known, since the shape parameter is taken as to be 2. The gamma function for 1.5 equals 0.886. V_{ave} is the annual average wind speed at the hub height and is defined in IEC 61400-1 as follows [36]:

$$V_{ave} = 0.2V_{50} \tag{4-46}$$

where V_{50} is the 50 years wind speed at hub height, and is defined by the wind turbine class.

The energy yield is calculated by the combination of the power curve, wind speed probability density function and the availability of the wind farm. The availability of a wind farm depends on whether or not the site is onshore or offshore. The wind farm annual availability is taken

as 85.4% from the data provided from UK wind farms, Scorby sands, Kentish Flats and North Hoyle. On the other hand the annual availability for onshore wind farms is taken as 98% [50]. Hence, the annual energy production can be calculated as:

$$E_t = \eta_{availability} \int_{V_{cut\_in}}^{V_{cut\_out}} P(V) P_R(V)\, dV \tag{4-47}$$

4-5 Mass and Cost Models of the Rotor Nacelle Assembly

4-5-1 Introduction

Most of the mass and cost models of the project are taken from the NREL study of "Wind turbine design cost and scaling model". The details of the study are in appendix A. This section introduces the mass and cost models that are different from the NREL study. In order to be consistent with the cost models in the NREL study, which are based on 2002 US dollars, the currency was set the same and attention was paid to base the new cost models on a year close to 2002.

4-5-2 Mass and Cost models of the Blade

The blade consists of the root section, two spar caps, shear webs between them and skin that externally surrounds the shear webs and spar caps. The major contribution to the blade weight is coming from the root section, which is generally one third of the length of the blade but constitutes half of the mass of the blade [35]. The mass of the blade is calculated by computing the mass of the root section and the rest separately. The composite that is used in the blade is assumed to be fibreglass reinforced plastic (GRP), which is one of the most common materials in wind turbine blade. The density of the blade material is assumed to be 1400 kg/m^3 [51]. The circular and elliptic aerofoils are assumed to be circular and the mass of the root section can be calculated as follows for station 1 till 4 ($i = 2, 3, 4$):

$$M_{blade1} = \sum_{i=2}^{4} \rho_{blade} \pi \left(\frac{c_i^2 - (c_i - 2t_i)^2}{4}\right) \left[\left(\frac{r}{R}\right)_i - \left(\frac{r}{R}\right)_{i-1}\right] R \tag{4-48}$$

where c is the chord therefore the diameter for the root section, ρ is the GRP density, t is the root thickness of the section and $\left(\frac{r}{R}\right)_i$ is the dimensionless spanwise location. The rest of the stations are scaled from the reference wind turbine. The rest of the mass distribution, M_{blade2}, can be computed as follows [34]:

$$M_{blade2}(r) = M_{old}(r) f \cdot g \tag{4-49}$$

where f is the thickness factor and g is the scaling factor for the chord distribution. How to get these values has been elaborated in section 4-1-3. The mass per unit length values for each station, M_{blade2_i} is represented in table 4-2. Each section is multiplied with its length and the mass is computed as follows:

$$M_{blade2} = \sum_{i=5}^{17} M_{blade2_i} \left[\left(\frac{r}{R}\right)_i - \left(\frac{r}{R}\right)_{i-1}\right] R \tag{4-50}$$

It should be noted that during calculations the last station of the blade was considered to extend from the previous station until the end of the blade. Hence the total mass of the blade can be calculated by adding up the mass values calculated for the root and the rest of the blade sections.

$$M_{blade} = M_{blade1} + M_{blade2} \tag{4-51}$$

The blade price calculation depends on the mass of the blade therefore the effect of the design variables used in the blade design such as rotor radius or root section thickness is reflected in the objective function. The blade price, C_{blade} is given as [7]:

$$C_{blade} = 13.084 M_{blade} - 4452.2 \tag{4-52}$$

Once the cost and mass models of the blade is determined the objective function for the second level optimization of the rotor can be selected. Here the contribution of the rotor design in the second level to the objective function should be taken into consideration. Since during the rotor optimization the tip speed ratio and the rotor radius is already fixed by the first level optimizer the contribution of the rotor design to the objective function becomes the cost of the blade. Since the cost of the blade depends on the mass of the blade, the objective function of the rotor optimization in the second level is selected as the mass of the blade.

4-5-3 Mass and Cost models of the Gearbox

There are two types of gearbox configuration that are focused on this project. One is the single stage planetary gearbox and the other is the three stage gearbox with first two stages of planetary configuration and a helical parallel shaft configuration for the last. The mass of the gearbox is determined by the diameter and the width of the gears. The mass of a planetary stage is defined by the mass of the ring wheel, the planets and the sun gears. If the number of planets is taken as 3 the resulting gear mass of the planetary stage becomes:

$$M_{planetary} = 3M_{planet} + M_{sun} + M_{ring} \tag{4-53}$$

For a parallel stage the mass of the gears are composed of the pinion and the gear mass. The gear mass of parallel stage is:

$$M_{parallel} = M_{pinion} + M_{gear} \tag{4-54}$$

The mass of sun, gear pinion and planets are computed in the same way. The diameter and thickness of each gear are taken into account with a factor k_1.

$$M_{planet} = M_{ring} = M_{sun} = M_{pinion} = M_{gear} = k_1 \rho_{steel} \frac{\pi d^2}{4} b \tag{4-55}$$

k_1 is a factor that takes into account the fact that gears are not produced as perfect cylinders. Generally the mass is reduced by removing material from the design. Thus the factor reduces the mass of gears by 50% in three stage gearboxes and 70% in single stage gearboxes. The mass of the ring wheel, M_{ring}, is calculated in the same way but with a different factor, since inside of the ring wheel is empty. The factor k_1 reduces the mass by 90% for the ring wheel in three stage gearboxes and 93% in the single stage gearboxes. DIN 20MnCr5 steel is chosen

as the material of the gears and it has a density, ρ_{steel}, of 7810 kg/m^3. The total mass of the three stage gearbox can be found as follows:

$$M_{gbx\_3s} = k_2(M_{planetary1} + M_{planetary2} + M_{parallel}) \tag{4-56}$$

where k_2 is a factor that takes into account the mass of the bearings, casing and the shafts within the gearbox. After a consideration of available wind turbine gearbox examples this value was selected as 1.2. Further investigation of these values has been done during the implementation of the model. The mass of the single stage gearbox with planetary stage can be computed as follows:

$$M_{gbx\_1s} = k_3 M_{planetary} \tag{4-57}$$

where k_3 just like the previous factor takes into account the additional masses. In a single stage gearbox the shafts are the low speed and the high speed shaft. These component mass and cost values are calculated separately. Therefore the factor k_3 takes into account the bearings, casing and the planet carrier in the element. Due to the compact nature of the planetary stages k_3 is taken as 1.15. The cost of a single stage gearbox is estimated by the specific cost of the gearbox, which is 6 $Euro/kg$ [10]:

$$C_{gbx\_1s} = 6M_{gbx\_1s} \tag{4-58}$$

The final cost of the three stage gearbox is calculated with the specific cost of 10 $Euro/kg$ [52].

$$C_{gbx\_3s} = 10M_{gbx\_3s} \tag{4-59}$$

Once again the objective function of the second level gearbox optimization is selected as the mass of the gearbox. Because the overall transmission ratio of the gearbox is determined by the first level optimizer and the contribution of the gearbox design to the first level objective function is the cost of the gearbox. Besides the cost of the gearbox directly depends on the mass of the gearbox.

4-5-4 Mass and Cost models of the Generator

The mass and cost models of the generator have been constructed by altering them from the NREL study of wind turbine design cost and scaling model. The cost and mass models represented by the NREL study depend on the rated power of the wind turbine. However in order to scale the generator properties with the high speed shaft torque, which is a more relevant quantity for the generator scaling, generator rotational speeds of 1200 rpm, 100 rpm and 20 rpm were considered for the three-stage high speed generator, single-stage drive with medium speed permanent magnet generator and direct drive drive train with permanent magnet generator respectively. Since the data for the drive train designs were extracted from the WindPACT drive train studies for the NREL Wind turbine design and cost model, the rotational speeds were appointed according to the drive train specifications given in the WindPACT alternative drive train design study reports [44] [47]. The mass model of the direct drive drive train permanent magnet generator is taken as it is in the NREL study, because it depends on the low speed shaft torque. The high speed shaft torque, T_{hss}, can be formulated with the design variables proposed in section 4-3-1 as follows:

$$T_{hss} = 2\pi r_g^2 l_g F_d \tag{4-60}$$

Thus the generator cost and mass models for different types of drive trains that are taken into consideration in this project can be formulated as follows:

Three-Stage High-Speed Generator

$$M_{gen\_3s} = 6.47\Big(100\pi^2 r_g^2 l_g F_d\Big)^{0.9223} \tag{4-61}$$

$$C_{gen\_3s} = 65\left(100\pi^2 r_g^2 l_g F_d\right) \tag{4-62}$$

Single-Stage Drive with Medium-Speed, Permanent-Magnet Generator

$$M_{gen\_1s} = 10.51\left(\frac{20\pi^2 r_g^2 l_g F_d}{3}\right)^{0.9223} \tag{4-63}$$

$$C_{gen\_1s} = 54.73\left(\frac{20\pi^2 r_g^2 l_g F_d}{3}\right) \tag{4-64}$$

Direct Drive

$$M_{gen\_dd} = 661.25\Big(2\pi r_g^2 l_g F_d\Big)^{0.606} \tag{4-65}$$

$$C_{gen\_dd} = 219.33\left(\frac{4\pi^2 r_g^2 l_g F_d}{3}\right) \tag{4-66}$$

Finally the objective function of the generator is selected as the mass of the gearbox since the mass and the cost models are all dependent on the volume and any selection among the two makes no distinction. This way the contribution of the second level generator optimizer to the first level objective function can be captured.

4-5-5 Decommissioning Cost

The NREL study of "Wind Turbine Design Cost and Scaling Model" provides a decommissioning cost for the offshore installations under the name Surety Bond. It does not introduce a decommissioning cost for onshore installations. Furthermore the decommissioning costs are assumed to be covered with the initial capital cost (ICC), which is not in line with the assumptions made in section 4-5-6. Thus a new model is implemented for the decommissioning costs that occur after a wind turbine reaches its life time.

The works of Kaiser and Snyder suggest that the decommissioning costs of an offshore wind farm is between 5 to 10% of the ICC [53]. So this project assumes the decommissioning costs to be 10% of the ICC. Likewise, the same approach is applied to the onshore installations as well. It was assumed that using a fixed percentage of the ICC will reflect the difference between the decommissioning costs of onshore and offshore applications through the distinct cost elements used in the ICCs for each wind site.

4-5-6 Levelized Production Cost

The levelized production cost was introduced in section 3-3-2. Several assumptions are made. Total cost for year 0 is composed of the ICC. From year 1 till year 20 total cost for a year is the annual operating expenses (AOE) and is constant. The decommissioning cost, C_{Decom}, is assumed to be covered in the year of shut down. The total electricity production of each year, E_t, that is presented in section 4-4-3 is assumed to be constant [31]. For these assumptions the levelized production costs can be determined from:

$$LPC = \frac{ICC}{aE_t} + \frac{AOE}{E_t} + \frac{C_{Decom}(1+r)^{-T}}{aE_t} \tag{4-67}$$

where a is the annuity factor and can be calculated as [31]:

$$a = \sum_{t=1}^{T} (1+r)^{-t} = \frac{1}{r}\left[1 - \left(\frac{1}{1+r}\right)^{T}\right] \tag{4-68}$$

Additionally, r is the real interest rate and it depends on two factors: *i*) annual interest rate on debts, i, and *ii*) annual inflation rate, v. Therefore the real interest rate changes according to the bank that is used for loans and the country. However it is a common practice to utilize 5% as the real interest rate. If not, the real interest rate can be calculated with the known values of annual interest rate on depths and annual inflation rate [54]:

$$1 + r = \frac{1+i}{1+v} \tag{4-69}$$

Finally this project assumes economic lifetime of a wind turbine is 20 years. For further information on how the cost of the components are calculated and for the detailed explanation of the ICC and AOE the reader is directed to appendix A.

4-6 Incorporating the Engineering Design tools

4-6-1 Introduction

This section introduces the adjustments that were made in order to combine the offshore wind farm design emulation of Dr. M.B. Zaaijer and the automatic Design of the RNA tool, that is developed in this project. The wind farm design emulation requires site conditions, size of the wind farm and the RNA properties as input [31]. The RNA design tool can provide the necessary properties for the integration. Therefore few extra calculations are included in the tool that allow the connection of the mentioned algorithms.

4-6-2 RNA Mass Eccentricity

The mass eccentricity calculation of the RNA is implemented in the tool because it is one of the inputs of the offshore wind farm emulation [31]. The mass eccentricity of the RNA is calculated by scaling the assumed eccentricities for the rotor and the nacelle. The given

eccentricities are -6.05 and 1 meter respectively. They are scaled linearly with the rotor radius of the new design. Thus the eccentricity can be calculated as follows:

$$d_{ecc} = \frac{M_{rotor}\frac{R_{new}}{R_{ref}}6.05 + M_{nacelle}\frac{R_{new}}{R_{ref}}}{M_{rotor} + M_{nacelle}} \tag{4-70}$$

where M_{rotor} includes the mass of the blades, hub, spinner, nose cone, pitch mechanisms and the bearings. $M_{nacelle}$ includes the rest of the components enclosed in the nacelle .

4-6-3 RNA Purchase Price

The RNA purchase price is calculated with the component costs models of the RNA. All of the costs of the RNA components are added together to find the RNA purchase price. This is an input that is utilized in the offshore wind farm emulation [31]. For the offshore wind sites this cost also includes the marinization costs.

4-6-4 Thrust

The last of the adjustments made in order to integrate the automatic RNA design tool to wind farm design emulation is the calculation of the thrust curve, maximal operational thrust and corresponding wind speed.

The thrust curve is computed as an array by finding the axial induction factor from the power coefficient of the wind turbine, with the following formula:

$$C_P = 4a(1-a)^2 \tag{4-71}$$

and calculating the thrust coefficient, and replacing it in the thrust formula for each wind speed. The thrust coefficient and the thrust is calculated with the given formulae:

$$C_T = 4a(1-a) \tag{4-72}$$

$$T = \frac{1}{2}\rho_{air}C_T\pi R^2U^2 \tag{4-73}$$

Finally the maximum operational thrust and its corresponding wind speed are found from the same array.

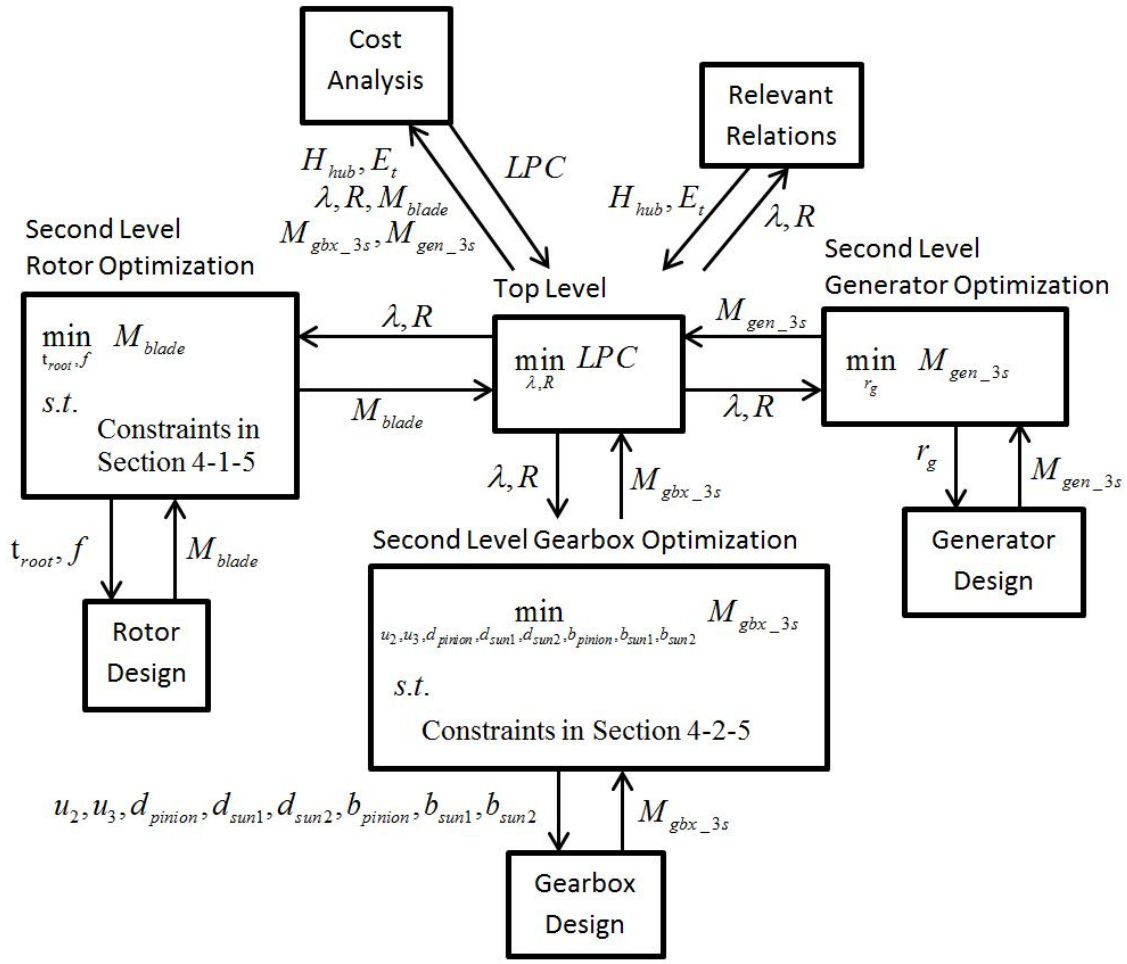

Figure 4-3: Multilevel structure of the optimization problem and the data flow between the nested optimizers

4-7 Mathematical Formulation of the Rotor Nacelle Assembly Optimization

This section provides the mathematical formulation of the optimization problem and gives the overall view visually. Figure 4-3 shows the flowchart of the multilevel optimization strategy. As an example, the optimization of the three stage gearbox with DFIG drive train is selected. In figure 4-3 the general formulation of each optimization are given with the design variables and the state variables that are introduced in this chapter. The objective functions of each optimization are minimized. The constraints that the optimizations are subject to are represented. For the formulation of the constraints the reader is directed to the relevant sections in this chapter. First and second level optimizations are identified and the data flow between the optimizers and the modules are shown. As it can be seen from the figure 4-3 the global design variables are controlled by the first level optimizer and the local design variables flow from the second level optimizers to the component design modules (rotor, gearbox,

generator). The mass of each component are fed to the first level for the calculation and evaluation of the levelized production cost. Further details on the objective functions, design variables and the data flow with respect to implementation of the RNA design tool are given in the next chapter.

Chapter 5

Implementation of the Automatic Design of Rotor Nacelle Assembly (RNA) Model

5-1 Overview

As the programming language for the implementation of the engineering model, Python was selected. Spyder has been utilized as the scientific Python development environment with the OpenMDAO framework. This section gives brief information about the tools that were utilized during the implementation of the engineering model and explains in detail the structure and layout of the RNA design emulation that is developed.

5-2 Python

Python is a commonly used, general-purpose, high level programming language and its syntax allows the users to express concepts in fewer lines of code than it would be in other languages [55]. The philosophy that lies at the heart of Python's design is listed in the work of Tim Peters, "The Zen of Python". The list includes adages such as [56]:

- Beautiful is better than ugly
- Explicit is better than implicit
- Simple is better than complex
- Complex is better than complicated
- Readability counts
- In the face of ambiguity, refuse the temptation to guess
- Now is better than never

Even though, the philosophy behind the programming language is absolutely attractive, further inspection among the programming languages has been done. The RNA design tool has similar software development, requirement and characteristics to the wind farm design emulation that is developed in the Ph.D. thesis of Dr. M.B. Zaaijer "Great Expectations for Offshore Wind Turbines". Therefore the evaluation of several programming languages against a list of criteria done in the thesis, is taken into consideration. Weights and scores for each criterion have been set to identify the best high level programming language for the offshore wind farm design emulation. The criteria that were considered essential were [31]:

- power and expressiveness
- ease of using the language
- ease of learning the language
- availability of compiler or interpreter (within the organisation)
- availability of third-party libraries
- efficiency (speed)
- quality of available tools
- possibilities for learning the language (tutorials, documentation, user-groups, etc)

As a result of this analysis Python scored the highest. Python was considered easy to learn and use, with an extensive library and active user-groups along with other advantages [31]. Considering all, the implementation of the tool was proceeded with Python.

5-3 Spyder

The scientific Python development environment that is adopted in this project is Spyder. Spyder has a MATLAB-like PYTHONPATH management dialogue box that works with all consoles. This was one of the key features of Spyder that resulted in the decision of its utilization, due to the previous experiences of the author in MATLAB. Furthermore, since Spyder is developed specifically for the Python language it also contains direct links to documentation such as Python, Matplotlib, NumPy, Scipy, etc., which were frequently used to utilize constants, built in functions and data structures. The numerical computing environment is created with the support of IPython, which is an enhanced interactive Python interpreter, and Python libraries. These libraries are NumPy for linear algebra, SciPy for signal and image processing and matplotlib for interactive 2D/3D plotting [57].

5-4 OpenMDAO

OpenMDAO is an open-source Multidisciplinary Design Analysis and Optimization (MDAO) framework, written in Python. It is built to develop design environments and integrated analysis for the engineering challenges. Essentially openMDAO is a software that links other pieces of software together. It provides the necessary means to combine design codes (analysis tools) from a variety of disciplines, at multiple levels and enables the user to manage the

interaction between them. The aim of the openMDAO software is to manage the actual data (the dataflow) and the arrangement of workflow in conjunction with the advanced solution techniques such as optimization algorithms. In addition, openMDAO has extensive built in optimization capabilities, which were extremely useful during the implementation of the engineering model [58].

OpenMDAO separates the dataflow from the workflow, by using four specific constructs, which makes it extremely flexible. The constructs that are utilized are: *i*) Component, *ii*) Assembly, *iii*) Driver and *iv*) Workflow. A component class instance preforms calculations to return the outputs according to the given input variables. An assembly instance is a container object, which confines within one or more child components. Furthermore, it defines the input and output data connections between the child components. These data connections determine the orientation of the data flow between the components. By default all assemblies contain one or more driver. The driver class controls the iteration process and contains a single workflow. The order of execution of child components involved in the assemblies, is dictated by the workflow. The drivers conduct the iteration by following the workflow, until a prescribed stopping condition is met. Thus, nesting a driver inside a workflow of another creates an iteration hierarchy, where multilevel optimization processes can be facilitated [59].

In this project two types of drivers are used. One simply runs the child components or assemblies in consecutive order as it is dictated by the workflow, and the other (optimizer) conducts an optimization procedure. The standard library of openMDAO includes several optimizers: *i*) COBYLAdriver, *ii*) CONMINdriver, *iii*) Genetic *iv*) NEWSUMTdriver and *v*) SLSQPdriver [58].

COBYLAdriver is a gradient-free optimizer that conducts a constrained optimization, only with inequality constraints, by linear approximation of the objective and constraint functions via linear interpolation [58].

CONMINdriver works with inequality constraints and implements the method of feasible directions to solve the non-linear programming problem [58].

Geneticis a gradient-free optimizer that works without constraints. It is based on PyEvolve, which is the general genetic algorithm framework written in Python [58] [60].

NEWSUMTdriver works with inequality constraints and utilizes Newton's method of sequence of unconstrained minimizations [58].

SLSQPdriver can work with both equality and inequality constraints and utilizes the sequential least squares programming [58].

The above mentioned optimizers that are available in the openMDAO library were tested for each of the optimizations that were operated. Their performance was compared to each other depending on their computational times and accuracy and precision of respective optimization results. As a result SLSQPdriver was selected for the second level optimizations and COBYLAdriver was selected for the first level optimization.

5-5 Structure and Layout

5-5-1 Overview

The engineering design tool is composed of three bi-level optimizations. For each drive train that is included in this project a two level optimization is conducted. The multi-level optimization of each drive train runs independently in an ordered fashion. Separation of each drive train optimization process, allows the users to evaluate and compare different type of drive trains used in wind turbines for a specified rated power and wind site. The iteration hierarchy overview of the engineering model can be seen in figure 5-1.

The blue boxes in figure 5-1 represent the components and the tan coloured boxes, with other components or drivers within, represent the assemblies. The purple boxes that are situated on the left top corner of each assembly are drivers.

5-5-2 Driver

The driver simply drives the components and the assemblies, in the order they are established in the workflow of the driver. The interface and the three selected drive train designs are executed and the results are displayed.

5-5-3 Interface

This component enables the user to provide input to the engineering model. In order to run the engineering tool, the user needs to select the rated power of the wind turbine that will be designed and the wind site where it will be utilized. These two selections are passed down to the rest of the assemblies for the design of each component.

5-5-4 Drive Train 0

Drive Train 0 represents the drive train with three stage gearbox and a Doubly Fed Induction Generator (DFIG). It is composed of four assemblies including itself and three components. The iteration hierarchy of the bi-level optimization that is taking place in the Drive Train 0 assembly is represented in figure 5-1. It involves the rotor, three stage gearbox and DFIG optimization assemblies along with Constraints, Relevant relations and Cost components.

Bi-level optimization of the first drive train can be observed from figure 5-1, as the purple box Drive train 0 is an optimizer (COBYLAdriver) and three more optimizers (rotor, gearbox and generator) are nested within it. The design variables for the master problem in the first level optimization are selected to be rotor radius and tip speed ratio, after the decomposition of the design process. The objective function is chosen to be the levelized production cost calculated in the Cost component. For each iteration within the nested formulations, the design variables are decided by the master problem and passed through to the second level assemblies (rotor, gearbox and generator optimizers).

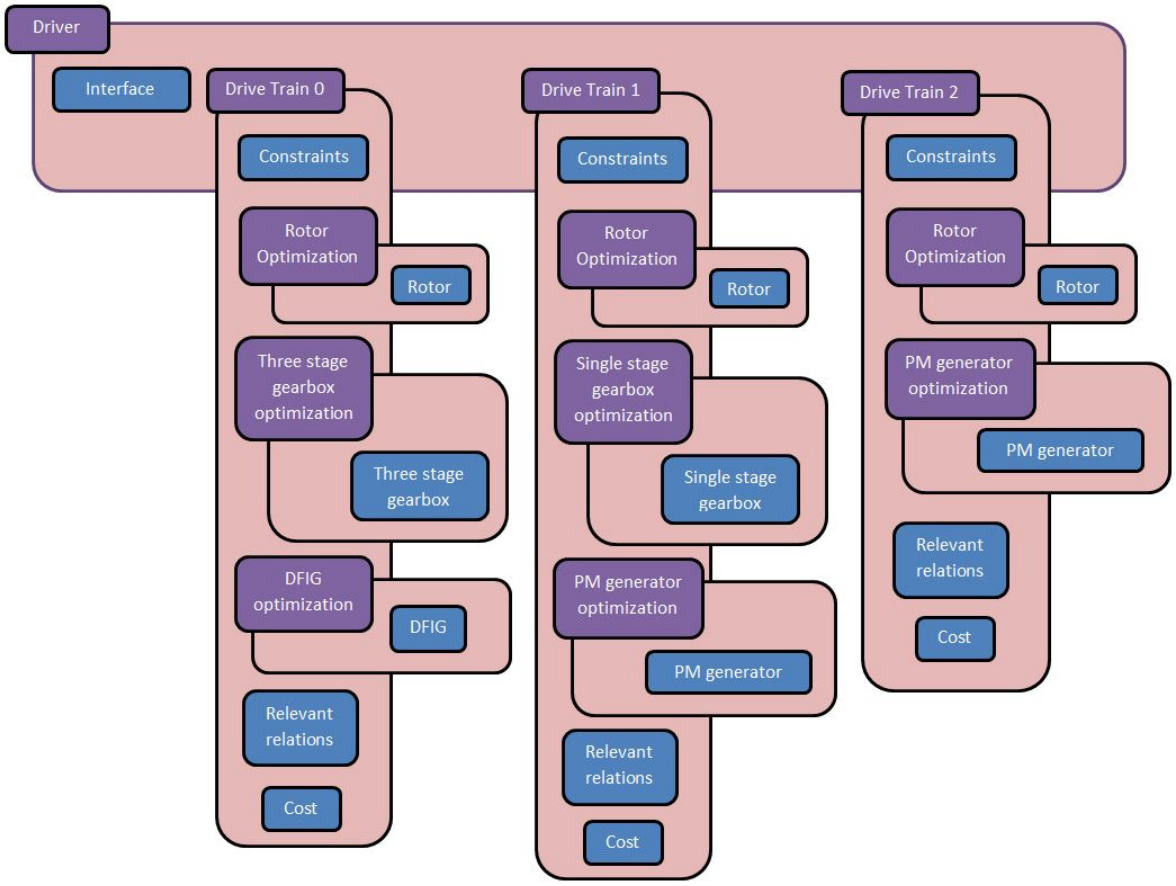

Figure 5-1: Iteration hierarchy of the multilevel optimization process

Ultimately, one of the most important aspects of the assembly is to connect the design variables and the state variables that are used in various components or assemblies. For example the annual energy production that is calculated in component Relevant relations, which is also used in Cost component.

Constraints

This component involves the calculation of certain constraints that change with the design variables. For example the maximum allowable blade tip deflection changes with varying rotor radius and hub height. Thus Constraints component was implemented in order to keep the design updated for each iteration. Evidently, the calculated constraints are passed through to the relevant optimizers in the second level.

Rotor Optimization

Rotor optimization assembly is composed of an optimizer (SLSQPdriver) and a component, Rotor. The design variables of this optimization are the root thickness and the skin thickness factor of the blade. Since the rotor radius and the tip speed ratio is selected to be global

design variables for the master problem, the rest of the design variables included in section 4-1-4 are used as local design variables in the second level optimization. On the other hand, the objective function of the optimization is selected as the mass of a rotor blade as it was pointed out in section 4-5-2. Finally, the rotor component includes the models introduced in section 4-1 for each iteration during the optimization.

Three Stage Gearbox Optimization

Three stage gearbox optimization is also composed of an optimizer (SLSQPdriver) and a component, Three stage gearbox. The design variables included in this optimization and the models used are presented in section 4-2-4. The objective function is selected as the mass of the element as it is in the rotor optimization, which was stated in section 4-5-3. Lastly, the Three stage gearbox component includes the models introduced in section 4-2 for each iteration during the optimization.

DFIG Optimization

This is the last assembly included in the workflow of Drive Train 0. It is also an optimization assembly with a component (DFIG) that includes the models introduced in section 4-3 for a DFIG. Ultimately the objective function of the DFIG Optimization is selected to be the mass of the generator, as it is given in section 4-5-4.

Relevant Relations

Relevant Relations is a simple component that calculates the state variables, such as the hub height or the net annual energy production (AEP). The models included in this component are presented in section 4-4.

Cost

Last of the components is the Cost, and it includes the cost models that are introduced in section 4-5 and appendix A. Above all, the most important function of the Cost component is to calculate the Levelized Production Cost (LPC) that is evaluated in the first level optimization.

5-5-5 Drive Train 1

The Drive Train 1 assembly represents the optimization process for the drive train with single stage gearbox and permanent magnet generator. There are few changes to the model compared to Drive Train 0 assembly as it can be seen from the iteration hierarchy of the Drive Train 1 in figure 5-1. Instead of three stage gearbox optimization and DFIG optimizations there are single stage gearbox optimization and Permanent magnet generator optimization. The rest of the properties of this assembly, its child components and nested assemblies are the same.

5-5-6 Drive Train 2

Drive Train 2 assembly illustrates the final drive train included in this project, the direct drive drive train. The iteration hierarchy with the assemblies and components included for Drive Train 2 is shown at the right hand side of figure 5-1. Noticeably a gearbox optimizer does not exist in this assembly. Moreover, the generator optimization is replaced by a component containing engineering models for a permanent magnet generator in a direct drive configuration. As it was stated for the Drive Train 1 assembly the rest of the properties of Drive Train 2 assembly are equivalent to those used in Drive Train 0 assembly.

Chapter 6

Appraisal of the Automatic Design of Rotor Nacelle Assembly (RNA) Tool

6-1 Overview

In this chapter the assessment of the RNA design tool will be done under three categories. First a comparison of the designs in different rated powers to given wind turbine design examples will be done. Second the responses of the wind turbine properties to different inputs will be investigated and finally performance of the RNA design tool will be analysed.

6-2 Emulation of the Designs

6-2-1 Overview

In this section the design results at different rated powers will be compared to wind turbine examples. Initially 5 MW NREL turbine will be compared to a design of the tool. Secondly 3 MW NREL cost analysis will be compared to the results of the design algorithm. Then for the larger scales of RNA designs, a comparison will be made to designs by the integrated aeroservoelastic design tool of Turaj Ashuri. After completing the system level comparisons a more detailed comparison for the main components with other examples from the literature and industry will be done.

6-2-2 Comparison to 5 MW NREL Offshore Wind Turbine

5 MW NREL wind turbine is widely used in both offshore and onshore wind energy research studies. A comparison between this study and the optimized design by the tool will prove the reasonableness of the new design. The NREL wind turbine has a multiple stage gearbox with high speed generator. Thus the design results of the drive train 0 are used for the comparison.

Table 6-1: Rotor properties of the 5 MW wind turbine design with drive train 0 in wind site class 1

Property	Optimized	NREL
Rotor radius	69.204 m	63.0 m
Tip speed ratio	6.218	7.55
Aerodynamic power coefficient	0.465	0.482
Tip deflection of the blade	6.082 m	5.0 m
Skin thickness factor of the blade	0.372	1
Rated wind speed	10.757 m/s	11.4 m/s
Rated rotational speed of the rotor	9.229 rpm	12.1 rpm

The general properties of the rotor designs are shown in table 6-1. First thing that draws attention is the larger rotor radius of the optimized design. The reasons behind this difference are difficult to investigate, however in an overall perspective larger rotor radius results in greater loads that increase the sizes of the consecutive components but on the other hand results in greater annual energy yield in below rated wind speeds. Nevertheless both of the designs are done in a way that will result in 5 MW power output at rated power, thus the size of the rotor radius becomes less consequential in above rated wind speeds for the annual energy yield. The concluding effect of the rotor radius can be seen in the objective function of the optimization.

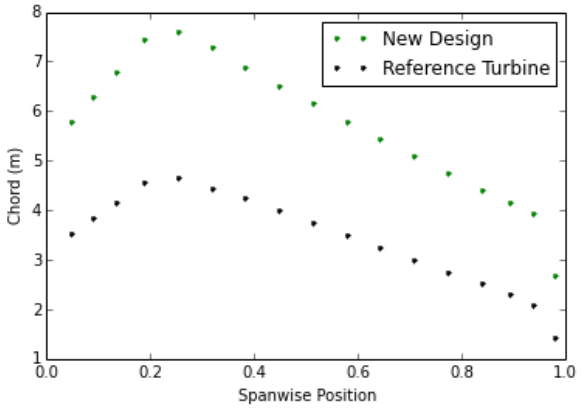

Figure 6-1: Chord distributions for 5 MW wind turbine design for offshore RNA with drive train 0 and NREL reference wind turbine

A consequence of having a larger rotor radius is the increase in the maximum tip deflection, that can be seen in table 6-1. One of the most important aspects of the tool that reflects on all of the designs emulated by the tool is the blade structural design. The blade tip deflection is the main driver of the rotor design in the tool. The emulation matches the tip deflection constraint on the highest possible value. Blade stiffness plays a major role in determining the blade tip deflection. In order to match the constraint, the stiffness is increased by increasing the chord and the skin thickness. Since the chord scaling factor has a significant influence on the stiffness, the tool increases the chord within the upper boundary set by the Betz optimum rotor. In order to do this, the tool lowers the tip speed ratio, but on the other hand the power

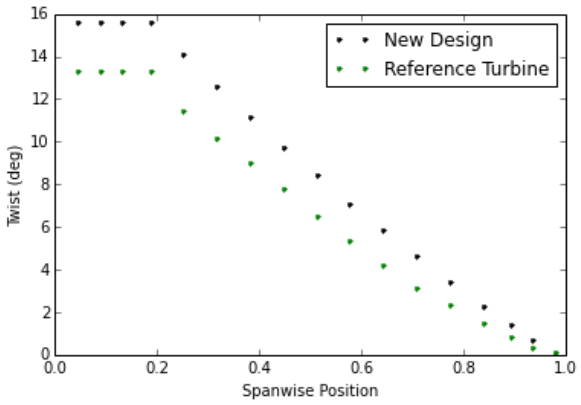

Figure 6-2: Twist distributions for 5 MW wind turbine design for offshore RNA with drive train 0 and NREL reference wind turbine

coefficient is lowered leading to larger rotor radius. Hence the tool finds the optimum value for the tip speed ratio taking into account both of the situations. The optimal solution has a slightly lower power coefficient, which indicates that an optimal solution to each component is not necessarily the optimum for the whole system. Moreover this type of blade design also generates blades that are lighter than realized designs. Higher chords allow the tool to lower the skin thickness factor significantly, without compromising stiffness, and lead to thinner, wider but more lightweight designs. The chord distribution of the reference turbine and the optimized design can be seen visually in figure 6-1.

Table 6-2: Mass properties of the optimized design and 5 MW NREL wind turbine

	Optimized	NREL
Blade Mass (kg)	16935	17740
Hub Mass (kg)	41925	56780
Rotor Mass (kg)	104714	110000
Nacelle Mass (kg)	157186	240000

The twist distributions of the designs are quite similar, the new design being slightly higher. Both of the designs have twist distributions very close to the Betz optimum rotor of their respective tip speed ratios. Since the same aerofoils in the same spanwise locations are used for both of the designs, the difference between the twist distributions is solely due to the difference in the tip speed ratios. Thus a comparison between the tip speed ratios will reveal the difference in the twist distributions. The NREL turbine has a tip speed ratio of 7.55 at peak power coefficient whereas the optimized design has 6.218 for it. So the twist distribution of the optimized design is expected to be higher than the NREL design. The comparison between the twist distributions can be seen in figure 6-2.

Lower tip speed ratio, resulting in lower power coefficient, and larger rotor radius of the optimized wind turbine results in lower rated wind speed and rated rotational speed of the rotor. This eventually has a burdening consequence on the gearbox design, as it increases the gear ratio of the gearbox and the torque. Consequently, this increases the size and the cost

of the gearbox. The optimizer finds an optimum solution, with lower rated rotational speed of the rotor and lower rated wind speed, that results in the lowest cost and highest energy yield of the wind turbine bearing in mind all of the constrictions. This resulted in a gearbox ratio of 130 whereas it is 97 for the NREL wind turbine.

The comparison of the component masses are illustrated in table 6-2. As it was mentioned previously, the optimized design results in lightweight blades, which are almost 1000 kg less than the NREL design even though the rotor radius is larger. The hub mass and cost is dependent on the mass of the blade. It was observed that the mass of the hub is significantly less than the NREL example as it was expected due to the lightweight blade in the optimized design. Lighter blade and hub mass results in a lighter rotor mass in the optimized design.

Nacelle mass is expected to be higher in the optimized design because of the higher rotor radius, however the opposite is seen. Firstly the nacelle mass of the NREL wind turbine is taken from the 5 MW REpower wind turbine. Secondly a difference can be seen in the gearbox designs, where the last stage of the gearbox in REpower wind turbine is a double helical spur gear stage instead of a helical parallel shaft stage. As a result it is seen that the nacelle masses are calculated differently due to modelling of this project and a slight change in the gearbox designs. Besides, further investigation reveals that even the rest of the components were lighter in weight, because the difference in nacelle masses is not only composed of the difference in the rotor radii. Even though most of the mass modelling of the components is done with the NREL mass models, a comparison to another NREL study (Definition of a 5-MW Reference Wind Turbine for Offshore System Development) results in different values.

The levelized production cost of the 5 MW NREL turbine is calculated with the cost component of the tool, therefore same cost models are applied with the given details of the wind turbine in the study. The energy yield of the NREL turbine was computed with the same drive train efficiency used in this project for the offshore wind site class with the given rated wind speed and the power coefficient. The resulting levelized production cost of the reference turbine is 0.0692 USD/kWh. On the other hand, the optimized design resulted in a levelized production cost of 0.0667 USD/kWh.

Overall, the RNA design tool generated a lighter design than the NREL wind turbine example with respect to the components that were discussed above. This is questionable since essentially a larger rotor radius should generate bigger and heavier components in the drive train. However the lack of data about the specific components in the NREL wind turbine makes it difficult to investigate further the differences. Differences in the designs result in relatively smaller difference in the levelized production costs. The tools design is 3.7% cheaper than the given example. This shows that the the NREL example can be further optimized to lower its levelized production cost.

6-2-3 Comparison to 3 MW NREL Offshore Wind Turbine Mass and Cost Analysis

In order to address the quality of the design results, design for a different rated power is checked. This will give insight in the reasonableness of the designs in a variety of rated powers. Thus, the tool is run for an offshore 3 MW wind turbine, in which the cost results

are compared to the output examples of the turbine provided by the NREL study of "Wind Turbine Design Cost and Scaling Model" [14].

The NREL example is a cost estimate summary for a shallow water offshore 3 MW wind turbine in 2005 USD. The basic drive train topology of the wind turbine is designed around a three stage gearbox with planetary and helical stages and generator with 1800 rpm nominal rotational speed [61]. Therefore the comparison is made with the drive train 0 design results. The example of NREL has a rotor radius of 45 m and hub height of 80 m. These are the only properties given other than the mass and cost details. The cost and mass results of the tools design and the NREL example are shown in table 6-3. It is important to acknowledge that the cost calculations are based on two different years, which suggests that the NREL example costs were escalated with Producer Price Indexes to compensate the fluctuations in the prices over the years.

Firstly the rotor radii are compared and it was observed that the rotor radius of the optimized design is 23% larger than the NREL example. The rotor radius of the optimized design is 55.5 m and the NREL design is 45 m, as it was stated before. Since this is one of the coordinating variables of the master problem it eventually affects most of the outcomes. The effect of the rotor radii to the component costs, net annual energy production (AEP) and gearbox design is detailed later in this section.

Noticeably the cost models that are a function of the rated power produce higher component cost for the NREL example due to the cost escalation mentioned above. These components are mechanical brake, high speed coupling with associated components, variable speed electronics, electrical connections, hydraulic and cooling system, offshore support structure, offshore transportation, port and staging equipment, offshore turbine installation, offshore electrical interface and connection, offshore permits, engineering and site assessment, scour protection and offshore levelized replacement cost. Likewise the fixed costs such as control, safety system, and condition monitoring and personnel access equipment are also higher for the NREL example due to the same reason. The only exception is the nacelle cover cost. Models for the nacelle cover cost in both of the designs only differ by the cost escalation factor added to the NREL model and they are both dependent on the rated power of the wind turbine. The table 6-3 shows lower nacelle cost in the NREL example, even though it is expected to be higher. But it should be noted that the nacelle cover cost in the NREL study was lowered to three significant digits, leaving the reader not knowing what the exact price of the component is. Compared to the other components that are discussed above the effect of the cost escalation seems to be minimal in the nacelle cover cost. Cost escalation factors of the components are expected to be different because the materials used and the labour intensity of the components are different.

The cost models that are a function of the rotor radius, regardless of the cost escalation, result in more expensive components for the optimized design, since the rotor radius is bigger than the NREL example. These components are pitch mechanisms and bearings, spinner, nose cone, low speed shaft, main bearings, yaw drive and bearing. Even though the main frame cost is dependent on the rotor radius, the NREL example is more expensive. This is due to the cost escalation and the fact that the cost of platform and railings are also included in the main frame cost for the NREL study.

The hub height in the optimal design is calculated as 64 m, which is significantly lower than the NREL design. This has an influence on other components. For example the hub height

Table 6-3: Cost and Mass analysis and comparison for the 3 MW wind turbine design with drive train 0 in wind site class 1

Component	NREL Cost (2005 USD)	NREL Mass (kg)	Optimized Cost (2002 USD)	Optimized Mass (kg)
Blade	106333	9603	107207	8537
Hub	69000	14842	112806	26543
Pitch Mechanism and Bearings	83000	6162	130886	5612
Spinner, Nose Cone	6000	1145	8533	1532
Low-Speed Shaft	59000	6251	80212	11444
Main Bearings	32000	1650	60724	1725
Gearbox	408000	20973	219757	21976
Mechanical Brake, HS cpling etc.	6000	-	5968	597
Generator	211000	10426	243750	12801
Variable speed Electronics	266000	-	237000	-
Yaw Drive and Bearing	46000	4312	78152	8627
Main Frame	168000	40426	93610	22029
Platforms and Railings	-	-	23956	2754
Electrical Connections	150000	-	120000	-
Hydraulic and cooling system	41000	240	36000	240
Nacelle Cover	38000	4273	38461	3846
Control, SS, CM	60000	-	55000	-
Rotor Nacelle Assembly	1962000	139509	2152241	145334
Tower	415000	200762	250634	167090
Marinization	321000	-	285805	-
Turbine Capital Cost	2698000	-	2402876	-
Offshore Support Structure	1114000	-	900000	-
Offshore Transportation	281000	-	253470	-
Port and Staging Equipment	74000	-	60000	-
Offshore Turbine Installation	371000	-	300000	-
Offshore Elctr. Interface and Con.	925000	-	780000	-
Offshore Permits, Eng., Site Assess.	119000	-	111000	-
Personnel Access Equipment	64000	-	60000	-
Scour Protection	204000	-	165000	-
Offshore Warranty Premium	357000	-	317561	-
Offshore Levelized Replacement Cost	55000	-	51000	-
Offshore Bottom Lease Cost	12000	-	13563	-
Offshore Operation and Maintenance	215000	-	251166	-
Surety Bond	176000	-	534991	-
Initial Capital Cost	6386000	-	5349906	-
Annual Operating Expenses	282000	-	315729	-
Levelized Production Cost	0.0950	-	0.0606	-

and the rotor swept area, so the rotor radius, have an affect on the tower cost. The tower cost of the NREL study is significantly larger due to the cost escalation of the rolled steel manufacturing and the larger hub height. The mass of the hub is larger in the optimized design, this is mainly caused by the coefficient that is implemented in the mass formula for taking into account the dynamics of the system. Consequently, this reflects upon the comparison of the hub costs, leading to a more expensive hub in the optimized design.

Considering all of the differences in the wind turbine component costs the turbine capital costs are very close to each other, with the optimized design being the smallest one. This directly affects the marinization and offshore warranty premium costs in a similar fashion. Difference in the surety bond is mainly because this project assumes 10% of the initial capital cost (ICC) whereas NREL study takes 3%. The larger rotor and lower rated wind speed of the optimized design also lead to a larger AEP. Hence the bottom lease cost and the operation and maintenance cost are greater in the optimized design.

Optimized components in the tool should be further investigated in both cost and mass aspects. The blade design resulted in lower mass due to the reasons given in the previous section, which eventually leads to lower cost. The gearbox mass is bigger in the optimized design, this is due to the bigger loads from the larger rotor and the mass coefficients used for the three stage gearbox mentioned in section 4-5-3. The cost comparison of the gearboxes reveals reasonable solutions for this rated power, when the sizes (masses) of the gearboxes and the cost escalation are taken into consideration. Finally the generator masses and costs are found to be close to each other with roughly 2% difference in both. The difference could be caused by different generator efficiencies taken, that lead to a bigger generator for the optimized design.

All things considered the initial capital cost is lower whereas the annual operating expenses are higher for the optimized design, leading to a lower levelized production cost of 0.0606 USD/kWh than the cost of energy, 0.095 USD/kWh for the NREL study. However, three things should be kept in mind: *i*) the costs are based on different years *ii*) the tower and surety bond costs are significantly different *iii*) the cost of electricity model in the NREL study is a different economic model than the levelized production cost of this project.

In order to compare the LPCs, firstly the difference in the base years is compensated. The only difference between the cost models of the NREL study and this project (except the blade, generator and gearbox cost models) is the additional coefficient that is present in front of all cost models in the NREL example to account for the cost elevation. These coefficients were investigated for the cost components that depend on the rated power. Because it is known that the only reason for different prices is the cost elevation. The costs were on average almost 30% more than this projects design. Therefore the ICC and the annual operating expenses (AOE) are increased by a conservative value of 30% for the optimized design. It should be remarked that this percentage was seen as a big increase. So the price elevation was also checked with the cost modelling in the Ph.D. thesis of Turaj Ashuri where the baseline year for the cost models was 2009. It was seen that the coefficients were slightly higher as expected. This points out that most of the cost escalation between 2002 and 2009 happened in the first three years. This analysis is also confirmed by the NREL "Wind Turbine Design Cost and Scaling Model" study where rapid changes in the cost of key materials in 2004 and 2005 is mentioned [14].

Secondly the differences between the tower costs were accounted for. In order to do this

200000 USD (the difference between the tower costs) was added to the 30% increased ICC of the optimized design. Then the surety bond for the NREL example was calculated with the cost model of this project.

Finally in order to compare the LPC of the two designs, final ICC, AOE and surety bond costs of the designs were placed into a LPC calculation. These resulted in an LPC of 0.0801 USD/kWh for the optimized design and 0.0812 USD/kWh for the NREL example. Hence the results are close but the optimized design is cheaper.

It is seen that the large difference in the rotor radii, therefore the cost, is compensated by the difference in the in the energy yield. The great difference in the energy yields (10020 MWh and 12558 MWh for NREL example and optimized design respectively) is expected, mainly due to the larger rotor radius of the optimized design. The large difference between the dimensions and costs of the towers constitute a drawback to the tool. However a tower design was not considered in the scope of this project.

6-2-4 Comparison to 10 and 20 MW Optimized Offshore Wind Turbines

Further investigation of the designs in the larger scales is done with the given optimized examples in the PhD. Thesis of Turaj Ashuri. 10 and 20 MW wind turbine designs with three stage gearbox and a DFIG for offshore applications are considered in this section for comparison, since that is the drive train configuration selected in Turaj Ashuri's work. This work includes an aeroservoelastic design and optimization with structural, control, cost and aerodynamic elements. The design results that are found in both of the emulations are presented in table 6-4. The cost values are represented in 1000 USD. Even though all of the designs that are taken into consideration are results of optimization processes the designs that are done by the tool that is constructed in this project will be called "optimized" for the sake of simplicity.

When the rotor radii are compared, it is seen that both of the optimization algorithms result in quite similar results. The rotor radius in 10 MW rated power is slightly higher in the RNA design tool. This will lead to larger sizes in the consecutive components but will also result in capturing more energy in the below rated region. Plus along with the rated rotational speed and the rated wind speed it will have an effect on the tip speed ratio which determines the maximum power coefficient. On the other hand the rotor radius in 20 MW rated power is slightly lower in the RNA design tool. Both of the rated rotational speeds are lower in the RNA design tool. Lowering the rated rotational speed of the rotor increases the gearbox ratio therefore its mass and cost. Nevertheless, lower rotational speeds could benefit the system more with tip speed ratios that result in higher power coefficients. Likewise the rated wind speeds are also below the given values in Ashuri's work. This increases the energy yield, because the rated power will be reached in a lower wind speed in the power curve. All of the above mentioned properties affect the tip speed ratio as it is mentioned previously. The tip speed ratios of the RNA design tool are lower in both of the situations. This is because the optimizer would like to keep the tip speed ratio in the region between 6 and 7 where highest values of power coefficient are achieved. On the contrary different tip speed ratios do not seem to affect the power coefficient of the designs in Ashuri's work, even a tip speed ratio of 9.1 has a corresponding power coefficient of 0.47. The balance between the rotor radius, rated rotational speed and wind speed, tip speed ratio and power coefficient is captured better in

Table 6-4: Optimization comparison of large offshore wind turbines in 10 and 20 MW rated power [7]

Property (Unit)	10 MW	20 MW	10 MW Optimized	20 MW Optimized
Rotor Radius (m)	91	143	94	142
Rated Rotational Speed (rpm)	8.5	6.5	7.1	4.5
Rated Wind Speed (m/s)	11.7	10.7	11.0	10.5
Tip Speed Ratio	6.92	9.1	6.35	6.47
Peak Power Coefficient	0.47	0.47	0.47	0.48
Max Chord length (m)	6.0	10.0	9.9	14.5
Skin Thickness of Root (cm)	12	19.3	6.1	9.3
Max Blade Deflection (m)	7.9	11.8	8.3	12.6
Gearbox Ratio	139	180	169	264
Hub Mass (ton)	56.2	180.0	98.5	306.3
Low Speed Shaft Mass (ton)	49.5	176.7	52.5	174.3
Gearbox Mass (ton)	84.1	173.7	136.6	520.5
Break, Cpling. etc. Mass (ton)	1.98	3.96	1.98	3.98
Generator Mass (ton)	31.5	59.7	38.9	73.6
Hydraulic etc. Mass (ton)	0.79	1.59	0.8	1.6
Nacelle Mass (ton)	379.9	1026.2	372.5	1197.7
TCC (USD)	15489.0	45618.0	10343.4	31572.6
ICC (USD)	29886.4	76714.4	32097.4	163819.1
AOE (USD)	1514.8	3269.8	1009.9	2109.8
AEP (MWh)	56273	122806	39844	83954
LPC (USD/kWh)	0.0711	0.0786	0.0924	0.1876

the RNA design tool. For instance in the RNA design tool, different tip speed ratios result in different power coefficients however this can not be seen in Ashuri's examples. The captured relationship puts constraints on the design variables and state variables (such as rotor radius, rated rotational speed of the rotor, rated wind speed, tip speed ratio, power coefficient) by reflecting their effect on the energy yield and cost of the components. For example the rated wind speed plays an important role on the calculation of the blade tip deflection, which affects the design, mass and cost of the blade.

As it was mentioned in section 6-2-2 the chords of the RNA design tool is larger than other examples, this can be seen for both of the rated power designs. One of the consequences of having bigger chords is the lower skin thickness in the optimized design. The root skin thicknesses are almost half of the ones in Ashuri's study. The blade designed by the RNA design tool is 47869 and 161283 kg for 10 and 20 MW respectively. For comparison, the blade masses in Ashuri's work are calculated according to the models given for the hub weight, which is depended on the blade mass. The blade masses in Ashuri's examples are calculated as 24728 and 92316 kg for 10 and 20 MW respectively. Due to the lower skin thicknesses the blades of the RNA design tool were expected to be lower in both of the rated powers, however this is not observed. Therefore the calculated blade masses for Ashuri's examples were further investigated. This was done by comparing the 5 MW wind turbine design blade

mass provided by Ashuri to the calculated 10 MW blade mass for Ashuri's example. 5 MW wind turbine blade in Ashuri's work is 22851 kg which is only 2 tons less than the calculated 10 MW blade. The blade weights in 5 and 10 MW rated powers are too close. The calculations doesn't seem to add up. So a comparison between the bladed masses are abandoned. The maximum blade deflections are larger in the RNA design tool. This is manly caused by the larger rotor radius as it is in 10 MW rated power or due to the tower design of the Ashuri's tool. The tower design in Ashuri's tool determines the tower diameter that is in the same level of the blade tip, whereas the RNA design tool scales the diameter. Finally the result of lower rated rotational speeds of the rotor can be seen in the higher gearbox ratios of the optimized design for both of the rated powers.

The hub mass models in both of the studies are the same. The reason they are lower in Ashuri's work is due to the lower blade masses that are calculated. Low speed shaft masses, mechanical brake high speed coupling and associated components, hydraulic and cooling systems are modelled in the same way. Thus the masses of these components are very similar due to the close rotor radii. The gearbox and the generator masses are greater in the optimized design, generator results being closer to Ashuri's work. The nacelle masses are very similar, even though the optimized design has heavier blades, gearboxes and generators. So with the given values of rated power, rotor radius, gearbox and generator masses, the total nacelle mass was calculated again for Ashuri's work. The resulting masses were 297 and 843.3 ton for 10 and 20 MW respectively. When the optimized results are compared with these values, it is seen that the difference is caused mainly by the gearbox and the generator and the rest of the difference is due to the rotor radii.

Economic comparison is made with the Turbine Capital Cost (TCC), Initial Capital Cost (ICC), Annual Operating Expenses (AOE), Annual Energy Production (AEP) and Levelized Production Cost (LPC). The turbine capital costs are lower in the optimized design even-though some of the components are heavier. This is because the economical modelling in Ashuri's work is based on 2009, thus corrections are applied that make them more expensive. The ICC calculation in Ashuri's work does not include the offshore transportation cost, which is one of the major contributors to the ICC calculation in the RNA design tool. That is mainly why the ICC costs are higher in the optimized design. In both of the cases AOE costs are calculated with the AEP and they are greater in Ashuri's work. The difference between the AEP values is due to three factors. Firstly availability of the wind farm is not taken into account in the PhD thesis. Secondly wind site classes are slightly different, where standard offshore wind site class values are utilized in this work and in the other wind site properties of the Dutch part of the North Sea are used. Finally the power curves are designed with different models of losses.

The table 6-4 shows the LPC values that were calculated with the given ICC, AEP and AOE values of the PhD thesis, since the economical analysis in Ashuri's work is based on levelized cost of electricity. Therefore at first sight the LPC value of Ashuri's work seems lower than the optimized design in both of the rated powers. But this comparison neglects the fact that the ICC does not include the offshore transportation and the AEP values are significantly different due to the reasons given above. So, if the offshore transportation costs are added to the ICC and the AEP are assumed to be the same in both works (taking the AEP values in the PhD. thesis) the LPC values change. The LPC values for 10 and 20 MW for aeroservoelastic design become 0.0898 and 0.1550 Euro/kwh respectively, whereas the results for the RNA design tool becomes 0.0654 and 0.1282 Euro/kwh.

Table 6-5: Wind turbine gearbox examples from the literature and the industry [10] [11] [12] [13] [14] [15] [16] [17]

Source	Rated Power (MW)	Type	Weight (kg)
Optimization Multibrid Sys.	3	Single-stage	15920
Comparison of DD and Geared Sys.	3	Single-stage	20000
Developments in Gen Sys.	3	Single-stage	20000
GE Drivetrain Technologies	2.7	Three-stage	17700
GE Drivetrain Technologies	2.9	Three-stage	21100
NREL Gearbox	3	Three-stage	20973
Comparison of DD and Geared Sys.	3	Three-stage	22000
Rexroth Bosh Group	3	Three-stage	23360
Wikov Gear	3	-	22250
Wikov Gear	3	-	25600
Eickhoff	3.3	Three-stage	30000
Eickhoff	3.6	Three-stage	28000
Optimization Multibrid Sys.	5	Single-stage	35020
Rexroth Bosh Group	5	Three-stage	40810
Wikov Gear	5	-	57000
Optimization Multibrid Sys.	10	Single-stage	180000

As a result the rotor radii of the tools were found to be very close. It is important to see that a global design variable of the RNA design tool is close to the result of another optimization algorithm. This shows the reasonableness of the tool. This also led to similar mass values in the drive train. Finally the LPC values are found lower in the RNA design tool as expected due to the different baseline years of the economical analyses.

6-2-5 Comparison of the Rotor Designs

The comparison of the rotor designs to the realized ones has been conducted in detail previously. Since the designs in all the rated powers and the wind site classes have the same significant differences from given examples and realized rotors, the reader is directed to section 6-2-2.

6-2-6 Comparison of the Gearbox Designs

Since the gearbox design is a part of the optimization process, the resulting designs are investigated and compared to either realized gearboxes or optimized ones in the literature. The existing gearbox designs do not reveal so much detail about the dimensions, but only masses, rated power and the type of the gearbox. Thus, the masses of the gearboxes for corresponding rated powers are compared. Some of the existing gearboxes and their details are stated in table 6-5. Hyphens are placed in the table 6-5 if the type of the gearbox was not provided in the source.

In most cases gearboxes that are above 5 MW rated power are under development and there are more examples of gearboxes for 3 MW and lower rated powers. For comparison results of

Table 6-6: Wind turbine gearbox mass and transmission ratios by the optimizer design

Rated Power (MW)	Wind Site Class	Gearbox Type	Gearbox Mass (kg)	Transmission Ratio
3	Offshore	Single-stage	25387	8.76
		Three-stage	21976	106.18
	Coastal	Single-stage	14178	6.94
		Three-stage	18099	91.21
	Inland	Single-stage	18267	7.67
		Three-stage	18385	92.38
5	Offshore	Single-stage	58477	10.02
		Three-stage	45843	126.57
	Coastal	Single-stage	44743	8.961
		Three-stage	40237	114.73
	Inland	Single-stage	55922	9.829
		Three-stage	44119	122.66
10	Offshore	Single-stage	252743	13.951
		Three-stage	136621	169.08
	Coastal	Single-stage	313412	15.35
		Three-stage	160631	189.84
	Inland	Single-stage	379932	16.726
		Three-stage	196327	210.85

the RNA design tool for 3, 5 and 10 MW rated powers are considered and they are separated into two designs as three stage gearbox and single stage gearbox in table 6-6.

The example 3 MW single stage gearbox masses range from 15920 to 20000 kg. The single stage gearbox designed by the RNA tool for 3 MW offshore applications is 25387 kg. However in wind site classes with lower wind speeds the gearbox mass is less because of the decreased loads. Nonetheless the resulting masses are within 27% vicinity of the given examples. The three stage gearbox designed by the RNA tool for 3 MW offshore wind turbine is 21976 kg, which is within the range that is attained by the examples. Likewise the other wind site classes have lighter gearboxes and they are within the given range of gearbox masses from 17700 to 25600 kg.

5 MW offshore designs of the RNA design tool have 58477 and 45843 kg single and three stage gearboxes respectively. This single stage gearbox mass is higher than the given example with 66% more mass and the three stage gearbox is within the range. The other single stage gearbox masses in different wind site classes are closer to the given example, the gearbox for the coastal design being the closest. Three stage gearboxes in other wind site classes are maximum 1.4% less in mass than the given example or they are within the given range.

Final comparison was made for a single stage gearbox in 10 MW wind turbine design and the RNA design tool resulted in 252743 kg of gearbox for offshore application. This is 40% higher

Table 6-7: Wind turbine generator examples from the literature and the industry [18] [11] [10]

Rated Power (MW)	Type	Stator Radius (m)	Stack Length (m)	Weight (ton)	Cost (kEuro)
3	DFIG 3G	0.42	0.75	5.25	320
3.2	DFIG 3G	-	-	7-10	-
3	PMG 1G	1.8	0.4	6.11	333
3	PMG 1G	1.7	0.4	4.59	398
3.6	PMG 1G	-	-	7-10	-
3	DD	2.5	1.2	24.1	432
3	DD	2.5	1.19	16.9	544
5	PMG 1G	1.9	0.35	7.29	719
5	DD	3.75	1.5	27.4	1082
10	PMG 1G	2.1	0.9	12.79	2088
10	DD	5	1.81	62.8	2420

than the suggested optimization result(Optimization Multibrid Sys.). The inland single stage gearbox designed by the RNA design tool is two times the given example, but the given example is not a realized gearbox.

The tool is able to design single stage gearboxes that are in maximum 66% vicinity of the example gearboxes between 3 MW and 5 MW range. Three stage gearboxes are designed in accordance with the given mass range by the examples. The highest differences are seen in the single stage gearboxes for the higher rated powers. This in a sense is already on the boundaries of the single stage applications, because the transmission ratios are slightly over 15:1 for the coastal and inland designs. Considering the great differences of gearbox masses between different manufacturers and literature examples, the gearbox designs by the RNA design tool are assumed to be reasonable.

6-2-7 Comparison of the Generator Designs

Generator designs for 3, 5 and 10 MW rated powers are mostly collected from the literature, where comparison between different drive trains and optimization processes are conducted. Either most of the realized generators are below 3 MW or the specifications do not involve volume, stator bore radius, axial stator stack length, mass nor the cost of the generators. Thus the relevant information for comparison of gearboxes was found in similar optimization or comparison studies.

The gathered generator designs are represented in the table 6-7. The first, third and sixth design is taken from a study that compares direct drive and geared systems [11]. The designs that are lacking the stator radius and stack lengths are taken from realized generators from ABB Ltd. [18]. The rest is taken from a similar study of optimization [10]. DFIG 3G corresponds to the drive train with three stage gearbox and a doubly fed induction generator, PMG 1G corresponds to drive train with single stage gearbox with permanent magnet generator and finally the DD is the direct drive drive train with permanent magnet generator.

Fist the generator designs that are given by the optimization tool for DFIG 3G and PMG 1G

Table 6-8: Wind turbine generator mass and dimensions by the optimizer design

Rated Power (MW)	Type	Stator Radius (m)	Stack Length (m)	Weight (ton)	Cost (USD)
3	DFIG 3G	0.53	0.46	12.8	243750
	PMG 1G	1.17	0.67	16.9	164190
5	DFIG 3G	0.64	0.52	20.5	406250
	PMG 1G	1.32	0.87	27.1	273650
10	DFIG 3G	0.82	0.63	38.8	812500
	PMG 1G	1.68	1.08	51.4	547300

generators are presented in table 6-8. The generator designs of the same type of drive train in different wind site classes result in the same outcomes, because the rotational speeds and the rated powers are kept the same. This leads to the same volume each time. So different wind site class designs are not shown separately in table 6-8. On the other hand the direct drive generator rotational speed is one of the state variables that are computed according to the design variables in the optimization. Therefore different wind site classes result in different generator designs due to the slight difference in the rotational speeds of the generators. Direct drive permanent magnet generator designs of the optimizer with respect to wind site classes are presented in table 6-9.

The 3 MW DFIG 3G generator design of the tool is compared to the given examples. The stator radius is 26% higher, whereas that stack length is 39% less from the comparison study (the first line in table 6-7). The weight of the given examples in table 6-7 range from 5.25 to 10 tons. Immediately a large difference in the comparison study and the realized generator is observed (the first and the second examples in the table 6-7). The gap between them ranges from 25% to 47.5%. The comparison study only takes into account the active material (iron, copper and magnets) in the generator weight calculation, whereas the given mass for the realized generator includes everything (casing, bearings etc.). This causes the large difference in the masses. So the analysis suggests that possible differences between the model results and the realized components are acceptable. The weight of the optimized generator is closer to the realized one, rather than the one given in the comparison study. But in both cases the optimization result is higher than the given examples. Even though the weight is greater the generator is cheaper in the optimization outcomes.

It should be noted that the currency of the given prices are different. The copper price given in the comparison study was investigated in the charts and data of the mining industry and it was observed that the copper price has been at most nearly 8 EURO/kg in the year 2011, between the years 2002 and 2014. The assumed copper price in the comparison study is 15 EURO/kg, thus it was not possible to locate the year that the prices were based upon. The assumed cost per kg prices of the materials are higher than expected, this is in line with the cost results, as the generator cost in the comparison study is significantly higher than the optimization result. The differences between the weight and cost modelling lead to significantly different results. The same difference is also observed in the PM 1G generators of 3, 5 and 10 MW.

Table 6-9: Wind turbine direct drive permanent generator mass and dimensions by the optimizer design for different wind site classes

Rated Power (MW)	Wind Site Class	Stator Radius (m)	Stack Length (m)	Weight (ton)	Cost (USD)
3	Offshore	2.15	1.21	68.5	973206
	Coastal	2.02	1.10	59.8	775990
	Inland	1.96	1.05	56.2	700852
5	Offshore	2.56	1.65	101.9	1873344
	Coastal	2.47	1.58	95.1	1671024
	Inland	2.40	1.52	89.6	1514637
10	Offshore	3.72	2.48	204.9	5929163
	Coastal	3.76	2.51	209.4	6147763
	Inland	3.93	2.64	563.6	7064523

The PM 1G design in 3 MW is 31% smaller and 67.5% larger in the stator radius and stack length respectively. This leads to a larger generator by the optimizer and its effect can be seen in the weight comparison. The given examples range from 4.59 to 10 tons. Once again the 3 MW PM 1G design example given in table 6-7 (fourth line) deviates from the realized generator with a large value of 54% in mass. On the other hand the optimized design by the RNA design tool is 69% heavier than the realized generator.

The comparison of the 5 and 10 MW generators is only done with the modelled examples in the comparison and the optimization studies in the literature. Thus, higher weights and lower costs in the designs of the RNA design tool are expected. The radius of the 5 MW PM 1G design of the tool is again 31% smaller, along with a stack length almost two and a half times larger. This leads to a generator weight almost 4 times heavier than the optimization example. As the rated power of the generator increases the difference between the weight of the optimized example and the new design is increasing. Looking at the mass of the realized generators a 10 MW permanent magnet generator is expected to be much higher than 12.79 tons as it is suggested in the optimization example in table 6-7. Finally 10 MW PM 1G design of the RNA tool is 20% less in the stator radius and 20% longer in the stack length. Thus the optimizer designs permanent magnet generators in a single stage gearbox configuration with smaller stator radii and larger stack lengths that result in heavier generators.

The 3 and 5 MW direct drive permanent magnet generator designs are in similar fashion with each other. In both of the cases the stator radius and the stack length of the generators are very close in each wind site class, offshore generator being the largest and inland generator being the smallest. The weight also follows the same pattern. The size of the generator is greater in the offshore applications because the rotational speed is lower which increases the torque on the generator.

The closest DD generator dimensions to the comparison and optimization examples in 3 MW range is the offshore application. In this rated power all the new design stator radii are lower than the given examples. Besides the stack length is 14% less than the given examples for inland configuration, which is the maximum difference seen among the stack lengths of 3 MW DD generators. In the 5 MW range designs of the optimizer the stator radii are lower than

the given example and the stack length are larger. The weight comparison for all rated powers and wind site classes are similar to the previous ones due to the reasons given above.

The largest DD generator in the 10 MW range is designed in the inland wind site class, due to the relation to the rotational speeds. Further investigation on how the optimizer responds to different input and the relations between the design variables and parameters will be studied in the section 6-3. Once again the optimizer designs stator radii smaller and the stack lengths larger, with on average 21 and 45 percent off values respectively for the inland wind site. The rest of the wind sites has closer values to the given stack length, but not for the stator radius values.

This analysis showed a great difference between the realized generator masses and the optimized solutions. The examples taken from the literature had lower masses compared to realized generators. The designs of the tool were closer to the realized generator examples, but higher in mass. Lack of realized generators and their differences in mass to the literature examples, hindered the appraisal of the generator designs.

6-3 Responses to Changes in Input Parameters

This section focuses on the responses of the design solutions to different inputs. There are two inputs involved by the user in the RNA design tool: *i*) rated power and *ii*) wind site class. Rated powers of 3, 5, 10 and 20 MW and three different wind sites (offshore, coastal and inland) will be compared for the same drive train configurations. The differences between the drive trains and how these differences evolve in different rated powers will be studied in chapter 7. Tables 6-10, 6-11, 6-12 and 6-13 provide the design variables and the properties of the design solutions in each wind site class for all of the drive train configurations at a certain rated power. Lastly the effect of increasing teeth number in the gearbox to the design will be investigated.

6-3-1 Changes in the Design Solutions for Different Rated Powers

In this section the responses of the design properties to an increase of the rated power will be analysed. Most of the properties of the wind turbine clearly increase with growing rated power, these are: rotor radius, maximum chord length, skin thickness of the root, maximum blade deflection, transmission ratio, stator radius and the stack length of the generator and masses and costs of each component. On the other hand rated rotational speed of the rotor and the rated wind speed are properties that decrease with increasing rated power, in order to have similar tip speed ratios in different rated powers. These changes are expected and they prove the reasonableness of the designs in different rated powers.

Also the tip speed ratio is increasing but not in a constant way. For example the tip speed ratios of the offshore DD, coastal DFIG 3G and PM 1G and inland DD designs in 3 and 5 MW rated powers have the same tip speed ratios. On the other hand the tip speed ratios of the offshore DFIG 3G, inland DFIG 3G and coastal DD designs has larger but very close tip speed ratios in 3 MW designs compared to 5 MW designs. Generally the data shows that the lowest tip speed ratios are seen in either 3 or 5 MW designs and the highest ones are seen in the 20 MW range. Since higher tip speed ratios correspond to higher power coefficients

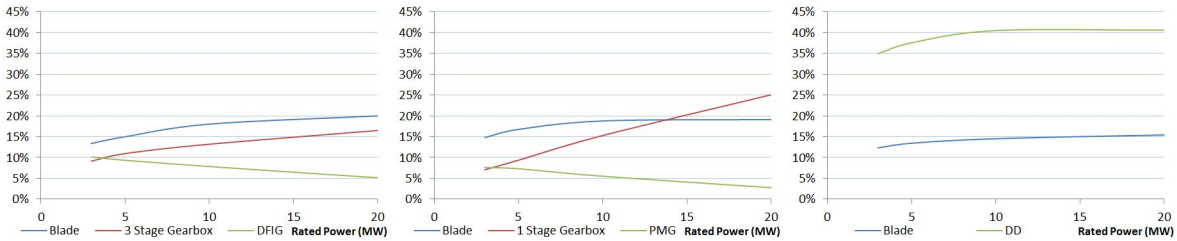

Figure 6-3: Blades, gearbox and generator cost percentages in the turbine capital cost for offshore region RNA design for DFIG 1G, PM 1G and DD respectively

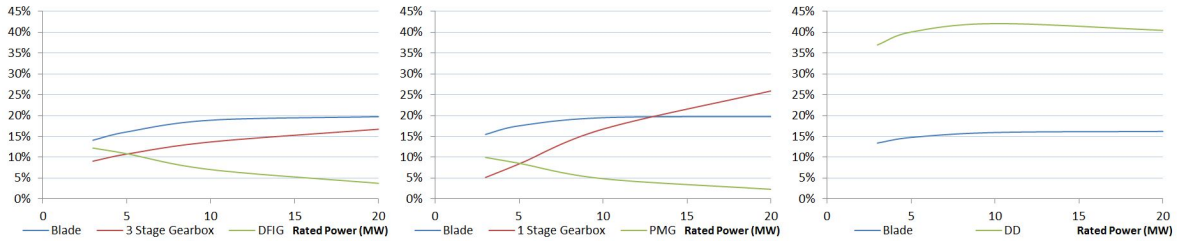

Figure 6-4: Blades, gearbox and generator cost percentages in the turbine capital cost for coastal region RNA design for DFIG 1G, PM 1G and DD respectively

in the model up to 7, it can be concluded that the decrease of the rated wind speed is tried to be compensated with increasing rotor radii and power coefficients. However it is more interesting to investigate the changes in the relative cost contributions of the blades, gearbox and the generator to the turbine capital costs. These changes are plotted for each component and drive train in different wind site classes in figures 6-3, 6-4 and 6-5 for offshore, coastal and inland respectively.

Essentially in all of the wind sites the changes in the relative costs of the components to the turbine capital cost are very similar. The real distinction is between the drive trains. In the DFIG 3G all of the blade costs start with approximately 15% and ends up with 20% of the turbine capital cost. The change in the blade costs is rather faster between 3 to 10 MW and than it slows down For the inland designs the relative blade costs are lower in 20 MW than 10 MW. The three stage gearbox also increases in relative cost in a similar fashion with higher slope compared to the blade relative cost in the second region after 10 MW from around 9% to 17%. On the other hand the generator starts decreasing its relative cost from approximately

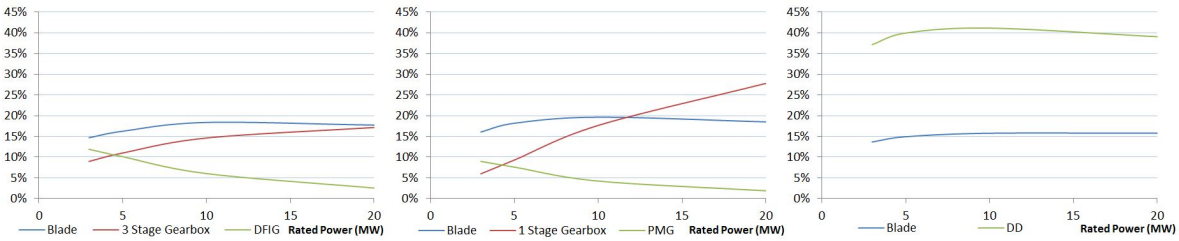

Figure 6-5: Blades, gearbox and generator cost percentages in the turbine capital cost for inland region RNA design for DFIG 1G, PM 1G and DD respectively

12% to 4%. This analysis shows that the weight of the gearbox and the blade design becomes more important for the turbine capital cost on the larger rated powers, whereas the generator cost impact on the turbine capital cost becomes less.

The relative costs of the PM 1G is quite similar to the previous drive train for the blade and the generator relative costs. The single stage gearbox increases much more than the three stage gearbox in relative cost from 3 MW to 20 MWs. It can be seen from the steeper increase of the relative cost that as the rated power increases the boundaries of a single stage gearbox design is forced. Where the three stage gearbox has a rather slight increase in the relative prices, the single stage gearbox rises from around 5% to 25%. From the graphs it can be computed that above 7 to 8 MW rated power, where the relative cost of the three and single stage gearboxes overlap, the designs will benefit from gearboxes with multiple stages.

Finally, the DD designs have more weight on the generator costs rather than the blade costs as expected, and the change in their individual relative costs are similar. For both of the components relative costs experience an increase between 3 to 10 MWs and than the slope decreases. The generator relative costs in the coastal and inland region decrease after 10 MW.

6-3-2 Changes in the Design Solutions for Different Wind Site Classes

In this section the changes of the RNA designs for specific drive trains in different wind site classes will be analysed. This analysis is conducted for all of the given rated powers. The way the design solutions of specific drive trains change in different wind site classes are usually the same for all the drive train configurations. For instance, the way the rotor radius changes from offshore to inland wind site classes for 3 MW is the same for all the drive trains. However, the optimizer guides the design solutions in different manners in different rated powers. Thus the alteration of the design solutions of a drive train can be classified under four sections: *i*) 3 MW *ii*) 5 MW *iii*) 10 MW and *iv*) 20 MWwith slight differences among different drive trains.

3 MW Design Solutions

The largest rotor radius is seen in the offshore applications and the smallest one in the coastal regions. At this rated power the offshore designs try to compensate for the differences in the expenses between offshore and onshore wind sites by producing more energy than the other wind classes and increases the rotor radius. Furthermore an increase in the rotor radius is more acceptable in the offshore designs rather than the other wind sites because the relative cost of the blades are lowest in the offshore applications at 3 MW rated power. The comparison of the relative costs of the blades in different wind sites can be observed in figures 6-3, 6-4 and 6-5. On the other hand coastal regions do not have the disadvantage of lower average wind speeds and the higher costs of offshore applications. In order to reach the same power output with lower average wind speeds the inland radii are greater than the coastal designs. This is an expected decision by the optimizer, as when the wind turbine manuals are checked for onshore 3 MW rated power the highest rotor radii are seen in the low wind speed regions. As a consequence lower rotor radii increase the rated wind speeds of the designs in coastal wind sites. This leaves the offshore designs with the lowest rated wind speeds. As anticipated, the maximum chord length is highest for the offshore and lowest for the coastal wind site classes due to the changes in the rotor radii with the exception of DD designs where the chord is

smallest for the inland sites. This is an effect of the higher tips speed ratios attributed in the inland designs for DD. Likewise the tip deflection also goes down with the decreased rotor radius, because it is essentially scaled with the rotor radius. The tip deflection is matched with the allowable distance by attributing proper thicknesses to the blades. The root thickness of the blades is lowest for offshore applications. This is a way for the optimizer to lower the mass and the cost of the blades as it was explained in section 6-2-2 and it is most apparent in the offshore design solutions. Nevertheless, the blade mass increases with increasing rotor radius.

Examples from realized wind turbines with higher rotor radii and lower rated wind speeds in low wind speed sites suggest that the rated rotational speed of the rotor should be decreased from coastal to inland regions in order to keep the tip speed ratio rather constant to have similar power coefficients in various wind sites. This is realized in the optimizer design as the inland regions have lower rated rotational speeds than coastal. Besides, the offshore designs with the highest radii and lowest rated wind speeds have also the lowest rated rotational speeds of the rotor. These rotational speeds result in highest tip speed ratios in the inland applications and lowest in the offshore wind sites. The corresponding power coefficients follow exactly the same trend as the tip speed ratios, all of them being between 6 and 7. This approach of the optimizer is realistic because it appoints the highest power coefficient to the lowest wind speed region. Another effect of the rotational speed is to the gearbox ratio and the gearbox mass. Lower rotational speeds on the rotor side increase the gearbox ratio, mass and the cost of the gearbox. So the gearbox ratio and the mass are highest for the offshore designs and lowest for the coastal ones.

The generator designs in all the wind site classes are exactly the same for the DFIG 3G and PM 1G where the rotational speeds of the generators are fixed, but the design changes for the DD. The stator radius, stack length and the mass always follows the same pattern. Their differences amongst the wind sites directly depend on the rotational speeds of the generators. So the higher rotational speeds lead to smaller generators. Therefore the biggest generators are found in the offshore applications and the smallest ones in the coastal designs.

As expected, the initial capital cost of the offshore applications is always the highest due to the extra burdens brought by the marine environment. Because of the smaller components caused by a smaller radius the initial capital cost of the coastal applications are the lowest. Similarly the offshore annual operating expenses are the highest due to the larger radii. But due to the lowest annual energy productions, the annual operating expenses are lowest for the inland designs. Also the annual energy production is highest in the offshore wind sites and this makes the annual operating expanses of the offshore designs even more expensive than the other two. These are expected outcomes of the optimizer. The way that the wind probability density function overlaps with the power curve determines the annual energy production. Factors affecting the differences in the outcome are the wind site class, rated wind speed, power coefficient and the rotor radius. It should be kept in mind that the availability of offshore wind sites is assumed to be significantly lower than the onshore applications (85% to 98%) which may lead to different results in other rated powers. Finally, the highest levelized production cost is seen in the offshore wind sites as expected and the lowest in the coastal wind sites. The advantages of the coastal regions reflect upon the levelized production costs as it benefits from mid-range wind speeds and onshore installations. The results are as expected and follow the realized wind turbine examples in different wind sites.

5 MW Design Solutions

The design trends of the optimizer in the 5 MW rated power for different wind sites vary slightly from 3 MW designs, without making a difference in the levelized production cost ranking among the wind sites. First off the largest rotor radii DD design solutions are in inland rather than offshore. Lower drive train efficiencies and average wind speeds force the DD rotor radii to increase to reach the designated power output at this rated power. This directly influences the rated wind speeds and makes them lowest for the inland regions. Also the tip deflection becomes the greatest in inland designs for DD. Another major difference between the two rated powers is the blade mass. At 5 MW designs the higher root thicknesses in the inland designs result in heavier blades than the offshore designs. The contribution of the blade thickness becomes more than the rotor radii effect on the blade mass at 5 MW range. The rest of the RNA property comparisons between wind site classes are the same with the 3 MW design solutions.

10 MW Design Solutions

The design trends of the optimizer in the 10 MW and above range are different than the previous section. The 10 MW designs in all drive trains respond the same to the changes in the wind site conditions. In this section the responses of the 10 MW designs to diffferent wind sites will be discussed.

At 10 MW rated power there are no commercialized wind turbines, thus the changes cannot be compared to realized wind turbines in different locations. First off the rotor radii are largest in the inland areas and smallest in the offshore regions. At this rated power the wind speeds are able to compensate for the smaller rotor radii in the offshore applications. Besides, inland rotor radius becomes larger due to the lower average wind speeds in the site. Furthermore the offshore application has the highest rated wind speed. From the data it can be seen that the rated wind speeds are more aligned with their corresponding average wind speeds of the site. The lack of high wind speeds in the inland areas is also assisted by the highest power coefficients. Further, the power coefficient of the offshore designs is the lowest even for the DFIG design. But for the DFIG the difference in the power coefficients between offshore and coastal regions cannot be seen in one decimal place in the table. Noticeably the tip speed ratios also follow the same pattern with the power coefficients. The maximum chord length and the maximum tip deflection are also the largest in the inland applications and smallest in the offshore regions as it is with the rotor radius. Once again the root thickness is found smallest in the offshore design to lower the cost of the blades. The highest root thickness is in inland area designs, which also leads to the heaviest blades amongst all the wind sites. The only exception to the situation is the DD design where the root thickness is the largest for the coastal areas, however this does not affect the blade mass ranking.

Rated rotational speeds of the rotor are lowest in the inland wind sites due to its relation to the rated wind speed and the tip speed ratio. This leads to biggest transmission ratios and gearboxes in the design. The generator dimensions and its mass respond to the rated rotational speeds and are largest in the inland areas and smallest in the offshore wind sites. It is important to note that the transmission ratios of the PM 1G designs in the coastal and inland applications are above 15. This value is the highest gear ratio that a single stage gearbox can have currently. Thus the PM 1G designs are eliminated for 10 MW rated powers

and above. The DD generator dimensions and mass follow the same analysis that was stated in 3 MW design comparison in different wind site classes and results in biggest dimensions in inland designs and smallest in the offshore designs.

The initial capital costs of the designs are highest for the offshore installations as expected and lowest for the coastal. The difference between the onshore installations is due to the larger rotor radius of the inland design. The annual energy production is the highest in the coastal applications and lowest in the inland wind sites. This is an expected outcome since an offshore wind site is expected to yield more energy than an inland application. But on the other hand larger rotor radii of the coastal regions combined with the lower availability of the offshore wind sites result in higher energy yields in the coastal areas.

Since the offshore levelized replacement cost and operation and maintenance are more expensive than the onshore applications the annual operating expenses are the highest for the offshore designs. Likewise lower energy yield in inland sites lead to the lowest annual operating costs. Finally the levelized production costs of the offshore designs are calculated the highest with coastal applications the cheapest. These results are the same with 5 MW and below designs however, the difference between the offshore and onshore levelized production costs are diminishing. The comparisons are as expected and the relations of the design variables among each other are reasonable.

20 MW Design Solutions

The changes in the designs between the 10 MW and 20 MW rated powers alter slightly. Firstly the differences between the rotor radii in comparison of the offshore and onshore applications increase significantly. In this case, as it was mentioned before the larger rotor radii cause the initial capital cost of the onshore designs to grow so much that they become more expensive than the offshore designs. However the annual operating expenses are still highest in the offshore installations which lead the levelized production cost of the offshore designs in the second place for cheapness. Once again the coastal applications are the cheapest in levelized production costs but inland has become more expensive than the ones on offshore sites. Futhermore the gap between the levelized production costs has diminished to maximum 6% between the coastal and offshore designs in comparison of the same drive trains.

The rest of the properties of the RNA are the same in respect to wind site comparisons with the 10 MW design solutions. Comparison among the design solutions with respect to wind site classes at 20 MW rated power showed some unexpected results as the offshore installations became cheaper than inland installations. However the reasoning behind the design of the tool shows the possibility of such outcomes.

6-3-3 Changes in the Design Solutions for Increasing Number of Teeth

Finally the effect of minimum number of teeth to the gearbox design is investigated. The 5 MW offshore wind turbine optimization process is run again with the minimum teeth number of 40 instead of 21. This changes the size and the dimensions of the gearbox along with the rest of the design. Some general properties along with gearbox dimensions and masses are presented in table 6-14. Only the dimensions of the sun in the first stage is provided in the table 6-14, because the effect of increasing the teeth number is the same for all of the gears.

Table 6-14: General and gearbox properties of the 5 MW DFIG 3G and PM 1G designs with minimum number of teeth 21 and 40

	Min. no. of teeth 21		Min. no. of teeth 40	
Property (Unit)	DFIG 3G	PM 1G	DFIG 3G	PM 1G
Rotor Radius (m)	69.2	66.2	66.5	66.0
Rated Rotational Speed (rpm)	9.2	10.0	10.0	10.1
Sun Diameter (m)	1.21	0.85	1.63	1.23
Sun Width (m)	0.76	0.57	0.54	0.43
Gearbox Ratio	130	10	120	9.9
Gearbox Mass (kg)	47577	58478	73216	90796

The number of teeth not only has an effect on the gearbox design but also on the global design of the RNA. The levelized production costs for DFIG 3G and PM 1G are increased, the rotor radii are decreased and rotational speed is increased among other differences. The increased teeth numbers increase the mass of the gearboxes, regardless of the fact that the transmission ratios are decreased by the increasing rotor rotational speeds. The tooth bending stress calculation is dependent on the tooth width and pitch, as in when they increase the bending stress decreases. Moreover the surface fatigue stress is dependent on the tooth width and diameter in the same way. So the optimizer chooses to increase the diameter to keep the pitch high (for the sake of lowering tooth bending stresses according to the constraints) and the surface fatigue stresses low. The increase in the diameter allows more narrow gears to be designed. Nevertheless larger diameters have a more considerable effect on the mass of the gearbox, due to the increase of the circular sectional gear area. As a result, it is concluded that the gearbox design is lighter and cheaper with lower number of gear teeth.

The response of the optimizer to the change in the minimum number of teeth of the gears shows that the multilevel perspective is effective. This shows even a slightest change in one of the components results in differences in the system level. These are the trade-offs and relations between the components that are aimed to be captured by the multilevel optimization of the RNA design tool.

6-4 Practical Performance of the Automatic Design of RNA Tool

6-4-1 Encountered Problems of the Automatic Design of RNA Tool

During the implementation of the engineering model, the employment of optimization routines have resulted in errors from time to time. Three types of errors were encountered:

- Positive directional derivative for linesearch
- Iteration limit exceeded
- Numerical overflow in the objective

SLSQPdriver, the optimization algorithm that is used in this project works by choosing a decent direction, and performs a linesearch to that direction. The first error listed, means

that the optimizer reaches a position where it cannot manage to find a direction that the value of the objective function decreases fast enough and cannot verify that the current position is a minimum. The problem was solved by changing the initial conditions of the related design variables of the optimizer. For instance if the gearbox optimization encountered this problem, the initial condition of the width and the diameter of the sun in stage 1 was changed.

The second error was solved in the same manner. In order for the optimizer to reach the minima within the given iteration number, the initial conditions of the design variables of the optimizer with the error were set closer to an expected result.

The latter of the errors means that the evaluation of the objective function causes an overflow, meaning the value is too great. In these cases the objective function of the related optimizer was divided by a constant value. This approach does not alter the functions minima and its corresponding values for the design variables.

These problems were encountered, while design of different rated power wind turbines from 3 MW to 20 MW were optimized. The adjustments that were made in the initial conditions or the objective functions were collected in a table for a variety of different rated powers. The table can be seen in appendix B. Before the tool is run the conditions that are stated in appendix B must be applied to the tool. Even though this approach makes the tool harder to be used, it helps to overcome major difficulties in the optimization routines and makes the it applicable for a great range of rated powers.

6-4-2 Speed of the Automatic Design of RNA Tool

In this section the computational times and the number of iterations in each optimization will be analysed. This analysis is conducted on the 3 and 5 MW designs in offshore, coastal and inland regions. Larger wind turbines are not included in the analysis since the iteration numbers exceed the printing capabilities of Spyder. After a while initially printed lines are deleted in order to write more. Furthermore the amount of data that needs to be analysed becomes excessive. However overall timing of 10 and 20 MW designs will be discussed with respect to lower rated wind turbines. The number of iterations and the duration of each optimization are represented in tables 6-15 and 6-16 for 3 and 5 MW designs respectively.

The tables show the number of iterations that are done during the rotor, gearbox and generator optimizations. The iteration number of the modules and Multi-Criteria Analysis (MCA) evaluation shows the number of iterations done in the higher level optimization, because these modules and the MCA evaluation runs only during the iterations of the first level optimization. The duration of each optimization process, total sums for each drive train and the total run time of the tool are shown in the tables.

For each drive train in all of the wind site conditions the most time consuming process is the evaluation of the objective function and choosing the direction for the next iteration in the higher level optimizer. Even though the iteration numbers are lower than rotor, gearbox or generator optimizations, the MCA evaluation takes much more time due to the higher complexity of the optimization in the first level.

In all of the DFIG 3G designs, three stage gearbox optimization takes longer time and needs more iterations in order to reach the optimum. The longest optimization process for DFIG 3G design takes place in the coastal and offshore regions for 3 and 5 MW designs respectively.

An optimization is taking longer if the initial guesses of the design variables are more distant from the optimum. Also it was observed that generally as the rated power increases the computational times increase as well.

Table 6-17: Maximum and Minimum duration of one iteration seen in the rotor, gearbox and generator optimizations

	DFIG 3G		PM 1G		DD	
	Duration (s)		Duration (s)		Duration (s)	
	Max.	Min.	Max.	Min.	Max.	Min.
Rotor Optimization	0.116	0.011	0.107	0.011	0.107	0.020
Gearbox Optimization	1.222	0.052	0.056	0.007	-	-
Generator Optimizaton	0.02	0.002	0.019	0.002	0.027	0.005

For the PM 1G and DD designs the rotor optimization is the one that takes most of the time and generator design the least. This can be seen in the tables when the larger values of iteration numbers and duration in the rotor optimization are compared to the others. As it was in the DFIG 3G configurations, the longest wind site optimizations differ for different rated powers. For the 3 MW wind turbine longest computational times are in offshore whereas for 5 MW designs, it is inland. This is vice versa for the DD designs.

There are no general trends for a specific drive train design taking most of the computational times during each run. It is obvious from the data that increase in the duration of one iteration results in longer run times. The results given in the tables show that any design can be completed below five and half minutes. But this situation is closely related to the vicinity of the initial conditions to the optimums. The computational times do not exceed this time up to 20 MW rated power with three exceptions. These were 20 MW offshore, 20 MW inland and 10 MW inland designs. The latter took almost 43.5 minutes the other two were below 23.5 minutes.

Finally the improvement of each iteration is analysed. The timing of each iteration is printed in order to see if they are decreasing consecutively. Table 6-17 shows the maximum and minimum durations of the iterations done in the rotor, gearbox and generator optimizers in different drive trains. For all of the optimization processes the maximum duration was seen in the beginning and the lowest times in the end. This is an indicator of improvements during each iteration. Finally from the table 6-17 it can be seen that the most time consuming iteration steps are taking place in the three stage gearbox optimization.

Table 6-10: Optimized 3 MW wind turbines for all wind site classes and drive trains

	3 MW								
	Offshore			Coastal			Inland		
Property (Unit)	DFIG 3G	PM 1G	DD	DFIG 3G	PM 1G	DD	DFIG 3G	PM 1G	DD
Rotor Radius (m)	55.5	55.1	55.2	50.8	48.0	44.9	51.4	51.2	47.8
Rated Rotational Speed (rpm)	11.3	11.4	13.5	13.2	14.4	17.0	12.9	13.0	15.3
Rated Wind Speed (m/s)	10.5	10.5	11.0	11.1	11.5	12.0	11.0	11.0	11.5
Tip Speed Ratio	6.25	6.27	6.60	6.29	6.30	6.65	6.36	6.35	6.66
Peak Power Coefficient	0.467	0.468	0.480	0.468	0.469	0.482	0.472	0.471	0.482
Max Chord length (m)	6.03	5.95	5.03	5.47	5.15	4.35	5.41	5.40	4.61
Skin Thickness of Root (cm)	3.1	3.1	4.2	3.2	3.3	4.6	3.4	3.4	4.6
Max Blade Deflection (m)	4.9	4.8	4.5	4.4	4.2	3.9	4.5	4.5	4.2
Gearbox Ratio	106.1	8.8	-	91.2	6.9	-	92.4	7.7	-
Generator Stator Radius (m)	0.53	1.17	2.2	0.53	1.17	2.0	0.53	1.17	2.08
Generator Stack Length (m)	0.46	0.67	1.22	0.46	0.67	1.1	0.46	0.67	1.15
Blade Mass (ton)	8.54	8.47	9.10	7.51	6.84	7.52	8.01	7.83	8.41
Gearbox Mass (ton)	22.0	25.4	-	18.1	14.2	-	18.4	18.3	-
Generator Mass (ton)	12.8	16.9	90.6	12.8	16.9	73.5	12.8	16.9	80.9
ICC (USD)	5350	5067	5784	2854	2488	2924	2912	2691	3158
AOE (USD)	316	319	307	127	125	119	113	115	110
AEP (MWh)	12558	12708	12165	11772	11443	10816	10024	1026	9615
LPC (USD/kWh)	0.0606	0.0583	0.0649	0.0310	0.0290	0.0336	0.0355	0.0330	0.0388

Table 6-11: Optimized 5 MW wind turbines for all wind site classes and drive trains

	5 MW								
	Offshore			Coastal			Inland		
Property (Unit)	DFIG 3G	PM 1G	DD	DFIG 3G	PM 1G	DD	DFIG 3G	PM 1G	DD
Rotor Radius (m)	69.2	66.2	61.9	64.5	62.0	58.0	67.3	66.0	63.0
Rated Rotational Speed (rpm)	9.2	10.0	11.7	10.5	11.2	13.1	9.8	10.2	11.5
Rated Wind Speed (m/s)	10.8	11.0	11.5	11.2	11.5	12.0	10.9	11.0	11.4
Tip Speed Ratio	6.22	6.30	6.60	6.29	6.30	6.64	6.31	6.39	6.66
Peak Power Coefficient	0.465	0.469	0.480	0.468	0.469	0.482	0.469	0.473	0.482
Max Chord length (m)	7.60	7.11	6.07	6.95	6.65	5.62	7.20	6.88	6.07
Skin Thickness of Root (cm)	3.8	4.2	5.6	4.2	4.3	5.9	4.2	4.5	5.8
Max Blade Deflection (m)	6.1	5.8	5.4	5.7	5.4	5.1	5.9	5.8	5.5
Gearbox Ratio	130.0	10.0	-	114.7	9.0	-	122.7	9.8	-
Generator Stator Radius (m)	0.64	1.32	2.56	0.64	1.32	2.47	0.64	1.32	2.58
Generator Stack Length (m)	0.52	0.87	1.65	0.52	0.87	1.58	0.52	0.87	1.66
Blade Mass (ton)	16.93	16.33	17.43	15.65	14.63	16.04	16.96	17.04	18.56
Gearbox Mass (ton)	47.8	58.5	-	40.2	44.7	-	44.1	55.9	-
Generator Mass (ton)	20.5	27.1	165.7	20.5	27.1	149.1	20.5	27.1	168.9
ICC (USD)	10151	9471	10881	6141	5577	6527	6440	6019	7180
AOE (USD)	515	510	491	210	208	199	190	192	186
AEP (MWh)	20390	20171	19281	19329	19071	18026	16879	17107	16364
LPC (USD/kWh)	0.0667	0.0644	0.0725	0.0373	0.0352	0.0412	0.0430	0.0405	0.0479

Table 6-12: Optimized 10 MW wind turbines for all wind site classes and drive trains

	10 MW								
	Offshore			Coastal			Inland		
Property (Unit)	DFIG 3G	PM 1G	DD	DFIG 3G	PM 1G	DD	DFIG 3G	PM 1G	DD
Rotor Radius (m)	94.0	93.4	93.6	100.4	99.7	95.8	108.0	105.68	104.75
Rated Rotational Speed (rpm)	7.1	7.2	7.4	6.4	6.5	7.2	5.7	6.0	6.2
Rated Wind Speed (m/s)	11.0	11.0	11.0	10.5	10.5	10.8	10.0	10.1	10.2
Tip Speed Ratio	6.35	6.38	6.59	6.43	6.48	6.67	6.44	6.57	6.69
Peak Power Coefficient	0.471	0.473	0.480	0.475	0.476	0.482	0.475	0.479	0.483
Max Chord length (m)	9.92	9.77	9.20	10.35	10.13	9.21	11.09	10.47	10.02
Skin Thickness of Root (cm)	6.1	6.3	7.6	6.4	6.7	8.1	6.3	7.0	7.9
Max Blade Deflection (m)	8.30	8.25	8.26	8.88	8.81	8.46	9.56	9.35	9.27
Gearbox Ratio	169.1	14.0	-	187.0	15.3	-	210.8	16.7	-
Generator Stator Radius (m)	0.82	1.68	3.72	0.82	1.68	3.75	0.82	1.68	3.93
Generator Stack Length (m)	0.63	1.08	2.48	0.63	1.08	2.50	0.63	1.08	2.64
Blade Mass (ton)	47.87	47.82	54.53	55.80	56.10	59.28	63.25	64.97	69.38
Gearbox Mass (ton)	136.6	252.7	-	157.5	313.4	-	196.3	379.9	-
Generator Mass (ton)	38.9	51.4	479.5	38.9	51.4	492.2	38.9	51.4	563.6
ICC (USD)	32104	31620	36971	28888	28582	30914	30826	30359	34613
AOE (USD)	1010	1021	1025	450	456	420	420	423	420
AEP (MWh)	39844	40375	40551	42443	43156	41792	38689	39088	38771
LPC (USD/kWh)	0.0924	0.0905	0.1012	0.0673	0.0657	0.0740	0.0774	0.0756	0.0852

Table 6-13: Optimized 20 MW wind turbines for all wind site classes and drive trains

	20 MW								
	Offshore			Coastal			Inland		
Property (Unit)	DFIG 3G	PM 1G	DD	DFIG 3G	PM 1G	DD	DFIG 3G	PM 1G	DD
Rotor Radius (m)	142.4	150.9	152.3	164.1	162.3	164.2	177.7	175.9	178.0
Rated Rotational Speed (rpm)	4.5	4.2	4.2	3.6	3.8	3.7	3.2	3.3	3.3
Rated Wind Speed (m/s)	10.5	10.0	10.0	9.5	9.5	9.5	9.0	9.0	9.0
Tip Speed Ratio	6.47	6.63	6.68	6.58	6.80	6.75	6.63	6.48	6.77
Peak Power Coefficient	0.476	0.481	0.482	0.480	0.485	0.484	0.481	0.486	0.484
Max Chord length (m)	14.52	14.67	14.61	16.18	15.05	15.41	17.28	16.11	16.65
Skin Thickness of Root (cm)	9.3	10.4	11.0	9.8	11.7	11.4	9.9	11.8	11.2
Max Blade Deflection (m)	12.6	13.4	13.5	14.6	14.4	14.6	15.8	15.6	15.8
Gearbox Ratio	264.4	23.8	-	329.8	26.3	-	374.2	29.9	-
Generator Stator Radius (m)	1.04	2.10	5.61	1.04	2.10	5.61	1.04	2.10	5.77
Generator Stack Length (m)	0.78	1.38	3.84	0.78	1.38	4.31	0.78	1.38	4.67
Blade Mass (ton)	161.28	192.56	203.48	217.34	238.43	240.55	254.88	279.04	277.17
Gearbox Mass (ton)	520.6	1647.3	-	722.0	2039.5	-	873.5	2680.0	-
Generator Mass (ton)	73.6	97.4	1536.3	73.6	97.4	1708.2	73.6	97.4	1931.1
ICC (USD)	163819	172713	186542	192620	196676	207623	201883	208151	218638
AOE (USD)	2110	2212	2220	985	997	1001	931	946	950
AEP (MWh)	83954	88791	89181	95405	96885	97411	88773	90568	91150
LPC (USD/kWh)	0.1876	0.1869	0.1991	0.1784	0.1793	0.1878	0.1999	0.2018	0.2102

Table 6-15: Number of iterations and durations of the optimizations in 3 MW designs with the RNA design tool

		3 MW					
		Offshore		Coastal		Inland	
		No. of Iterations	Duration (s)	No. of Iter.	Duration (s)	No. of Iter.	Duration (s)
DFIG 3G	Rotor Optimization	300	0.961	3082	8.755	310	0.983
	Three Stage Gearbox Optimization	885	4.234	7561	33.856	895	4.199
	DFIG Optimization	91	0.088	1570	1.582	91	0.090
	Modules and MCA Evaluation	27	7.168	580	147.8	27	7.151
	Total	-	12.451	-	192.650	-	12.423
PM 1G	Rotor Optimization	2932	9.210	428	1.406	672	2.124
	Single Stage Gearbox Optimization	1189	2.180	157	0.283	249	0.468
	PMG Optimization	883	0.774	109	0.103	178	0.160
	Modules and MCA Evaluation	291	77.836	33	8.592	56	14.686
	Total	-	90.000	-	10.384	-	17.438
DD	Rotor Optimization	1079	3.343	549	1.673	2727	8.157
	PMG Optimization	684	0.696	353	0.356	2019	2.079
	Modules and MCA Evaluation	81	21.576	39	9.413	248	63.285
	Total	-	25.615	-	11.442	-	73.521
Total		-	142.883	-	228.636	-	119.727

Table 6-16: Number of iterations and durations of the optimizations in 5 MW designs with the RNA design tool

		5 MW					
		Offshore		Coastal		Inland	
		No. of Iterations	Duration (s)	No. of Iter.	Duration (s)	No. of Iter.	Duration (s)
DFIG 3G	Rotor Optimization	3503	9.673	1822	5.387	2048	5.775
	Three Stage Gearbox Optimization	8634	38.382	4674	21.686	5151	23.310
	DFIG Optimization	1951	1.790	871	0.831	1075	1.014
	Modules and MCA Evaluation	647	171.037	287	74.276	355	94.074
	Total	-	220.882	-	102.180	-	124.173
PM 1G	Rotor Optimization	648	2.061	522	1.730	2550	6.200
	Single Stage Gearbox Optimization	213	0.402	177	0.345	933	1.325
	PMG Optimization	163	0.153	136	0.130	703	0.488
	Modules and MCA Evaluation	50	13.055	41	10.396	230	61.746
	Total	-	15.671	-	12.601	-	69.759
DD	Rotor Optimization	2358	7.033	1947	5.903	494	1.588
	PMG Optimization	1669	1.663	1388	1.406	316	0.322
	Modules and MCA Evaluation	206	52.818	170	42.298	33	8.362
	Total	-	61.514	-	49.607	-	10.272
	Total	-	311.969	-	177.621	-	214.641

Chapter 7

Utility of the Automatic Design of Rotor Nacelle Assembly (RNA) Tool

7-1 Overview

In this section the usefulness of the RNA design tool are discussed. Utility and possible purposes of the tool is divided in three sections: for preliminary designs, utilization of the tool with other algorithms and comparisons of the designs. In the latter a drive train comparison example is given for a range of rated powers.

7-2 Preliminary Design of the RNA

The automatic design of the RNA design tool can be used for many purposes. Firstly it is a preliminary design tool that can guide the manufacturers in the unexplored rated powers. The tool is able to capture the relationships between components and their individual importances to the selected objective function. Thus it designs an optimum for the whole system and not for each component. Nonetheless this does not mean that the component designs are not optimized to their maximum operational capacity. In general, the designs from the RNA design tool are similar to the available and realized examples in the literature and industry but slightly different and lead to a lower levelized production cost. Furthermore the tool is sensitive to the changes in the inputs and even slight changes such as the minimum number of teeth of the gears in the gearbox, which are studied in the previous section. The designs alter with these differences and not only in the components that are directly related to the different inputs. This shows that the relationships between the components are captured properly.

7-3 Working with Other Design Tools

The RNA design tool can be used combined with other optimization tools. Since the tool is able to design RNA for different wind site classes it can be used with wind farm design tools,

where the properties of the RNA are necessary for input. Also different rated powers can be applied at the same wind farm and differences between the results can be analysed to reach an optimum combination of rated power, number of turbines and layout. For instance the tool can be run consecutively with the wind farm design emulation of Dr. Michiel Zaaijer for the purposes given above.

7-4 Comparison of the Designs

Besides from preliminary design, the tool can also be used for comparing different designs. This is possible because of the flexibility of the user to be able to select different inputs to the tool. Furthermore each time the tool is run it provides three different drive train designs. Thus the tool provides the possibility to compare RNA designs in different rated powers, wind site classes and drive trains. The different drive train designs are one of the main functions of the algorithm as it constructs three RNA with selected drive trains for the given rated power and the wind site class. In order to demonstrate the utility of the RNA design tool a comparison between the drive trains will be conducted in this section. The properties that are given in tables 6-10, 6-11, 6-12 and 6-13 will be compared for different drive trains at different rated powers.

There are three types of trends between the different drive trains in different rated powers. The comparison of the drive trains is quite similar in rated powers of 3 and 5 MWs and the other two trends can be seen in 10 and 20 MW rated powers. General behaviour of these trends will be explained consecutively.

7-4-1 Comparison of the Drive Trains at 5 MW and Below Rated Power

In the first place it is seen that the rated rotational speed is kept slightly higher in the PM 1G than DFIG 3G to lower the size of the single stage gearbox and the rated rotational speed is kept highest in DD in order to keep the PM generator smaller. The power coefficient and the tip speed ratio are kept highest in DD due to the lower drive train efficiencies appointed to the drive train. But on the other hand during the optimization of the DD the optimizer chooses to increase the rated wind speed instead of the rotor radius. This is because an increase in the rotor radius does not affect the power produced as much as the rated wind speed, that is why the rotor radius of the DD is the lowest. Also as it can be seen from figures 6-3, 6-4 and 6-5 in below 5 MW rated power the relative costs of the major components such as the rotor, gearbox and the generator adds up to a maximum relative cost of 35% for DFIG 3G and PM 1G drive trains, whereas it is almost 50% for the DD. This forces the optimizer to lower the sizes of the rotor and the generator by decreasing the rotor radius and increasing the rated rotational speed of the rotor. Moreover the permanent magnet generator used in the DD is one of the most expensive components used in all of the drive trains, due to this reason the optimizer tries to lower the costs of the rest of the components by lowering the rotor radius. Nonetheless the initial capital cost of the DD is always the highest. Besides higher rated wind speeds, lower drive train efficiency and lower rotor radii always result in the lowest annual energy production for the DD. High initial capital costs and low annual energy production result in the highest levelized production costs for the DD.

Three stage gearbox is usually heavier than the single stage gearbox in the 3 MW range, however for larger wind turbines this situation reverses and produces heavier single stage gearboxes than three stage gearboxes. The optimizer is allowed to move in this direction because the cost price in Euro/kg of the single stage gearbox is less than the one for the three stage gearbox. PM 1G has the highest drive train efficiency. This allows the optimizer to lower its rotor radius to decrease its initial capital costs, which as a result produces the lowest levelized production costs among all the drive trains.

The relative average levelized production costs of DFIG 3G and DD are calculated according to the PM 1G. On average the DFIG 3G and DD are found to be 6 and 15% more expensive respectively for 3 MW rated power and for both of the cases the difference is highest in the inland designs and lowest on the offshore applications. For the 5 MW rated power DFIG 3G is 5% more expensive whereas DD is 16%.

7-4-2 Comparison of the Drive Trains at 10 MW Rated Power

The differences between the drive trains are not completely different from the previous rated powers, therefore the most significant alterations between 10 MW and 5 MW and below will be pointed out in this section. The annual energy productions are highest in the PM 1G designs for the onshore applications. On the other hand for the offshore designs the highest annual energy production is seen in the DD designs. Nevertheless this is not enough to close the gap between the levelized production costs of DD and other drive trains as it is once again the highest among them. The levelized production costs of the DFIG 3G is 2% larger than the PM 1G whereas the DD is 12% more expensive. It is seen that the difference between the DFIG 3G and PM 1G has decreased significantly. One of the important observations is that at this rated power the cost of the single stage gearbox passes the three stage gearbox cost. Besides this can be seen from the lower relative costs of the DFIG 3G. Finally it should be noted that the increase in the single stage gearbox is expected since the possible transmission ratios are passed in the onshore design.

7-4-3 Comparison of the Drive Trains at 20 MW Rated Power

There are two types of comparison in 20 MW rated power, one is for the offshore wind site designs which is fairly similar to the comparison in the 10 MW range and the other is for the onshore designs. The comparison of the drive trains has one significant difference from 10 MW comparison of the drive trains. At this rated power the DD designs always has the highest rotor radius and because of this the annual energy productions of the DD designs are always highest. From from figures 6-3, 6-4 and 6-5 it can be seen that the relative costs of the major components in the DFIG 3G and PM 1G are adding up to maximum of 50% of the turbine capital cost and the relative rotor and generator costs in the DD adds up to 55%. The difference between the relative costs diminished compared to lower rated power designs. This allows the optimizer to increase the rotor radii of the DD more than it was for the lower rated powers. At 20 MW the relative costs of the major components in DFIG 3G and PM 1G become more sensitive to the changes in the rotor radius, whereas the DD relative costs are almost the same. The difference can be seen in all of the wind sites of the 20 MW designs.

On onshore designs where the rotational speeds decrease even more than the offshore applications, the cost of the single stage gearbox becomes much more expensive than a three stage gearbox. This results in the lowest initial capital costs for the DFIG 3G drive trains, which eventually leads to the lowest levelized production costs in both cases. This is one of the most interesting observations for the onshore applications at 20 MW rated power.

Chapter 8

Conclusions

The primary objective of this project was to have and validate an engineering model that performs a multi-level preliminary design optimization of the Rotor Nacelle Assembly (RNA). The model was aimed to focus on the trade-offs and interactions between the components of the RNA for selected drive trains in offshore and onshore wind farms. Furthermore it was targeted to use physical models that allow rapid assessment with necessary accuracy and address the functionalities mostly desired by the users.

Firstly, the multi-level optimization process was investigated and an overview of the optimization was constructed by applying the decomposition methods to the possible design variables and constraints of the components involved in the design. This way the multilevel perspective of the project was achieved. Later, engineering design models were constructed for rotor, gearbox and generator. Besides, cost models for all of the wind turbine and farm elements were introduced. During the modelling part the targets of the project were realized by instituting three different drive trains and wind site classes to the designs. From these models the constraints and global and local design variables were drawn.

In the previous project the implementation of the engineering design optimization was not successful. It was concluded that Matlab's optimization toolbox was not suitable for implementation of the design algorithm. This problem with Matlab was solved by selecting another high level programming language, namely Python, to work with. Additionally an extra multidisciplinary analysis and optimization framework was utilized. This has been a suitable choice for conducting higher level optimizations, since the automatic design of RNA was implemented successfully. But, above all the success of the implementation depended on the different modelling of the RNA in this project.

The tool was verified by doing performance tests and checking the responses to the changes in the input parameters. Also the results were compared among themselves and to examples found in the literature and the industry. This analysis was done for 3, 5, 10 and 20 MW rated power wind turbines in offshore, coastal and inland wind sites. The comparisons to selected examples revealed the reasonableness of the designs with similar design and state variables and the differences between them benefited the designs with lower levelized production costs.

Expected trends for scaling of the wind turbines and reasonable differences between the designs in different wind site classes were found. Comparison of the drive trains in different rated powers showed the advantages and the disadvantages of different topologies. On the other hand unexpected results such as offshore levelized production costs being lower than for inland applications at 20 MW rated power, due to the large increase in the rotor diameters in inland sites, have been discovered. Different type of rotor designs with lower skin thicknesses and larger chords have been constructed by the tool. Heavier single stage gearboxes and generators designed by the tool differentiated the results from the given examples for comparison.

Performance tests showed that the runtime of the tool is below five and half minutes which is assumed to be acceptable for rapid assessments. There were only some minor exceptions of run times that took longer time to find an optimum. Finally the utilization of the tool was demonstrated. The tool can be integrated with other design tools for a complete optimization of wind farms or allows comparison between different designs and lastly can guide the wind turbine manufacturers in the uncharted rated powers with a preliminary design.

Another drawback of the project is that there has been no contact with any possible users, except Dr. Michiel Zaaijer who designed the offshore wind farm design emulation. In order to be able to integrate the RNA design tool with the wind farm design emulation more calculations were added to this project. This has been the only additional implementation to the tool in order to address the functionalities desired by the users. However this drawback was tried to be overcome by implementing greater variety of inputs by the users. So possible design scenarios were considered and implemented in the functionalities of the tool. For example the tool was designed to provide three wind site classes and drive trains in a great range of rated power to the users.

Chapter 9

Recommendations

It would be beneficial to extend the algorithm by implementing an initial guess code for the optimization process. The computational times of the tool will definitely benefit from this and the longer run times that were observed for some exceptional optimizations in 10 and 20 MW rated power can be eliminated.

As of now the computational times are below five and half minutes and this can be extended to seven and half which can be accepted as a reasonable time for a preliminary design optimizer. This will provide the opportunity to improve the generator modelling, which is the simplest amongst all. During the project a more elaborate model for the generator was not implemented because it was believed that increasing the design variables further in the optimization would result in excessive computational times. However implementation of the initial guess code and allowing the runtime to extend to seven and half minutes will create more time for further computation of the detailed generator design.

Implementing a constraint for the tip speed of the rotor in onshore applications, could alter the designs slightly. The tip speed constraint would affect the tip speed ratio, rotor radius, rated wind speed and the rated rotational speed of the rotor. The effects of this approach can be analysed and differences in the designs can be observed. On the other hand an improved gearbox mass model would be useful for future work in the gearbox design. The coefficients used in the model were checked with realized gearboxes up to an extent. Despite that, further study of the gearbox is needed for more accurate results.

One of the most interesting studies would be to test the Rotor Nacelle Assembly (RNA) design tool with a wind farm design optimizer. This would reveal the optimum configurations for wind farms without loosing the connection between the wind turbine and farm designs.

Appendix A

Mass and Cost Models

A-1 Introduction

The mass and cost models for the major components of the wind turbine and the wind farm have been used. The relations are generally based on design parameters and higher level design variables such as rotor diameter, wind turbine rating or hub height. On the other hand some relations have either have fixed values for different concepts and scales or have their local key turbine descriptors. The wind turbine configuration that the mass and cost models are based on is three bladed, upwind, pitch controlled, variable speed wind turbine and its variants. The results of the model are based on 2002 dollars in order to provide consistency. In case of lack of cost data from 2002 the value was converted to 2002 dollars before developing the cost and scale factors. Economic models for onshore and offshore systems will be introduced in this section [14].

A-1-1 Initial Capital Cost

The initial capital cost (ICC) includes the cost of the turbine system and balance of station. The construction financing or financing fees are not present in any of the cost, because they are taken into account in the fixed charge rate (FCR). Furthermore the costs also don't include a debt service reserve fund, which is assumed to be zero for balance sheet financing. The cost elements that are introduced in the model is as follows [14]:

- Rotor
  - Blades
  - Hub
  - Pitch mechanisms and bearings
  - Spinner, nose cone
- Drive train, nacelle

  - Low-speed shaft
  - Bearings
  - Gearbox
  - Mechanical brake, high-speed coupling, and associated components
  - Generator
  - Variable speed electronics
  - Yaw drive and bearing
  - Main frame
  - Electrical connections
  - Hydraulic and cooling systems
  - Nacelle cover
- Control, safety system, and condition monitoring
- Tower
- Balance of station
  - Foundation/support structure
  - Transportation
  - Roads, civil work
  - Assembly and installation
  - Electrical interface/connections
  - Engineering permits

For the model of offshore applications teh following elements are also introduced:

- Marinization (added cost to handle marine environment)
- Port and staging equipment
- Personal access equipment
- Scour protection
- Surety bond (to cover decommissioning)
- Offshore warranty premium

A-1-2 Annual Operating Expenses

Land Lease Cost/Bottom Lease Cost

This cost is the rental or lease fees that are charged for turbine installation. It applies both on onshore and offshore applications and it is expressed in units of $/kWh [14].

Levelized operation and maintenance cost (OM) Cost

Levelized OM cost is one of the biggest contributors to the annual operating expenses (AOE). It includes labour, parts and supplies for scheduled and unscheduled turbine maintenance, parts and supplies for equipment and facilities maintenance and labour for administration and support. It is expressed in units of $/kWh [14].

Levelized Replacement/Overhaul Cost

levelized replacement/overhaul cost (LRC) analyse the cost of overhauls and major replacements over the lifetime of the wind turbine and it is expressed in $/kW [14].

A-1-3 Net Annual Energy Production

The net net annual energy production (AEP) is calculated for a given annual average wind speed. The gross AEP need to be adjusted depending on the blade soiling losses, array losses, machine availability, power coefficient, mechanical and electrical conversion losses [14].

A-2 Land Based Component Formulas

A-2-1 Blades

The mass and cost models of the blade are introduced in section 4-5-2.

A-2-2 Hub

The scaling of hub mass and cost has started with the WindPACT project and it was continued and advanced by the data from industry websites and Low Wind Speed Technology (LWST) projects. However the mass calculation of the hub does not take in to account the dynamics of the system but only the peak root moments based on static analysis. Therefore a coefficient of 1.92 was placed in front of the formula to better estimate the hub mass. Thus the mass of the hub depends on the mass of a single blade mass in the following formula [14]:

$$M_{hub} = 1.92(0.954M_{blade} + 5680.3) \tag{A-1}$$

The equation for the hub mass is [14]:

$$C_{hub} = 4.25M_{hub} \tag{A-2}$$

A-2-3 Pitch Mechanisms and Bearings

The model that was started with the WindPACT rotor design study data was finalized with information from the industry and LWST projects. Bearing mass actuator and drives were taken in to account. The actuator and drive mass was assumed to be 32.8% of the bearing mass plus 555 kg [14].

$$M_{pbearing} = 0.1295(3M_{blade}) + 491.31 \tag{A-3}$$

$$M_{pitchtot} = 1.328M_{pbearing} + 555 \tag{A-4}$$

The cost of the pitch bearing system is a function of the rotor diameter, D. The actuator and the pitch housing was estimated to be 128% of the bearing cost. So the total cost of the pitch system is [14]:

$$C_{pitchtot} = 2.28(0.2106D^{2.6578}) \tag{A-5}$$

A-2-4 Spinner, Nose Cone

New formula was derived from data in WindPACT drive train and LWST reports. The mass and the cost of the nose cone is a function of the rotor diameter [14]:

$$M_{ncone} = 18.5D - 520.5 \tag{A-6}$$

$$C_{ncone} = 5.57M_{ncone} \tag{A-7}$$

A-2-5 Low-Speed Shaft

Once again the rotor diameter was used in order to formulate the mass and cost models. Several drive train configurations do not use the low-speed shaft so for direct drive, single-stage drive or multi-generator drive systems the low-speed shaft model is not necessary [14].

$$M_{lss} = 0.0142D^{2.888} \tag{A-8}$$

$$C_{lss} = 0.01D^{2.887} \tag{A-9}$$

A-2-6 Main Bearings

A correction on the mass and cost models that was reported in the WindPACT rotor design was made. Bearing mass and the bearing housing was assumed to be same weight [14].

$$M_{mbearing} = \left(\frac{8D}{600} - 0.033\right) 0.0092D^{2.5} \tag{A-10}$$

$$C_{mbearing} = 17.6\,(2M_{mbearing}) \tag{A-11}$$

A-2-7 Gearbox

The mass and cost models of the blade are introduced in section 4-5-3.

A-2-8 Mechanical Brake, High-Speed Coupling, and Associated Components

Machine rating is used for the determination of the cost and the mass, is depending on the assumption that a kilogram of the component costs 10$.

$$C_{brk-cpl} = 1.9894P - 0.1141 \tag{A-12}$$

$$M_{brk-cpl} = C_{brk-cpl}/10 \tag{A-13}$$

A-2-9 Generator

The generator mass and cost model is detailed in section 4-5-4.

A-2-10 Variable-Speed Electronics

The mass of the variable speed electronics are ignored due to the fact that they are very low compared to other components. The power converter that is modelled in this analysis is assumed to be capable of handling full power output. The cost is calculated as a function of the rated machine power as follows:

$$C_{vse} = 79P \tag{A-14}$$

A-2-11 Yaw Drive and Bearing

The calculations of the yaw bearing cost is based on the rotor diameter. The total cost of the yaw subsystem is assumed to be twice of the yaw bearing cost. In the mass calculation the bearing housing mass was assumed to be 60% of the bearing mass. The calculation is based on rotor diameter.

$$M_{yaw} = 1.6\left(0.0009D^{3.314}\right) \tag{A-15}$$

$$C_{yaw} = 2\left(0.0339D^{2.964}\right) \tag{A-16}$$

A-2-12 Mainframe

The platforms and the railings of the mainframe is calculated on based on price per kilogram values. The cost of the main frame was calculated using rotor diameter. However different type of drive train configurations requires different type of mainframe. Therefore the distinction between concepts has been made. The difference between the mainframes is due to different distribution of loads between types. This results in varying length of the mainframe. The mass functions of the mainframe also depend on the rotor diameter and the same power law was applied to all of them. Finally the additional mass of the platforms and railings were assumed to be 12.5%. The costs for platform and railings were calculated on $/kg basis.

Three-Stage Drive with High-Speed Generator

$$M_{mframe\_3s} = 2.233D^{1.953} \tag{A-17}$$

$$C_{mframe\_3s} = 9.489D^{1.953} \tag{A-18}$$

Single-Stage Drive with Medium-Speed, Permanent-Magnet Generator

$$M_{mframe\_1s} = 1.295D^{1.953} \tag{A-19}$$

$$C_{mframe\_1s} = 303.96D^{1.067} \tag{A-20}$$

Direct Drive

$$M_{mframe\_dd} = 1.228D^{1.953} \tag{A-21}$$

$$C_{mframe\_dd} = 627.28D^{0.85} \tag{A-22}$$

Platforms and Railings

$$M_{plat-rail} = 0.125 M_{mframe} \tag{A-23}$$

$$C_{plat-rail} = 8.7 M_{plat-rail} \tag{A-24}$$

A-2-13 Electrical Connections

The switchgear and tower wiring is included in this model. Cost is calculated by the machine rating in kW

$$C_{elcon} = 40P \tag{A-25}$$

A-2-14 Hydraulic and Cooling Systems

In this model the mass is dependent on the machine rating in kW and the cost is calculated by price per machine rating in kW.

$$M_{hyd-cool} = 0.08P \tag{A-26}$$

$$C_{hyd-cool} = 12P \tag{A-27}$$

A-2-15 Nacelle Cover

In this analysis the nacelle cover of all the drive trains are considered the same. Therefore one function is derived for all the configurations.

$$C_{nacelle} = 11.537P + 3849.7 \tag{A-28}$$

$$M_{nacelle} = C_{nacelle}/10 \tag{A-29}$$

A-2-16 Control, Safety System, Condition Monitoring

WindPACT studies have acknowledged \$10 000 for the control, safety system, condition monitoring of a 750 kW wind turbine. However this data was applicable to 1999 designs. Now the importance of condition monitoring is more valued by the operators. This was taken account by increasing the cost of the system to \$35 000 regardless of the machine rating for the onshore applications. As for the offshore applications the number was increased to \$55 000, due to utilization of more sophisticated and extensive systems.

A-2-17 Tower

The towers that are taken in to consideration are all steel tubular towers. The tower mass scaling is done according to the rotor swept area and the hub height. There are two tower designs that are considered. First one is the initial WindPACT rotor study base line, where turbines are designed for trade-offs between buckling and overturning moment for set of load conditions. Also fatigue loads are estimated. The second one is the WindPACT rotor study

final design, where advanced technologies such as tower feedback in control system, flap-twist coupling in the blade and reduced blade solidity in conjunction with higher tip speed are used. Commercial turbines were compared with these scaling rules, assuming different rotors have similar thrust coefficients. The baseline scaling relationship represents the commercial wind turbines in a somewhat conservative way. The final design scaling reflects towers with advanced technology innovation and projects masses that are lower than what is commercially available. This project takes into account the latter tower design.

$$M_{atwr} = 0.2694AH_{hub} + 1779 \tag{A-30}$$

The cost is scaled with using the cost of steel in 2002 dollars.

$$C_{twr} = 1.5M_{twr} \tag{A-31}$$

A-2-18 Foundation

The foundation that is studied is a hollow drilled pier. The foundation mass was not calculated only the cost function was established. The function is dependent on the rotor swept area and hub height, which are directly proportional to overturning moment.

$$C_{fndtn} = 303.24(AH_{hub})^{0.4037} \tag{A-32}$$

A-2-19 Transportation

The cost estimation is a function of the machine rating. The costs reflect the onshore turbines transportation. A transportation cost factor, k_{trans} is used in this analysis.

$$k_{trans} = 1.581 \cdot 10^{-5}P^2 - 0.0375P + 54.7 \tag{A-33}$$

with the transportation cost factor the cost of transportation is calculated as follows:

$$C_{trans} = k_{trans}P \tag{A-34}$$

A-2-20 Roads, Civil Work

These expenses are about the modification of road widths, crane pads to handle larger machines. The function depends on machine rating in kW. As the transportation cost a civil works cost factor, k_{civil} is used:

$$k_{civil} = 2.17 \cdot 10^{-6}P^2 - 0.0145P + 69.54 \tag{A-35}$$

$$C_{civil} = k_{civil}P \tag{A-36}$$

A-2-21 Assembly and Installation

A model that takes into account the physical size of the largest components was used. The cost is dependent on the hub height and the rotor diameter.

$$C_{assem-ins} = 1.965(H_{hub}D)^{1.1736} \tag{A-37}$$

A-2-22 Electrical Interface/Connections

The turbine transformer and the turbines share of cables to substation is included in this cost model. A cost factor, k_{elc} is used to calculate the cost.

$$k_{elc} = 3.49 \cdot 10^{-6} P^2 - 0.0221P + 109.7 \tag{A-38}$$

$$C_{elc} = k_{elc} P \tag{A-39}$$

A-2-23 Engineering, Permits

The cost of designing and permitting the entire wind facility per wind turbine is studied in this model. These costs are dependent on locations, environmental conditions, availability of electrical grid access, and local permitting requirements. A cost factor, $k_{eng-Permt}$, is used to calculate the cost.

$$k_{eng-permt} = 9.94 \cdot 10^{-4} P + 20.31 \tag{A-40}$$

$$C_{eng-permt} = k_{eng-permt} P \tag{A-41}$$

A-2-24 Levelized Replacement Cost

This is a sinking fund factor to model the long-term replacement and overhauling of major turbine elements such as generators , blades and gearboxes. It is uses a cost factor, k_{LRC}, that depends on the machine rating in kW.

$$k_{LRC} = 10.7P \tag{A-42}$$

$$C_{LRC} = k_{LRC} P \tag{A-43}$$

A-2-25 Operations and Maintenance

OM costs cover the scheduled and unscheduled maintenance and operations cost of a wind farm. A fixed cost of $ 0.007kWh is used in this model. The calculation is made depending on the AEP as follows:

$$C_{OM} = 0.007 E_t \tag{A-44}$$

A-2-26 Land Lease Costs

Normally a lease fee is paid for the land that is used by the wind turbines. This fee is mostly dependent on the wind class of the site, potential market price for the wind, nature and value of the land. The cost model used is dependent on the AEP.

$$C_{_{LLC}} = 0.00108 E_t \tag{A-45}$$

A-3 Offshore Based Component Formulas

A-3-1 Introduction

In order to evaluate offshore wind technology the model is expanded. Most of the land based components that are introduced are also applicable to offshore design, however some of the models that were used are different for offshore and onshore. In addition few more offshore specific components are included. The models handle shallow water installations. The installations are based on 500 MW wind farm that is 5 miles far from coast with 10 m depth. The spacing between the turbines is 7 rotor diameters. Installed wind turbines have a rated power of 3 MW, 80 m hub height and 90 m rotor diameter. The cost models that are introduced are in 2003 dollars.

A-3-2 Marinization

The components that are used in the offshore wind farms need to survive in the offshore ocean environment. Therefore the marinization component of the cost model covers the preparation of these components such as: improved seals for gearboxes, generators, electrical components, electrical connections, special coatings and paintings. The marinization cost is assumed to be 13.5% of the turbine and tower costs.

$$C_{marin} = 0.135 C_{turb-twr} \tag{A-46}$$

A-3-3 Offshore Support Structure

The onshore wind turbines are installed upon a solid foundation, but the offshore turbines needs to be attached from the sea level to the seabed. This model assumes a steel pile driven into the seabed. The cost model depends on the machine rating.

$$C_{OSS} = 300P \tag{A-47}$$

A-3-4 Offshore Transportation

There are two types of transportation costs when installing offshore wind turbines. One is the transportation of the turbine components to the port staging and assembly area. The other one is the transportation of the turbine to the installation area. Latter is taken into consideration in the offshore installation costs. The costs of transportation can be significantly reduced by locating the fabrication facilities next to a port or the staging areas, due to the high costs of transporting large structures over the road or the rail. A cost factor is introduced in $\$/kW$ that depends on the machine rating in order to model the offshore transportation costs.

$$k_{OTC} = 1.581 \cdot 10^{-5} P^2 - 0.0375P + 54.7 \tag{A-48}$$

$$C_{OTC} = k_{OTC} P \tag{A-49}$$

A-3-5 Port and Staging Equipment

Installation in the offshore wind farms requires specific components. Special ships and barges are used to install, towers, turbines, piles, underwater electrical lines. Furthermore for the ongoing operation and maintenance of the wind farm these ships need to be employed. The model is formulated depending on the machine rating.

$$C_{port-stage} = 20P \tag{A-50}$$

A-3-6 Offshore Turbine Installation

The erection of a turbine in the sea needs cranes and special barges that are able to keep its position under the influence of winds and currents. On the other hand this model also includes the transportation of the turbine components to the installation site at the sea. The model depends on the machine rating as follows:

$$C_{OTI} = 100P \tag{A-51}$$

A-3-7 Offshore Electrical Interface and Connection

The electricity produces in offshore wind turbines is transmitted by the electrical transmission system of the wind farm. Likewise the electrical cables that are connected between the turbines are also necessary to gather the turbine power. Therefore the cost model is taking into account the cabling between the turbines and the connection to the grid onshore. It should be noted that the model is reflecting the cost analysis of a wind farm situated 5 miles away from the shore with 7 rotor diameter distance between the wind turbines and a water depth of 10 m. The calculation depends on the machine rating.

$$C_{offelc} = 260P \tag{A-52}$$

A-3-8 Offshore Permits, Engineering, and Site Assessment

Developing detailed engineering plans permitting and measuring wind conditions for a wind site is more time consuming than a land based process. The equation for the cost depends on the machine rating in kW.

$$C_{offeng-prmt} = 37P \tag{A-53}$$

A-3-9 Personnel Access Equipment

The servicing of the offshore wind farms can be done by marine vessels, small boats or helicopters. The safety of the personnel that is performing the services requires personnel access equipments along with the regular ones like fall protection equipment. This model takes into consideration the need of special boat access ramps or docking equipment, lifesaving equipment, special tool lifts and emergency survival equipment that is placed in each turbine. The cost for these equipments is estimated with a fix prize of $60,000 per turbine.

A-3-10 Scour Protection

The piles that are used for mounting the wind turbines to the seabed will loosen up due to scouring. The currents will eventually have a tendency to move the bottom material from the base. To prevent such foundation failure, rip rap (graded boulder and rock) are placed around the foundation.

$$C_{scour} = 55P \tag{A-54}$$

A-3-11 Surety Bond

Once the lifetime of a offshore wind farm has come to an end, the foundations and the support structures needs to be removed for the sake of navigational restrictions. This model analyses the cost of decommissioning and makes sure a surety bond is provided for. The cost is a percentage of the ICC without the offshore warranty premium.

$$C_{surety} = 0.03(ICC - C_{warranty}) \tag{A-55}$$

A-3-12 Offshore Warranty Premium

Offshore wind turbines are operating in more extreme conditions than the on-land wind turbines, therefore they are under greater risks of failure. The cost for offshore warranty premium is reflected as a percentage of the turbine and tower cost.

$$C_{warranty} = 0.15C_{turb-twr} \tag{A-56}$$

A-3-13 Offshore Levelized Replacement Cost

As in the on-land wind parks the offshore LRC is a fund to cover long-term overhauls and replacements of components in the wind turbine. Since offshore installations are operating in harsher conditions they are replaced more frequently than on-land based installations. The cost is formulated depending on the machine rating.

$$C_{offLRC} = 17P \tag{A-57}$$

A-3-14 Offshore Bottom Lease Cost

The sea that a offshore wind turbine occupies is leased for building a offshore wind farm. The rights to these spaces are mostly held by the State governments or the Federal governments. The cost in this model than is based on the cost of leasing per energy production per year.

$$C_{BLC} = 0.00108AEP \tag{A-58}$$

A-3-15 Offshore OM

The offshore operation is done with special transportation equipment in a remote location under harsh operating environment, therefore it is expected to be more expensive that on-land based OM. The cost of offshore OM is calculated depending on the energy production per year.

$$C_{offOM} = 0.02AEP \tag{A-59}$$

Appendix B

Running the Engineering Design Tool

This appendix involves the initial conditions of the design variables before running the tool, according to the rated power input. Furthermore objective functions involved needs to be adjusted according to the rated power of the wind turbine as well, due to the reasons given in section 6-4-1. First two of the figures involve the general set up of the design variables and the methods for above and below 10 MW. If any changes needs to be done for a specific rated power they are demonstrated below the general set-ups.

Table B-1: Set-up for 10 MW and below

Rated Power	Wind Site Class	File	Design Variable	Method	Adjustment
10 MW and below	All wind site classes	Cost0.py	rotor_radius	-	set to 62 m
		Cost1.py	rotor_radius	-	set to 62 m
		Cost2.py	rotor_radius	-	set to 62 m
		Rotor0.py	-	MassBlade_optDFIG	divide by 10^6
		Rotor1.py	-	MassBlade_opt	divide by 10^4
		Rotor2.py	-	MassBlade_optDD	divide by 10^4
		Three_stage_gearbox	sun1_tooth_width	-	set to 0.5 m
		Three_stage_gearbox	sun2_tooth_width	-	set to 0.2 m
		Three_stage_gearbox	pinion_tooth_width	-	set to 0.2 m
		Three_stage_gearbox	-	objfunc	divide by 10^7
3 MW		Cost0.py	rotor_radius	-	set to 60 m

Table B-2: General set-up for above 10 MW rated power and 15 MW

Rated Power	Wind Site Class	File	Design Variable	Method	Adjustment
Above 10 MW	All wind site classes	Three_stage_gearbox	sun1_tooth_width	-	set to 1.3 m
		Three_stage_gearbox	sun2_tooth_width	-	set to 0.5 m
		Three_stage_gearbox	pinion_tooth_width	-	set to 0.5 m
15 MW	Wind site classes 1	Rotor0.py	-	MassBlade_optDFIG	divide by 10^7
		Rotor1.py	-	MassBlade_opt	divide by 10^6
		Rotor2.py	-	MassBlade_optDD	divide by 10^7
		Cost0.py	rotor_radius	-	set to 140 m
		Cost1.py	rotor_radius	-	set to 140 m
		Cost2.py	rotor_radius	-	set to 140 m
		Three_stage_gearbox	-	objfunc	divide by 10^8
15 MW	Wind site classes 2	Rotor0.py	-	MassBlade_optDFIG	divide by 10^8
		Rotor1.py	-	MassBlade_opt	divide by 10^6
		Rotor2.py	-	MassBlade_optDD	divide by 10^6
		Cost0.py	rotor_radius	-	set to 140 m
		Cost1.py	rotor_radius	-	set to 140 m
		Cost2.py	rotor_radius	-	set to 140 m
		Three_stage_gearbox	-	objfunc	divide by 10^8
15 MW	Wind site classes 0	Rotor0.py	-	MassBlade_optDFIG	divide by 10^8
		Rotor1.py	-	MassBlade_opt	divide by 10^6
		Rotor2.py	-	MassBlade_optDD	divide by 10^6
		Cost0.py	rotor_radius	-	set to 140 m
		Cost1.py	rotor_radius	-	set to 140 m
		Cost2.py	rotor_radius	-	set to 140 m
		Three_stage_gearbox	-	objfunc	divide by 10^8

Table B-3: Set-up for 20 MW rated power

Rated Power	Wind Site Class	File	Desing Variable	Method	Adjustment
20 MW	Wind site class 0	Rotor0.py	-	MassBlade_optDFIG	divide by 10^8
		Rotor1.py	-	MassBlade_opt	divide by 10^6
		Rotor2.py	-	MassBlade_optDD	divide by 10^6
		Cost0.py	rotor_radius	-	set to 120 m
		Cost1.py	rotor_radius	-	set to 140 m
		Cost2.py	rotor_radius	-	set to 120 m
		Three_stage_gearbox	-	objfunc	divide by 10^8
20 MW	Wind site class 1	Rotor0.py	-	MassBlade_optDFIG	divide by 10^6
		Rotor1.py	-	MassBlade_opt	divide by 10^6
		Rotor2.py	-	MassBlade_optDD	divide by 10^7
		Cost0.py	rotor_radius	-	set to 140 m
		Cost1.py	rotor_radius	-	set to 140 m
		Cost2.py	rotor_radius	-	set to 140 m
		Three_stage_gearbox		objfunc	divide by 10^8
20 MW	Wind site class 2	Rotor0.py	-	MassBlade_optDFIG	divide by 10^6
		Rotor1.py	-	MassBlade_opt	divide by 10^6
		Rotor2.py	-	MassBlade_optDD	divide by 10^7
		Cost0.py	rotor_radius	-	set to 140 m
		Cost1.py	rotor_radius	-	set to 140 m
		Cost2.py	rotor_radius	-	set to 140 m
		Three_stage_gearbox	-	objfunc	divide by 10^8

Bibliography

[1] J. K. Kaldellis and M. Kapsali, "Shifting towards offshore wind energy-recent activity and future development," *Energy Policy*, vol. 53, pp. 136–148, 2013.

[2] M. Bilgili, A. Yasar, and E. Simsek, "Offshore wind power development in europe and its comparison with onshore counterpart," *Renewable and Sustainable Energy Reviews*, vol. 15, no. 2, pp. 905 – 915, 2011.

[3] M. López and J.-C. Vannier, "Sistema aislado de conversión eólica con control de máxima transferencia de potencia," *Ingeniare. Revista chilena de ingeniería*, vol. 17, no. 3, pp. 329–336, 2009.

[4] J. F. Manwell, J. G. McGowan, and A. L. Rogers, "Wind energy explained: Theory, design and application," 2010.

[5] J. T. Allison, *Complex system optimization: A review of analytical target cascading, collaborative optimization, and other formulations*. PhD thesis, The University of Michigan, 2004.

[6] J. M. Jonkman, S. Butterfield, W. Musial, and G. Scott, *Definition of a 5-MW reference wind turbine for offshore system development*. National Renewable Energy Laboratory Golden, CO, 2009.

[7] T. Ashuri, *Beyond Classical Upscaling: Integrated Aeroservoelastic Design and Optimization of Large Offshore Wind Turbines*. PhD thesis, Ph. D. Thesis, Delft University of Technology, The Netherlands, 2012.

[8] G. Henriot, *Gears and planetary gear trains*. Brevini, 2001.

[9] R. C. Juvinall and K. M. Marshek, *Fundamentals of machine component design*, vol. 83. John Wiley & Sons, 1991.

[10] H. Li, Z. Chen, and H. Polinder, "Optimization of multibrid permanent-magnet wind generator systems," *Energy Conversion, IEEE Transactions on*, vol. 24, no. 1, pp. 82–92, 2009.

[11] H. Polinder, F. F. Van der Pijl, G.-J. De Vilder, and P. J. Tavner, "Comparison of direct-drive and geared generator concepts for wind turbines," *Energy conversion, IEEE transactions on*, vol. 21, no. 3, pp. 725–733, 2006.

[12] H. Polinder and J. Morren, "Developments in wind turbine generator systems," *Electrimacs. Hammamet, Tunisia*, pp. 67–78, 2005.

[13] G. D. Technologies, "Wind turbine gearbox systems."

[14] L. J. Fingersh, M. M. Hand, and A. S. Laxson, *Wind turbine design cost and scaling model*. National Renewable Energy Laboratory Golden, CO, 2006.

[15] B. R. AG, "Gearboxes for wind turbines."

[16] W. Gear, "Light weight and reliable gearboxes for wind turbine drives," 2014.

[17] E. A. GmbH, "Lasting power from wind eicogear."

[18] A. Ltd., "Generators for wind turbines," 2014.

[19] J. D. Speth, *The Bridge ath the Edge of the World*. Yale University Press, 2008.

[20] L. Lizuma, Z. Avotniece, S. Rupainis, and A. Teilans, "Assessment of the present and future offshore wind power potential: A case study in a target territory of the baltic sea near the latvian coast," *The Scientific World Journal*, vol. 2013, 2013.

[21] REN21, *Renewables 2013: Global status report*. REN21 Secretaritat, Paris, 2013.

[22] A. Westwood, "Turbine capacity," *Refocus*, vol. 5, no. 3, p. 17, 2004.

[23] M. Ragheb, "Optimal rotor tip speed ratio," *Available from NetFiles at the University of Illinois at Urbana-Champaign, Last modified*, 2009.

[24] M. Ragheb and A. M. Ragheb, "Wind turbines theory-the betz equation and optimal rotor tip speed ratio," *R. Carriveau, Fundamental and Advanced Topics in Wind Power*, pp. 19–37, 2011.

[25] T. Burton, N. Jenkins, D. Sharpe, and E. Bossanyi, *Wind energy handbook*. John Wiley & Sons, 2011.

[26] Z. H. Z. Guevara, "Insight into properties of an ideal wind turbine and its subsystems," tech. rep., TU Delft, 2010.

[27] A. J. d. Wit, *A unified approach towards decomposition and coordiation for multi-level optimization*. PhD thesis, TU Delft, 2009.

[28] S. Tosserams, L. P. Etman, and J. Rooda, "A classification of methods for distributed system optimization based on formulation structure," *Structural and Multidisciplinary Optimization*, vol. 39, no. 5, pp. 503–517, 2009.

[29] R. Saigal, "Matrix partitioning methods for interior point algorithms," *Ann Arbor*, vol. 1001, pp. 48109–2117, 1992.

[30] T. C. Wagner and P. Y. Papalambros, "General framework for decomposition analysis in optimal design.," *ASME DES ENG DIV PUBL DE., ASME, NEW YORK, NY(USA), 1993,*, vol. 65, pp. 315–325, 1993.

[31] M. B. Zaaijer, *Great Expectations for Offshore Wind Turbines.* PhD thesis, TU Delft, 2013.

[32] M. Zaaijer, H. Hendriks, S. Herman, A. Winnemuller, T. Topper, R. van den Berg, and W. op den Velde, "Optimisation through conceptual variation of a baseline wind farm," in *Proceedings of MAREC*, 2002.

[33] R. S. Krishnamachari and P. Y. Papalambros, "Hierarchical decomposition synthesis in optimal systems design," *Journal of Mechanical Design*, vol. 119, no. 4, pp. 448–457, 1997.

[34] S. Goossens, "Rotor design model," tech. rep., TU Delft, n.d.

[35] P. Jamieson, *Innovation in wind turbine design.* John Wiley & Sons, 2011.

[36] W. Turbines, "Part 1: Design requirements, iec 61400-1," 2005.

[37] R. van Rooij, "Terminology, reference systems and conventions," tech. rep., TU Delft, 2001.

[38] A. Ragheb and M. Ragheb, "Wind turbine gearbox technologies," in *Nuclear & Renewable Energy Conference (INREC), 2010 1st International*, pp. 1–8, IEEE, 2010.

[39] A. Derks, "Development of a wind turbine drive train engineering model," Master's thesis, TU Delft, 2008.

[40] A. Stokes, *Gear handbook: design and calculations.* Society of Automotive Engineers, 1992.

[41] E. Properties, "Young modulus for some materials," *The Engineering ToolBox (http://www. engineeringtoolbox. com/young-modulus-d_417. html). Retrieved*, vol. 5, 2013.

[42] C.-H. Liou, F. Oswald, D. Townsend, and H. H. Lin, "Effect of contact ratio on spur gear dynamic load with no tooth profile modifications," *Journal of Mechanical Design*, vol. 118, no. 3, pp. 439–443, 1996.

[43] W. Musial, S. Butterfield, and B. McNiff, "Improving wind turbine gearbox reliability," in *Proceedings of the European wind energy conference*, 2007.

[44] R. Poore and T. Lettenmaier, "Alternative design study report: Windpact advanced wind turbine drive train designs study; november 1, 2000–february 28, 2002," tech. rep., National Renewable Energy Laboratory (NREL), Golden, CO., 2003.

[45] H. Polinder, S. W. de Haan, M. R. Dubois, and J. G. Slootweg, "Basic operation principles and electrical conversion systems of wind turbines," *EPE JOURNAL*, vol. 15, no. 4, p. 43, 2005.

[46] T. Jokinen *et al.*, *Design of rotating electrical machines*. John Wiley & Sons, 2008.

[47] G. Bywaters, V. John, J. Lynch, P. Mattila, G. Norton, J. Stowell, M. Salata, O. Labath, A. Chertok, and D. Hablanian, "Northern power systems windpact drive train alternative design study report; period of performance: April 12, 2001 to january 31, 2005," tech. rep., National Renewable Energy Laboratory (NREL), Golden, CO., 2004.

[48] M. Segeren, "Support structure design-offshore wind farm design," 2013.

[49] *IEC 61400-1: Wind turbines part1: Design Requirements*. IEC, 2005.

[50] E. Koutoulakos, "Wind turbine reliability characteristics and offshore availability assessment," *Master's thesis, TU Delft*, 2008.

[51] S. Habali and I. Saleh, "Local design, testing and manufacturing of small mixed airfoil wind turbine blades of glass fiber reinforced plastics: part i: design of the blade and root," *Energy conversion and management*, vol. 41, no. 3, pp. 249–280, 2000.

[52] H. Li and Z. Chen, "Design optimization and evaluation of different wind generator systems," in *Electrical Machines and Systems, 2008. ICEMS 2008. International Conference on*, pp. 2396–2401, IEEE, 2008.

[53] M. J. Kaiser and B. Snyder, "Offshore wind energy installation and decommissioning cost estimation in the us outer continental shelf," *US Dept. of the Interior, Bureau of Ocean Energy Management, Regulation and Enforcement, Herndon, VA TA&R*, vol. 648, 2010.

[54] M. Zaaijer and G. van Bussel, "Integrated analysis of wind turbine and wind farm," in *Symposium Offshore-Wind-Energy-Structure, Design and Environmental Aspects of Offshore-Wind-Energy-Converters, Hannover, DE*, 2002.

[55] G. v. Rossum *et al.*, "Python programming language," *URL http://www. python. org*, 1989.

[56] T. Peters, "The zen of python," in *Pro Python*, pp. 301–302, Springer, 2010.

[57] P. Raybaut, "Documentation," 2009.

[58] "An open-source mdao frmawork written in python," 2012.

[59] C. Heath and J. Gray, "Openmdao: Framework for flexible multidisciplinary design, analysis and optimization methods," in *Proceedings of the 53rd AIAA Structures, Structural Dynamics and Materials Conference, Honolulu, HI*, 2012.

[60] C. S. Perone, "Pyevolve: a python open-source framework for genetic algorithms," *ACM SIGEVOlution*, vol. 4, no. 1, pp. 12–20, 2009.

[61] W. Musial and B. Ram, "Large-scale offshore wind power in the united states: Assessment of opportunities and barriers," tech. rep., National Renewable Energy Laboratory (NREL), Golden, CO., 2010.

Glossary

List of Acronyms

RNA	Rotor Nacelle Assembly
OWF	Offshore Wind Farm
LPC	Levelized Production Cost
PMSG	Permanent Magnet Synchronous Generator
DFIG	Doubly Fed Induction Generator
MDO	Multidisciplinary Design Optimization
FIO	Fully Integrated Optimization
MP	mathematical programming
FCR	fixed charge rate
ICC	initial capital cost
AEP	net annual energy production
AOE	annual operating expenses
OM	operation and maintenance cost
LRC	levelized replacement/overhaul cost
LWST	Low Wind Speed Technology
IEC	International Electrotechnical Commision
GL	Germanischer Lloyd
GRP	fibreglass reinforced plastic

Nomenclature

Latin Symbols

a	Induction factor
a'	Radial induction factor
B	Number of blades
b	Gear tooth width
c	chord
C_D	Drag coefficient
C_L	Lift coefficient
C_P	Power coefficient
C_p	Coefficient of material elastic property
C_R	Reliability factor
C_T	Thrust coefficient
C_{2a}	Influence of ageing partial safety factor for composite materials
C_{3a}	Temperature effect partial safety factor for composite materials
C_{4a}	Hand layup laminate partial safety factor for composite materials
C_{5a}	Post cured laminate partial safety factor for composite materials
$C_{_{LLC}}$	Land lease costs
$C_{assem-ins}$	Cost of the assemble and installation
C_{blade1}	Cost of the blade root
C_{BLC}	Offshore bottom lease cost
$C_{brk-cpl}$	Cost of the mechanical brake, high-speed coupling, and associated components
C_{civil}	Cost of the roads and civil work

C_{elcon}	Cost of the electrical connections
C_{elc}	Cost of the electrical and interface connections
$C_{eng-permt}$	Cost of the engineering and the permits
C_{fndtn}	Cost of the foundation
C_{gbx_1s}	Cost of single stage gearbox
C_{gbx_3s}	Cost of three stage gearbox
C_{gen_1s}	Cost of single stage PM generator
C_{gen_3s}	Cost of DFIG
C_{gen_mp}	Cost of direct drive PM generator
C_{hub}	Cost of the hub
$C_{hyd-dool}$	Cost of the hydraulic and cooling systems
C_{Li}	Life factor
C_{LRC}	Levelized replacement cost
C_{lss}	Cost of the low speed shaft
C_{marin}	Marinization costs
$C_{mbearing}$	Cost of the main bearings
C_{mframe_1s}	Cost of the PM1s drive train mainframe
C_{mframe_3s}	Cost of the DFIG3s drive train mainframe
C_{mframe_dd}	Cost of the DD drive train mainframe
$C_{nacelle}$	Cost of the nacelle
C_{ncone}	Cost of the nose cone
C_{offelc}	Offshore electrical interface connection costs
$C_{offeng-prmt}$	Offshore permit, engineering and site assessment costs
C_{offLRC}	Offshore levelized replacement cost
C_{offOM}	Offshore operation and maintenance cost
C_{OM}	Cost of the operation and maintenance
C_{OSS}	Offshore support structure
C_{OTC}	Offshore transportation costs
C_{OTI}	Offshore turbine installation cost
$C_{pitchtot}$	Cost of the pitch mechanisms and the bearings
$C_{plat-rail}$	Cost of the platforms and rails
$C_{port-stage}$	Costs of port and staging equipment
C_{scour}	Scour protection cost
C_{surety}	Surety bond cost
C_{trans}	Cost of the transportation
$C_{turb-twr}$	Turbine and tower costs
C_{twr}	Cost of the tower
C_t	Total costs for year t

C_{vse}	Cost of the variable speed electronics
$C_{warranty}$	Offshore warranty premium
C_{yaw}	Cost of the yaw drive and bearing
CR	Contact ratio
d	pitch diameter
d_g	Gear diameter
d_i	Inner diameter of the blade root
d_o	Outer diameter of the blade root
d_{pinion}	Pinion diameter
d_{root}	Blade root diameter
E	Young's modulus
E_t	Total electricity production in year t
EI	Blade flapwise stiffness
EI_{ref}	Reference wind turbine blade flapwise stiffness
f	Thickness factor for the blade
F_d	Air gap force density
F_t	Tangential force on teeth
g	Scaling factor of the chord distribution
H_{hub}	Hub height
I	Geometry factor
i	Annual interest rate on depths
I_b	Area moment of inertia of the blade root cross section
k	Shape parameter
k_1	Non-uniformity factor
k_2	Mass factor for three stage gearbox
k_3	Mass factor for single stage gearbox
K_m	Mounting factor
K_o	Overload correction factor
K_v	Velocity factor
k_{civil}	Cost factor for roads and civil works
k_{elc}	Cost factor for the electrical and interface connections
$k_{eng-permt}$	Cost factor for the engineering and permits
k_{LRC}	Cost factor for the levelized replacement cost
k_{OTC}	Cost factor for the offshore transportation
k_t	Cost factor for transportation
l_g	Generator length
m	Gear module
M_{blade1}	Mass of the blade root

M_{blade2}	Mass of the rest of the blade
M_{blade}	Total mass of the blade
$M_{brk-cpl}$	Mass of the mechanical brake, high-speed coupling, and associated components
M_{flp}	Flapwise bending moment at the root
M_{gbx_1s}	Mass of three single gearbox
M_{gbx_3s}	Mass of three stage gearbox
M_{gear}	Mass of the gears
M_{gen_1s}	Mass of single stage PM generator
M_{gen_3s}	Mass of DFIG
M_{gen_mp}	Mass of direct drive PM generator
M_{hub}	Mass of the hub
$M_{hyd-dool}$	Mass of the hydraulic and cooling systems
M_{lss}	Mass of the low speed shaft
$M_{mbearing}$	Mass of the main bearings
M_{mframe_1s}	Mass of the PM1s drive train mainframe
M_{mframe_3s}	Mass of the DFIG3s drive train mainframe
M_{mframe_dd}	Mass of the DD drive train mainframe
$M_{nacelle}$	Mass of the nacelle
M_{ncone}	Mass of the nose cone
$M_{parallel}$	Mass of the parallel stage
$M_{pbearing}$	Mass of the bearings
M_{pinion}	Mass of the pinion gears
$M_{pitchtot}$	Mass of the pitch mechanisms and the bearings
$M_{planetary}$	Mass of the planetary stage
M_{planet}	Mass of the planet gears
$M_{plat-rail}$	Mass of the platforms and rails
M_{ring}	Mass of the ring wheel
M_{sun}	Mass of the sun gears
M_{yaw}	Mass of the yaw drive and bearing
n_g	Rotational speed of the gear
n_p	Angular velocity of gear
n_p	Rotational speed of the pinion
n_{pole}	Number of poles
P	Power of the wind turbine
p	Pitch
p_a	Axial pitch
P_p	Power in gearbox
P_R	Rayleigh probability density function

R	Rotor radius
r	Real interest rate
r_g	Generator radius
r_p	Pitch radius
R_{ref}	Reference wind turbine rotor radius
R_t	Total revenues for year t
S_H	Surface fatigue strength of tooth
S_{fe}	Surface fatigue strength of steel
T	Economic life time
T_g	Torque transferred to the gear
T_p	Torque transferred to the pinion
T_{hss}	High speed shaft torque
T_{rated}	Rated torque of the rotor
t_{root_ref}	Reference turbine blade root skin thickness
t_{root}	Skin thickness of the blade root
U	Rated wind speed
u	Transmission ratio
v	Annual inflation rate
V_g	Generator volume
V_p	Pitch line velocity
V_{50}	50 year wind speed at hub height
V_{ave}	Annual average wind speed at the hub height
V_{hub}	Wind velocity at hub height
v_{tip}	Tip speed
x	Distance from the flapwise neutral axis in the blade
Y	Levis form factor
y	Blade tip deflection
YS_{gear}	Yield stress of the gear
z	Number of teeth
z_g	Number of teeth in gear
z_p	Number of teeth in pinion
z_{planet}	Number of teeth in planet gear
z_{ring}	Number of teeth in ring wheel
z_{sun}	Number of teeth in sun gear

Greek Symbols

α	Angle of attack

β	Blade twist
$\Delta z_{clearence}$	Clearance height
$\eta_{availability}$	Annual availability of the wind park
γ_{M0}	General material factor
λ	Tip speed ratio
λ_r	Local tip speed ratio
ν	Poisson ratio
ω	Rated rotational speed of the rotor
ω_{gen}	Generator rotational seed
ϕ	Inflow angle
ρ_{air}	Air density
ρ_{steel}	Steel density
σ_b	Bending stress at gear teeth
σ_c	Surface fatigue stress at gear teeth
$\sigma_{flp,\max}$	Maximum flapwise stress at the blade root
φ	Pressure angle